

**School of Electrical Engineering,
Computing and Mathematical Sciences**

**Real-time Condition Monitoring and Asset Management of Oil-
Immersed Power Transformers**

Lan Maggie Jin

0000-0002-4753-9543

**This thesis is presented for the Degree of
Master of Philosophy (Electrical and Computer Engineering)
of
Curtin University**

January 2024

Declaration

To the best of my knowledge and belief this thesis contains no material previously published by any other person except where due acknowledgment has been made.

This thesis contains no material which has been accepted for the award of any other degree or diploma in any university.

(Include where applicable)

Signature:

Date:

Acknowledgements

I would like to express my appreciation to all those who have contributed to the successful completion of my thesis. I am profoundly thankful to Professor Ahmed Abu-Siada and Dr Dowon Kim for their exceptional mentorship, insightful guidance, and continuous encouragement throughout my research. Their expertise, dedication, and willingness to share their knowledge have been instrumental in shaping the direction and quality of this work.

I also like to sincerely acknowledge and express my gratitude to BHP corporation for providing me with a scholarship that enabled me to conduct this research.

I extend my sincere appreciation to the staffs of Curtin University for their support in providing access to essential research resources. Their administrative assistance and technical guidance have been deeply appreciated.

Lastly, I would like to thank my family and friends for their unwavering support and encouragement, which have been crucial factors in this challenging journey.

Abstract

In the realm of electric power systems, oil-immersed power transformers stand out as critical and expensive assets. The failure of a power transformer would not only result in downtime to the entire transmission and distribution networks but may also cause personnel and environmental hazards due to oil leak and fire. Owing to their vital function and high cost, the implementation of effective asset management strategies for power transformers becomes imperative. This ensures the continuity of uninterrupted power supply, mitigating financial risks, and maintaining overall grid stability. While extensive effort has been invested by the industry in developing various condition monitoring and fault diagnosis apparatuses, it is not economically feasible to apply rigorous inspection and extensive testing to all power transformer fleets in the network. The fundamental purpose of asset management is to balance cost and reliability of the system.

With the global trend to establish digital substation automation systems, transformer online condition monitoring has been given much attention by utilities and researchers alike. Among the current available online condition monitoring technologies, Dissolved Gas Analysis (DGA) has long been recognized as a valuable diagnostic tool for detecting potential faults and monitoring transformers' conditions. This study focuses on the integration of online DGA method into asset management practices for oil-immersed power transformers, employing an advanced data analytics technique known as Convolutional Neural Network (CNN), which is a type of deep machine learning algorithms.

The formulated model for transformer asset management comprises two core modules: the Fault Diagnostic module and Life Management module, both of which have been trained utilizing CNN algorithms. The devised Fault Diagnostic module utilizes five-gas (H_2 , CH_4 , C_2H_4 , C_2H_6 , and C_2H_2) measurements collected from the online DGA device to predict potential faults, providing a corresponding probability of failure. Concurrently, the established Life Management module employs two-gas (CO and CO_2) measurements from the online DGA device to forecast the percentage of remaining life and the extent of degradation. Notably, the outcomes exhibit a commendable performance with an approximate accuracy rate of 86% for the Fault Diagnostic module and about 85% for the Life Management module.

List of Publications

1. Lan Jin, Dowon Kim, A. Abu-Siada, Shantanu Kumar, "Oil-immersed Power Transformer Condition Monitoring Methodologies: A Review", *Energies*, 15(9), 3379, May 2022.
2. Lan Jin, Dowon Kim, A. Abu-Siada, "State-of-the-art Review on Asset Management Methodologies for Oil-immersed Power Transformers", *Electric Power Systems Research*, 218, 109194, April 2023
3. Lan Jin, Dowon Kim, Kit Yan Chan, A. Abu-Siada, "Deep Machine Learning-based Asset Management Approach for Oil-Immersed Power Transformers using Dissolved Gas Analysis", in *IEEE Access*, vol. 12, pp. 27794-27809, Feb 2024, doi: 10.1109/ACCESS.2024.3366905.

Attribution Statement for Thesis Chapter Based on Published Work

This thesis incorporates material from the following published papers:

Chapter 2 of this thesis is published as “Oil-immersed Power Transformer Condition Monitoring Methodologies: A Review”.

Authors: Lan Jin, Dowon Kim, A. Abu-Siada, Shantanu Kumar
Source: Energies, 15(9), 3379, May 2022

Chapter 3 of this thesis is published as “State-of-the-art Review on Asset Management Methodologies for Oil-immersed Power Transformers”.

Authors: Lan Jin, Dowon Kim, A. Abu-Siada
Source: Electric Power Systems Research, 218, 109194, April 2023

Chapter 4 of this thesis is published as “Deep Machine Learning-based Asset Management Approach for Oil-Immersed Power Transformers using Dissolved Gas Analysis”.

Authors: Lan Jin, Dowon Kim, Kit Yan Chan, A. Abu-Siada
Source: IEEE Access, vol. 12, pp. 27794-27809, Feb 2024

The candidate made significant contributions to the above three journal papers, primarily focusing on the conception and design, acquisition of data and methods pertinent to dissolved gas analysis, data conditioning and manipulation by setting to consistent format, utilizing advanced analysis and statistical methods, particularly leveraging machine learning techniques, comparing results, interpretation and discussion. Moreover, the candidate contributed to manuscript preparation and effectively incorporated valuable feedback from reviewers.

The co-authors significantly contributed to all three journal papers by reviewing results, validating the main author’s contributions and the novelty of the findings, engaging in discussions, conducting comprehensive reviews of the manuscripts, and evaluating reviewers’ comments.

Name	Author: Lan Maggie Jin	Supervisor: Ahmed Abu-Siada
Signature		

Table of Contents

Declaration.....	1
Acknowledgements	2
Abstract.....	3
List of Publications	4a
Table of Contents.....	5
List of Figures	8
List of Tables	10
List of Abbreviations	12
Chapter 1 Introduction	14
1.1. Background and Challenges.....	14
1.2. Objectives and Contribution of the Thesis	16
1.3. Thesis Outline	16
Chapter 2 Oil-immersed Power Transformer Condition Monitoring Methodologies	18
2.1. Introduction.....	18
2.2. Offline Condition Monitoring Methods.....	20
2.2.1 Degree of Polymerization of Insulation Paper	20
2.2.2 Furan Analysis	21
2.2.3 Interfacial Tension Analysis and Acidity.....	22
2.2.4 Oil Dielectric Breakdown Voltage	22
2.2.5 Insulation Resistance Test.....	23
2.2.6 Dissipation Factor Measurement.....	24
2.2.7 Dielectric Response Methods	25
2.2.8 Sweep Frequency Response Analysis	29
2.2.9 Transformer Turns Ratio Test	30
2.3. Online Condition Monitoring Methods	31
2.3.1 Dissolved gas analysis	31
2.3.2 Partial Discharge	40
2.3.3 Thermal Measurements.....	46
2.3.4 Vibration Analysis	47

2.4.	Challenges and Opportunities	47
2.5.	Summary.....	48
Chapter 3	Asset Management Methodologies for Oil-immersed Power Transformers.....	49
3.1.	Introduction.....	49
3.2.	Fault Diagnosis.....	50
3.2.1	Condition monitoring methods	51
3.2.2	Fault Analysing Methods	55
3.3.	Reliability Assessment	64
3.3.1	Health Index.....	64
3.3.2	Health index algorithms.....	66
3.4.	Life Management.....	69
3.4.1	Thermal-based Method	70
3.4.2	DP-value method	72
3.5.	Future Improvement areas.....	75
3.5.1	Failure modes definition	75
3.5.2	Hybrid models.....	75
3.6.	Summary.....	76
Chapter 4	Deep Machine Learning-based Asset Management Approach for Oil-Immersed Power transformers using Dissolved Gas Analysis.....	77
4.1.	Introduction.....	77
4.2.	Methodologies Utilized in Developing the Asset Management Model.....	78
A.	Data Pre-processing – Normalization	78
B.	Data Pre-processing – Balance Datasets	79
C.	Convolution Neural Network.....	81
4.3.	Proposed Asset Management Model.....	83
A.	Fault Diagnostic module	84
B.	Life Management module.	86
4.4.	Results and Discussion.....	88
A.	Fault Diagnostic module	88
B.	Life Management module	102
C.	Contribution and significance.....	109

4.5. Summary.....	109
Chapter 5 Conclusions and Future Work.....	111
5.1. Conclusions.....	111
5.2. Future Work.....	113
References.....	115
Appendix A Python Script for Fault Diagnostic Module Training.....	131
Appendix B Python Script for Life Management Module Training.....	134
Appendix C Python Script for Asset Management Model.....	136

List of Figures

Figure 1.1 ANFIS diagnostic structure for DGA analysis.	15
Figure 2.1 Distribution of failures for Australian power transformers during the period 2000 to 2015.....	18
Figure 2.2 The parameters to be monitored for oil-immersed power transformer components.....	19
Figure 2.3 Offline and online condition monitoring methods for oil-immersed power transformer.....	20
Figure 2.4 Chemical structure of cellulose.....	20
Figure 2.5 Typical IR measurements versus time of the applied voltage.	23
Figure 2.6 (a) Equivalent circuit represents a dielectric and (b) phasor diagram.....	24
Figure 2.7 Equivalent circuit for bushing PF monitoring.....	25
Figure 2.8 (a) Basic RVM measuring circuit and (b) measurements.....	26
Figure 2.9 Example of RVM polarization spectrum.	26
Figure 2.10 (a) Basic PDC measuring circuit and (b) waveform of polarization and depolarization currents. ...	27
Figure 2.11 Example of relationship between polarization/depolarization currents and insulation conductivity.	28
Figure 2.12 (a) Basic FDS measuring circuit and (b) typical FDS response.....	29
Figure 2.13 FRA measurement example, (a) Transfer function amplitude. (b) Transfer function phase angle. 30	30
Figure 2.14 Headspace extraction structure diagram and membrane structure.	32
Figure 2.15 Online GC system using SOFC detector.	33
Figure 2.16 Example of voltage signal output of SOFC detector equivalent to gas concentrations.....	33
Figure 2.17 The principle of photo-acoustic effect.....	34
Figure 2.18 Schematic diagram of PAS detection unit.....	34
Figure 2.19 The electromagnetic spectrum for various wavelength regions of light.....	35
Figure 2.20 Diagram of H ₂ atoms react with Pd surface.	36
Figure 2.21 Classic Duval Triangle from IEEE C57.104.	39
Figure 2.22 Duval pentagon 1 from IEEE C57.104.	40
Figure 2.23 The process of PD measurement.	41
Figure 2.24 (a) Signal of tuned UHF narrowband method and (b) bandwidth of UHF broadband method.....	41
Figure 2.25 Fabry-Perot interference sensor structure.....	42
Figure 2.26 Example of output electrical signal from Fabry-Perot optical sensor.....	43
Figure 2.27 Diagram of Mach-Zehnder interferometer structure.....	43
Figure 2.28 Diagram of Michelson interferometer structure.....	43
Figure 2.29 Diagram of Sagnac interferometer structure.....	44
Figure 2.30 Working principle of FBG.....	44
Figure 2.31 Diagram of Fibre Bragg Grating interferometer structure.....	44
Figure 2.32 Detection principle of TEV signals.....	45
Figure 2.33 Diagram of HFCT structure.....	46
Figure 2.34 An example of thermal image taken by infrared camera.....	46
Figure 3.1 Basic structure of asset management.....	49
Figure 3.2 The basic structure of condition assessment in asset management.....	50

Figure 3.3 (a) Duval Triangle 1. (b) Duval Pentagon 1.....	57
Figure 3.4 Structure of Fuzzy Logic data analysis.....	59
Figure 3.5 An example of Decision Tree structure.....	60
Figure 3.6 Principal diagram of SVM with two classes.	61
Figure 3.7 An example of Bayesian Network model.....	62
Figure 3.8 Basic structure of Artificial Neural Network.	63
Figure 3.9 Basic structure of ANFIS model.....	64
Figure 3.10 HI model used by current industry practice.	65
Figure 3.11 Scoring-weighting method used in industry.	66
Figure 3.12 Using Kalman filter for thermal model.	72
Figure 3.13 Sources of faults.....	75
Figure 4.1 (a) Raw H2 Data (in ppm) collected from DGA sensor. (b) Data processed using Minimum- Maximum normalization.....	79
Figure 4.2 (a) Data distribution before SMOTE and (b) Data distribution after SMOTE. (for reference to label numbers, see Table 3).....	81
Figure 4.3 The structure of Convolution Neural Network.	82
Figure 4.4 General structure of neural networks with 2 hidden layers.....	83
Figure 4.5 Proposed workflow for the oil-immersed power transformer asset management model.	84
Figure 4.6 Fault Diagnostic module: (a) Training and validation loss plot. (b) Training and validation accuracy plot.....	91
Figure 4.7 Confusion matrix of the proposed Fault Diagnostic module.	91
Figure 4.8 The training and validation loss plot for the Life management module.....	104
Figure 5.1 Asset Management Module Interface.....	112

List of Tables

Table 1.1 Engineering crafted parameters used in machine learning training for DGA analysis.	15
Table 2.1 Furan compounds and associated types of stresses.	21
Table 2.2 The correlation between 2-FAL and DP for paper insulation with condition level.....	22
Table 2.3 Fault types and key gases corresponding to each fault.	32
Table 2.4 Primary faults associated with key gases.....	35
Table 2.5 The summary of KGM from IEEE C57.104.....	37
Table 2.6 Rogers Ratio Method (RRM) from IEEE C57.104.....	37
Table 2.7 Doernenburg Ratio Method (DRM) from IEEE C57.104.....	38
Table 2.8 Limit concentrations of dissolved gases from IEEE C57.104.....	38
Table 2.9 Abbreviations of basic faults.	39
Table 2.10 Comparison of different optical detection technologies.	42
Table 3.1 Primary and sub-types of faults that can be diagnosed using DGA.	51
Table 3.2 Partial discharge detection methods	52
Table 3.3 Conventional fault diagnostic methods.....	55
Table 3.4 Proposed AI methods for each condition monitoring method.....	58
Table 3.5 AI methods used for HI algorithm.....	68
Table 3.6 various DP-Furan correlational models.....	73
Table 3.7 Examples of hybrid model used in condition assessment.	76
Table 4.1 Datasets for Fault Diagnostic module training.....	80
Table 4.2 Six fundamental types of faults diagnosed using DGA.....	84
Table 4.3 Possible conditions represented using binary numbers.	86
Table 4.4 Fault Diagnostic module outputs and corresponding Asset Management statement.....	86
Table 4.5 DP values and their associated significance [150].	88
Table 4.6 Optimal parameters of the developed Fault Diagnostic module.....	89
Table 4.7 Comparison between the diagnostic result from the Fault Diagnostic module and actual condition from inspection. (All gases are measured in PPM).....	93
Table 4.8 Comparison between the diagnostic results from the Fault Diagnostic module and actual condition during inspection for Korea Electric Power Corporation (KEPCO) historical data. (All gases are measured in PPM).....	97
Table 4.9 Comparison of diagnostic results: proposed module vs. the traditional methods for the IEC TC 10 database. (All gases are measured in PPM).....	97
Table 4.10 Comparison of diagnostic results: proposed module vs. the traditional methods for Korea Electric Power Corporation (KEPCO) historical data. (All gases are measured in PPM).....	101
Table 4.11 Training datasets for Life Management module.....	102
Table 4.12 Optimal parameters of the developed Life Management module.....	103
Table 4.13 Comparison between the predicted result from the Life Management module and actual condition from dataset.	105
Table 4.14 CO ₂ and CO concentration ranges and the corresponding levels of deterioration [207].	105

Table 4.15 Comparison between the predicted result from the Life Management module and estimated condition according to Table 4.14106

List of Abbreviations

2-FAL	2-furaldehyde
AE	Acoustic emission
AI	Artificial intelligence
ANFIS	Adaptive neuro fuzzy inference system
ANN	Artificial neural network
BDV	Dielectric breakdown voltage
C ₂ H ₂	Acetylene
C ₂ H ₄	Ethylene
C ₂ H ₆	Ethane
CC	Correlation coefficient
CH ₄	Methane
CNN	Convolutional neural network
CO	Carbon monoxide
CO ₂	Carbon dioxide
DAQ	Data acquisition
DF	Dissipation factor
DGA	Dissolved gas analysis
DP	Degree of polymerization
DPM	Duval pentagon method
DRM	Doernenburg ratio method
DTM	Duval triangle method
EM	Electromagnetic
EMI	Electromagnetic interference
EoL	End of life
FAT	Factory acceptance testing
FBG	Fibre Bragg grating
FDS	Frequency domain spectroscopy
FEM	Finite element modelling
FID	Flame Ionization Detector
FP	Fabry-Perot
GC/MS	Gas chromatography-mass spectrometry
GIS	Gas-insulated switchgear
H ₂	Hydrogen
HFCT	High-frequency current transformer
HI	Health index
HPLC	High performance liquid chromatography
HST	Hot-spot temperature
IFT	Interfacial tension
IR	Insulation resistance
KEPCO	Korea electric power corporation
KGM	Key gas method

KNN	K-nearest neighbour
MF	Membership function
ML	Machine learning
N ₂	Nitrogen
NN	Neutralization number
O ₂	Oxygen
OLTC	On-load tap changer
OQF	Oil quality factor
PAS	Photo-acoustic spectroscopy
PD	Partial discharge
PDC	Polarization/depolarization currents
PF	Power factor
PI	Polarization index
PIF	Paper insulation factor
ppm	Parts per million
PRPD	Phase-resolved partial discharge
ReLU	Rectified linear unit
RRM	Roger's ratio method
RUL	Remaining useful life
RVM	Recovery/return voltage measurements
SD	Standard deviation
SFRA	Sweep frequency response analysis
SMOTE	Synthetic minority over-sampling technique
SNR	Signal- to -noise ratio
SOFC	Solid oxide fuel cell
SVM	Support vector machine
TCD	Thermal conductivity detector
TDOA	Time differences of arrival
TECs	Thermal equivalent circuits
TEV	Transient earth voltage
TOT	Top-oil temperature
TTR	Transformer turns ratio
UHF	Ultrahigh frequency
UV-Vis	Ultraviolet-to-visible

Chapter 1 Introduction

1.1. Background and Challenges

Oil-immersed power transformers find extensive application in power systems, primarily owing to their capability to manage elevated voltage levels. Power transformers represent key links in electricity grids that have a direct influence on the reliability of the entire network [1]. As they are performing under continuous thermal, electrical, and mechanical stresses, power transformers, in particular aged transformers, are prone to various types of faults that deteriorate its performance and reduce its operational life [2]. Therefore, it is necessary to assess the health condition of power transformers, provide strategic management plans for each transformer and determine the most economical management approach. Without effective asset management in place, it is difficult to make decisions about maintenance and replacement priorities [3]. Transformer asset management is used to help industry to achieve an optimal balance between technical performance, operating expenses, and capital investment [4]. Improper decisions could result in high maintenance costs and long periods of unavailability of the transformer.

The traditional operational and maintenance strategies are time-based, wherein transformers undergo periodic check-ups regardless of their current condition. Over the years, various condition monitoring methods have been evolved to detect diverse faults in power transformers [5]. The development of online condition monitoring sensors offers the opportunity to implement condition-based maintenance. Real-time condition monitoring increases the likelihood of detecting incipient faults, reducing the probability of failures, improving safety operation, controlling unscheduled maintenance, and assisting in prioritizing the maintenance and replacement schedule based on individual transformers' conditions.

Several online condition monitoring methods have been applied to oil-immersed power transformers, further enhancing the capability to assess their health. For instance, partial discharge sensors are employed to detect partial discharge faults, providing crucial insights into potential issues. Thermal sensors contribute by identifying thermal faults, ensuring timely intervention to prevent further escalation. Additionally, vibration sensors are designed to detect abnormal conditions, enabling a proactive response to deviations from normal operation.

In industry applications, Dissolved Gas Analysis (DGA) stands out as a predominant method for scrutinizing power transformer oil and identifying potential incipient faults [6]. The widespread adoption of the DGA method in industry is attributed to its capability to offer a comprehensive diagnosis. This method proves particularly effective as it can identify six primary faults, encompassing critical issues such as partial discharge and thermal faults, which has become an essential asset management tool. The traditional offline DGA method involves periodic sampling and laboratory analysis, often resulting in delayed detection and response to emerging faults. To address these limitations, the advanced online DGA units have been emerged to offer real-time monitoring and continuous data acquisition. This results

in a substantial amount of data to be interpreted. Various conventional DGA interpretation methods, derived from ANSI/IEEE standard and IEC publication 599, have been extensively utilised in the power industry [7, 8]. These methods, including Key gas method, Rogers Ratios, Doernenburg Ratios, Duval Triangles and Pentagons, have proven valuable but exhibit certain limitations such as out-of-code ratios, distinct boundaries, and the exclusion of gas evolution. These limitations may lead to incorrect and inconsistent fault diagnoses [9]. As a result, the accuracy of diagnostic results relies more on expertise and experience of analysts.

Exploring alternative approaches, recent research has delved into the application of artificial intelligence (AI) methods, particularly machine learning, to enhance DGA interpretation. Previous studies scrutinizing conventional AI methods have identified several drawbacks. Notably, to enhance the accuracy of conventional machine learning methods often involves the utilization of carefully engineering crafted parameters, as illustrated in Table 1.1. However, the increased number of parameters could slow down the training process.

Table 1.1 Engineering crafted parameters used in machine learning training for DGA analysis.

Engineering Crafted Parameters	
%CH ₄	C ₂ H ₄ /C ₂ H ₆
%C ₂ H ₄	C ₂ H ₂ /C ₂ H ₄
%C ₂ H ₂	C ₂ H ₂ /CH ₄
CH ₄ /H ₂	C ₂ H ₆ /C ₂ H ₂
CO ₂ /CO	C ₂ H ₂ /H ₂

Furthermore, the diagnosis of co-existing conditions requires multiple training models. An example is given in Figure 1.1 using Adaptive Neuro Fuzzy Inference System (ANFIS) machine learning method. As shown in the Figure, a minimum of three training models is required, namely, partial discharge criticality, discharge (arcing) criticality and thermal criticality. Once again, this multi-model approach has potential to slow down the training process.

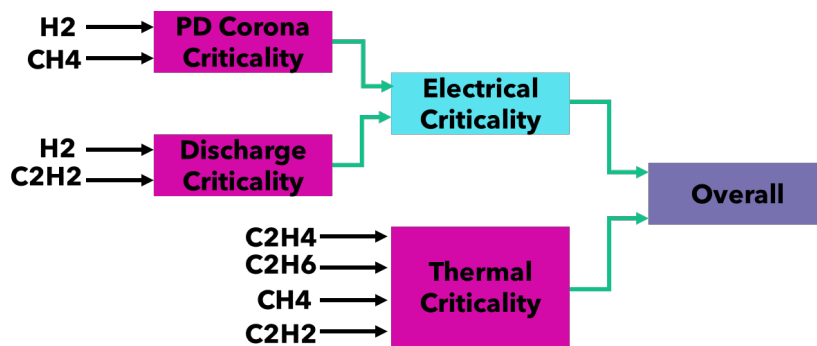


Figure 1.1 ANFIS diagnostic structure for DGA analysis.

1.2. Objectives and Contribution of the Thesis

The primary objective of this thesis is to formulate a novel asset management strategy grounded in data acquired from the online DGA unit for power transformers. The specific objectives and contributions of this work encompass:

- Crafting an asset management strategy that leverages data exclusively from online DGA devices, which have gained popularity in the power industry. This approach ensures comprehensive fault diagnosis and assessment of deterioration conditions within power transformers, utilizing real-time data from these advanced DGA devices.
- Identifying the essential input data required for effective asset management, the newly developed asset management model specifically incorporates seven-gas measurements obtained from online DGA devices.
- Developing machine learning algorithms capable of recognizing data patterns within existing diagnosed datasets. Within the newly developed asset management framework, a Convolutional Neural Network (CNN) classification algorithm is employed to train the Fault Diagnostic module, while a CNN regression algorithm is utilized to train the Life Management module. This advanced approach enhances the system's ability to effectively identify and classify fault conditions, as well as predict the remaining lifespan of power transformers.
- Curating diverse datasets containing DGA measurements and target output from a variety of sources to enhance the performance and adaptability of the asset management approach.

1.3. Thesis Outline

This thesis is composed of five chapters, and the content of Chapters 2 through 5 is outlined below.

Chapter 2 provides an extensive literature review encompassing a wide range of condition monitoring techniques applied to oil-immersed power transformers. This review covers both online and offline methodologies, offering a comprehensive examination of each approach. Additionally, the principles and drawbacks of each method are thoroughly explained to provide a detailed understanding of their applications and limitations.

Chapter 3 delivers a comprehensive literature review addressing the domain of oil-immersed power transformer asset management. The primary focus is on three crucial modules essential to effective transformer asset management: the Fault Diagnostic module, the Reliability Assessment module based on Health Index, and the Life Management module. It is important to note that all three modules acquire data from condition monitoring. Within the review, each module is examined in detail, encompassing both traditional conventional methods and emerging artificial intelligence-based approaches.

Chapter 4 describes the development of the proposed oil-immersed power transformer asset management model based on only online DGA measurements. This model adopts a deep machine learning-based approach called convolutional neural network. The chapter elucidates the architecture and functionality of two pivotal modules integrated into the proposed model: the Fault Diagnostic module and

the Life Management module. It is noteworthy that contemporary online DGA units can measure up to nine different gases. Within the proposed Fault Diagnostic module, five gases are utilised to assess and indicate the transformer's condition, identifying potential discharge, thermal, partial discharge issues, or affirming a fault-free state. Simultaneously, the Life Management module relies on measurements from two gases to evaluate the level of insulation paper deterioration, providing an estimate of the remaining life of the transformer. In addition to detailing the modules' architecture, the chapter extensively discusses the validation results of each module over actual transformer condition.

Finally, in Chapter 5, the overall research conclusion and recommendations for future work are presented. In conclusion, this chapter encapsulates the key findings derived from the entire research endeavour. Additionally, the chapter outlines valuable recommendations for future research directions and potential areas of further exploration in the field of oil-immersed power transformer asset management.

Chapter 2 Oil-immersed Power Transformer Condition Monitoring Methodologies

2.1. Introduction

Oil-immersed power transformers play a pivotal role in power systems. These transformers endure continuous thermal, electrical, and mechanical stresses, making them prone to a range of potential faults. Faults such as windings and core mechanical deformation, partial discharge, overheating and arcing result in deterioration to the transformer mechanical integrity and degradation to the dielectric insulation system [10]. While the transformer may operate normally with incipient faults, some faults such as winding axial displacement can progress rapidly and lead to catastrophic consequences if not detected and rectified at early stage [11]. Short-circuit faults and overloading can further increase the probability of unexpected failures of power transformers.

In 2017, the University of Queensland conducted a comprehensive survey on power transformer failures within Australia, focusing on a significant portion of the national transformer fleet. The study encompassed 6057 power transformers, representing approximately 98% of Australia’s transformer inventory [12]. The collected data, covering the period from 2000 to 2015, revealed 199 reported transformer failures, accounting for 3.29% of the analysed transformers. The statistics reveal a high number of non-catastrophic failures occurs in the 30 to 49 years age group while a higher catastrophic failure rate occurs in age groups 0 to 9 years and above 49 years. The causes of the failures have been categorized into five major groups: bushings, on-load tap changer (OLTC), windings, insulation systems, and others with failure distribution profile as shown in Figure 2.1 [12]. This survey emphasized the critical need for the adoption of reliable condition monitoring techniques across various power transformer components. The essential parameters for monitoring each key components are illustrated in Figure 2.2 [13, 14].

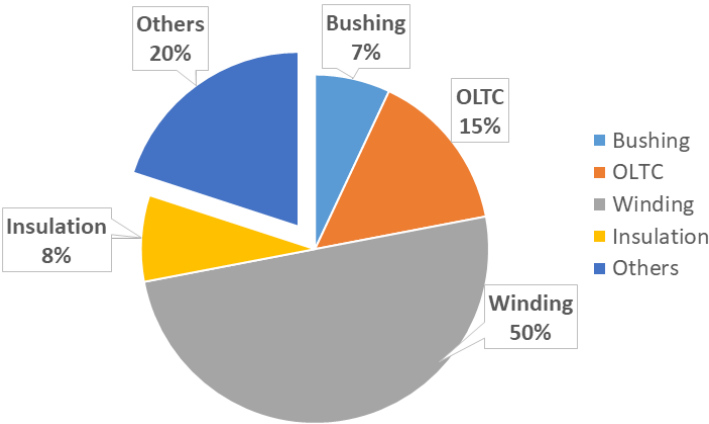


Figure 2.1 Distribution of failures for Australian power transformers during the period 2000 to 2015.

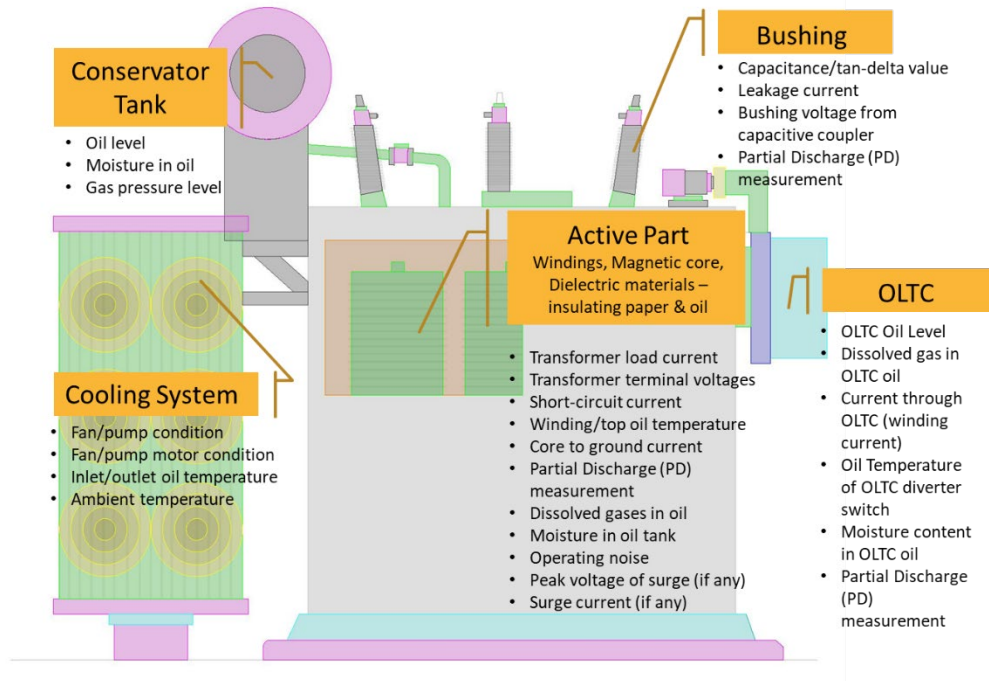


Figure 2.2 The parameters to be monitored for oil-immersed power transformer components.

Over the years, wide variety of sensor technologies applicable to both online or offline fault diagnostic methods have been developed for power transformer condition monitoring systems [15]. In this chapter, we explore nine typical offline diagnostic methods for power transformers.

In contrast to offline testing methods, online condition monitoring offers numerous advantages, including the provision of timely information regarding the health of the transformer, early detection of incipient faults to facilitate informed and timely decision-making by asset managers, a reduction in the likelihood of unplanned downtime resulting from catastrophic failures, mitigating of production cost losses due to transformer outages, and a decrease in the risk to personnel, as it requires less frequent access to high voltage substations. Hence, there is an imperative to continually enhance online condition monitoring methods for oil-immersed power transformers. Four commonly known online methods are presented in this chapter. An overview of both offline and online condition monitoring techniques for oil-immersed power transformers currently employed in the industry is depicted in Figure 2.3. The overarching goal of this comprehensive review is to introduce and explore various online and offline condition monitoring methods for power transformers.

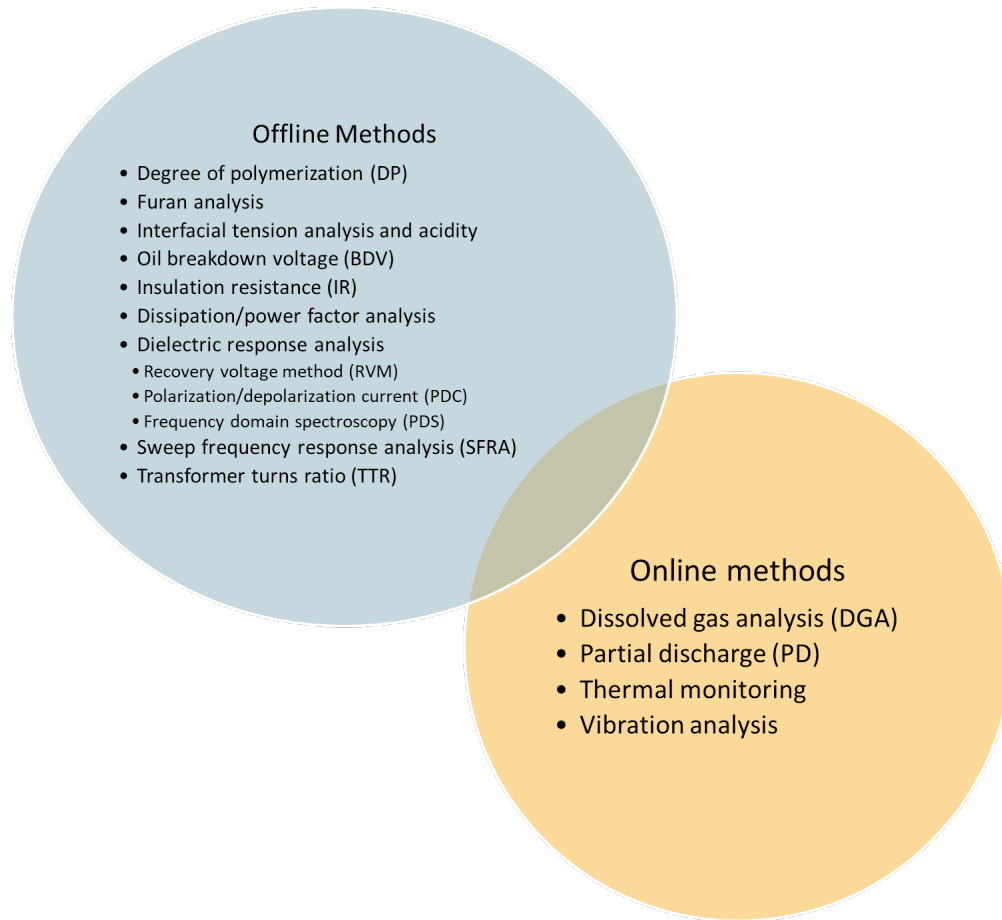


Figure 2.3 Offline and online condition monitoring methods for oil-immersed power transformer.

2.2. Offline Condition Monitoring Methods

2.2.1 Degree of Polymerization of Insulation Paper

The transformer's insulation paper and pressboard are constructed from cellulose polymer. As transformer aging over the time, the structure of cellulose polymer as shown in Figure 2.4 becomes increasingly fragile. This fragility results in degradation of the paper insulation, losing its dielectric and mechanical strength. The length of the cellulose chain is measured by the number of monomer units in the polymer, also known as degree of polymerization (DP). The quality of cellulose is a function of the DP value that can be measured using average viscosity method [16, 17].

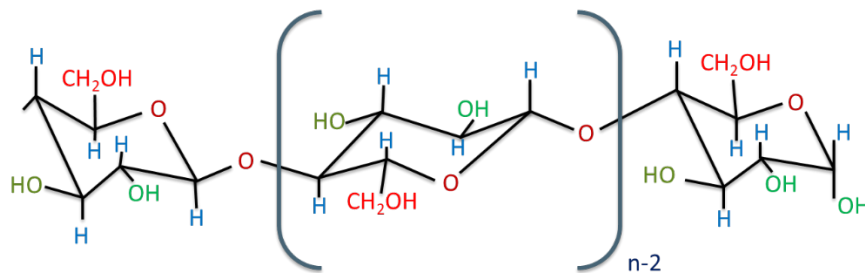


Figure 2.4 Chemical structure of cellulose.

In general, new transformers exhibit DP values in the range of 1000-1400 [18]. When the DP value drops to the range of 100-250, it is considered end of paper’s useful life, which is corresponding to end of transformer life [18]. Measuring DP involves collecting paper samples from various locations within the transformer windings, which is impractical for transformers in active service. Therefore, this method is only performed during planning for transformer replacement. Alternatively, indirect methods, such as Furan analysis, can be used to estimate the DP value of the insulation paper.

2.2.2 Furan Analysis

The utilization of furan analysis presents a viable diagnostic approach for evaluating the condition of paper insulation in oil-immersed power transformers. The degradation of cellulose, induced by factors such as elevated temperatures, oxygen exposure, moisture, and acidic content, results in the generation of five distinct furan compounds, as detailed in Table 2.1 [19, 20].

Table 2.1 Furan compounds and associated types of stresses.

Furan Compound	Symbol	Nature of Stress
2-furaldehyde	2-FAL	Overheating
5-methyl-2-furaldehyde	5-M ₂ F	Local severe overheating
5-hydroxymethyl-2-furaldehyde	5-H ₂ F	Oxidation
2-acetyl furan	2-ACF	Lightning
2-furfurol	2-FOL	High moisture

The concentration of these furan compounds, typically measured in parts per million (ppm), can be measured using high performance liquid chromatography (HPLC) or gas chromatography-mass spectrometry (GC/MS) in a laboratory environment [21]. In industry practice, 2-FAL stands out as the predominant compound due to its substantial generation rate and stability in oil [19]. Notably, there exists a strong correlation between 2-FAL measurements and the DP value, as detailed in Table 2.2, a relationship supported by existing literatures and IEEE guidelines [18, 22]. This correlation facilitates a non-intrusive diagnostic alternative to the DP test, traditionally conducted in a laboratory setting by trained personnel using expensive equipment. However, a standardized code linking furan analysis to DP for biodegradable oil and thermally upgraded paper has yet to be established.

A novel approach, introduced in [23], combines ultraviolet-to-visible (UV-Vis) spectroscopic technology with artificial intelligence to estimate the concentration of the 2-FAL compound in transformer oil samples. The UV-Vis spectroscopic diagnostic method relies on measuring the absorbance of light by contaminants present in the transformer oil [24]. Consequently, this technology can not only assess the quality of the transformer oil but also quantify the reduction in its operational lifespan [24, 25]. The proposed UV-Vis spectroscopic method features low cost, easy to perform by unexperienced personnel and can be conducted onsite or implemented online. However, this method has not yet undergone extensive testing on operational transformers.

Table 2.2 The correlation between 2-FAL and DP for paper insulation with condition level

2-FAL (ppm)	DP Value	Degree of Degradation
0-0.1	1200-700	Healthy
0.1–1.0	700-450	Moderate
1-10	450-250	Extensive
>10	< 250	End of Life

2.2.3 Interfacial Tension Analysis and Acidity

Interfacial tension (IFT) analysis and acidity number measurement are used to assess oil quality. The presence of contaminants and degradation by-products can significantly impact the physical and electrical properties of insulation oil, leading to a reduction in IFT. Additionally, the process of oil oxidation gives rise to the formation of acidic by-products [26]. To determine IFT, a planar ring with circumference d is inserted into a container filled with insulating oil and water mixture, then measures the interfacial force (F , dyne/cm) required to lift the ring 10mm upward through the oil-water interface [26]. IFT analysis is detailed in standard ASTM D971. In general, transformers $\leq 69\text{kV}$ with $\text{IFT} \leq 22$ dynes/cm; and transformers $> 69\text{kV}$ with $\text{IFT} \leq 25$ dynes/cm are considered to approach the end of insulating oil service life. The conventional IFT test requires a trained person and expensive equipment to conduct the measurements. Therefore, the test is normally performed in a laboratory environment. There has been research on using UV-Vis spectrum method to determine the IFT value of transformer oil sample [27]. This spectroscopic measurement is based on measuring energy level in atoms and molecules. The measurements can then be analysed using artificial intelligence software tool to estimate the IFT value. This method has an online application feasibility but has not been tested on practical field yet.

The Acidity number, also known as neutralization number (NN), provides insights into the acid content within insulating oil. It quantifies the mass of potassium hydroxide (KOH) in milligrams (mg) required to neutralize the acid in one gram (gm) of the oil. The NN tends to increase as the transformer ages, and its limitations are outlined in the ASTM D974 standard. In general, transformers $\leq 69\text{kV}$ with $\text{NN} \geq 0.20$ mg KOH/gm; transformers of rated voltage between 69kV, 230kV with $\text{NN} \geq 0.15$ mg KOH/gm; and transformers $\geq 230\text{kV}$ with $\text{NN} \geq 0.10$ mg KOH/gm are considered in critical condition in terms of oil quality.

2.2.4 Oil Dielectric Breakdown Voltage

The oil dielectric breakdown voltage (BDV) test is a common method used to determine the breakdown voltage of insulating oil. As transformers age, the insulating oil degrades, and decomposes resulting in moisture, sludge, gases, and impurities that decrease the dielectric strength of the insulating oil [28].

The BDV test can be conducted on-site using a mobile test device. According to the standard IEC 60156, the test is conducted by applying a steady incremental voltage 2kV/s until breakdown occurs at the electrode, which is immersed in the insulating oil sample. The test is repeated at least six times and the average value of the measurements is considered as the oil BDV [29]. The correlation of the transformer

oil dielectric strength and the oil BDV is detailed in the standard IEEE C57.106 [30]. Generally, oil of a BDV lower than 30kV calls for further investigation and correction action [31].

It's worth noting that there are ongoing developments in the creation of online BDV test unit. The concept involves installing a detection unit in proximity to a transformer and connecting it to the primary oil tank, permitting a continuous closed-loop circulation of oil through the measuring unit.

2.2.5 Insulation Resistance Test

The insulation resistance (IR) test is designed to evaluate the insulation resistance of power transformers. IR value reveals the insulation degradation due to contamination, moisture, and severe cracking. The test is performed by applying a constant DC voltage for 10 minutes between windings or windings and ground [32, 33]. IR values are measured every minute or less in MΩ using a metering instrument called Megger or Megohmmeter. Typical trend of IR measurements is shown in Figure 2.5 [33]. A single IR result is not enough to determine the insulation status [34]. An insulator is considered as a capacitor that with the application of voltage, a charging current will flow. If the insulation is contaminated, the charging time is typically 1 minute [33]. After 10 minutes of testing, the IR value can reach a stable level. Historical trending results for IR is useful to monitor insulation condition over years [34]. If the IR value drops from the previous test, further investigation and analysis will be required.

The polarization index (PI) represents another parameter used for evaluating the insulation condition. PI is typically calculated using IR measurements taken at 1 minute (IR_{1min}) and 10 minutes (IR_{10min}) as given by (2.1) [33, 35]. A sharp decline in PI is an indication to severe insulation degradation [34].

$$PI = \frac{IR_{10min} (M\Omega)}{IR_{1min} (M\Omega)} \quad (2.1)$$

The limitation of IR test is its inability to identify the IR value of each individual insulation system such as bushings, paper, and oil.

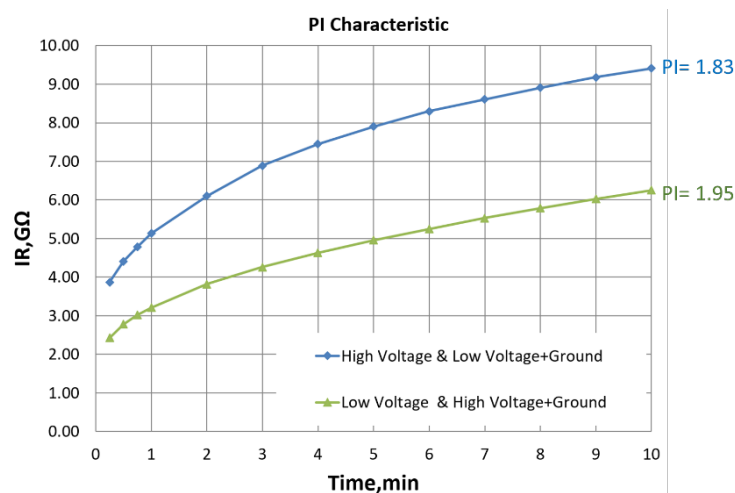


Figure 2.5 Typical IR measurements versus time of the applied voltage.

2.2.6 Dissipation Factor Measurement

Dissipation factor (DF) analysis is used to assess bushings and insulation condition. This offline test is performed periodically on bushings and windings [36]. In an ideal scenario, insulation, essentially a dielectric material, can be considered as a pure capacitor. Over time, the permittivity of the material changes due to aging, and it causes capacitive current variations. Additionally, the degradation of the material leads to an increase in resistive leakage currents.

The dissipation factor, also known as power factor or tan delta, presents the ratio between the capacitance current and resistive current components flowing through the insulation. Figure 2.6 (a) illustrates a simplified equivalent model of a dielectric structure. On an isolated transformer, AC voltage of up to 10kV is applied through the bushings [37]. In an ideal scenario, the insulation exhibits capacitive current leading the applied voltage by 90 degrees, as depicted in Figure 2.6 (b) [38]. Consequently, the total current I equals the capacitive current I_C , and the DF ($\tan \delta$) is zero.

However, the presence of some leakage current (resistive current I_R) through the insulation's surface increases due to the contamination or carbonization in the insulation, and it represents the resistive loss, also called watt-loss. The term tan delta ($\tan \delta$) presents the ratio between the resistive I_R and capacitive I_C current components, and power factor ($\cos \theta$) represents the fraction of I_R with respect to the total current I .

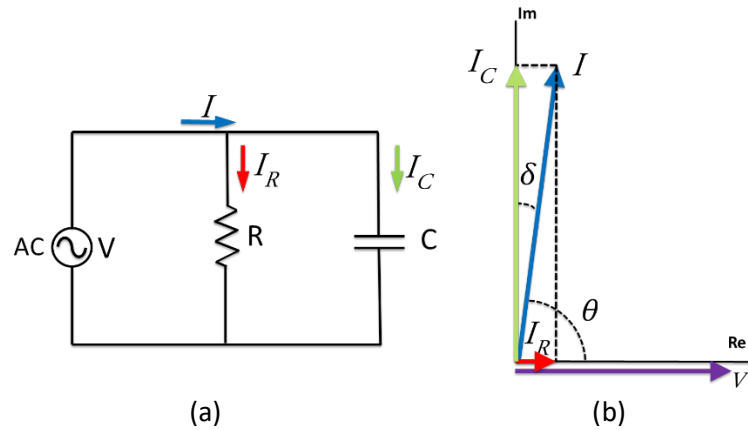


Figure 2.6 (a) Equivalent circuit represents a dielectric and (b) phasor diagram.

The DF and power factor (PF) calculations are given by (2.2) and (2.3) respectively [37, 38]. Any changes in these values indicate power dissipated in the insulation. Lower DF and PF means lower dielectric losses [39]. For mineral-oil-immersed power transformers in normal condition, PF is lower than 0.5%. PF value between 0.5% and 1% could be acceptable whereas a PF value over 1% is an indication for insulation degradation [39].

$$\% \text{ Dissipation Factor (DF)} = \% \tan(\delta) = \frac{I_R}{I_C} \times 100\% \quad (2.2)$$

$$\% \text{ Power Factor (PF)} = \% \cos(\theta) = \frac{I_R}{I} \times 100\% \quad (2.3)$$

The value of DF represents the average index of the dielectric integrity considering both capacitive and resistive currents in the apparatus. For detailed analysis of insulation quality, the trend of I_C and I_R variation is investigated. The main drawback of DF analysis is that it provides an average condition of insulation integrity, and the results are sensitive to the ambient temperature [39]. This test is generally performed on-site during commissioning, regular maintenance, or malfunction investigation. The results of DF measurement are compared to previous DF rates for analysing the trend of insulation degradation.

Online PF measurement is available for assessing the insulation condition of bushings. Figure 2.7 shows the equivalent circuit for bushings PF setup [37]. The bushing has dielectric resistance R_X shunted by a capacitance C_X , with bushing tap U_2 connected to the ground through an impedance Z_M . The voltage U_2 is compared to a reference voltage U_1 . Bushing condition changes result in changes in the amplitude and phase of U_2 with respect to the reference voltage.

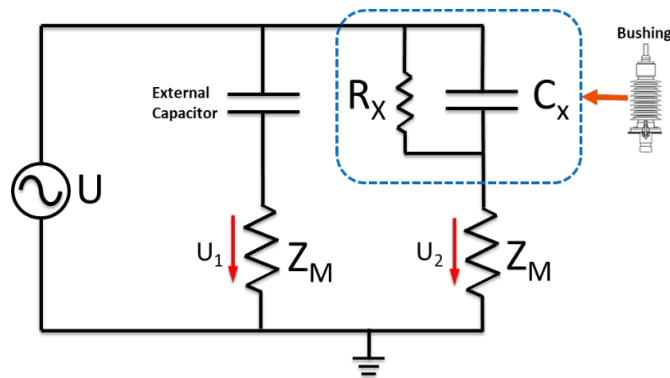


Figure 2.7 Equivalent circuit for bushing PF monitoring.

2.2.7 Dielectric Response Methods

Impurities such as moisture and aging by-products in oil-paper insulation system increase the dielectric losses [40]. Moisture content and contaminations such as sludge result in polarization within the dielectric molecules [41]. Moisture, temperature, aging, and other factors lead to different characteristics of polarization. These phenomena can be identified by the dielectric response methods listed below [42]:

- Recovery/return voltage measurements (RVM)
- Dielectric spectroscopy in time domain – polarization/depolarization currents (PDC)
- Dielectric spectroscopy in frequency domain/Frequency domain spectroscopy (FDS)

These three techniques are elaborated below.

2.2.7.1 Recovery/Return Voltage Measurement

Recovery voltage measurement (RVM) is utilized to analyse the slow polarization process of the oil and paper insulation [42, 43]. The basic measuring circuit for RVM is shown in Figure 2.8 (a). By applying a step DC voltage U_0 and closing switch S_1 , the insulation is charged for a specific time period t_c . This results in a polarization current flow through the insulation after which the insulation is short-circuited by opening switch S_1 and closing switch S_2 for a certain time t_d , allowing depolarization current to flow. Switch S_2 is

opened after the short-circuit period while switch S3 is closed to measure the recovery voltage. The charging/discharging time and recovery voltage are shown in Figure 2.8 (b). The initial slope dU_r/dt of the recovery voltage reveals the polarization characteristics [43, 44].

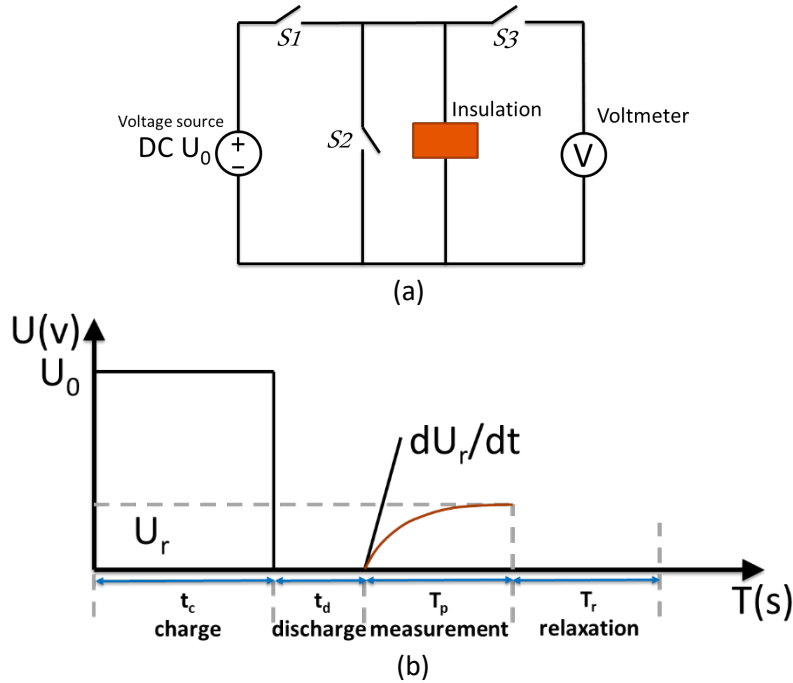


Figure 2.8 (a) Basic RVM measuring circuit and (b) measurements.

Interpretation of RVM results hinges on both the magnitude and the position of the maximum recovery voltage [45]. In the polarization spectrum profile presented in Figure 2.9, parameters such as the maximum recovery voltage U_{rmax} along with the central time constant are utilized for assessing the insulation condition [46-48]. The central time constant is the charging time to the peak value of the recovery voltage.

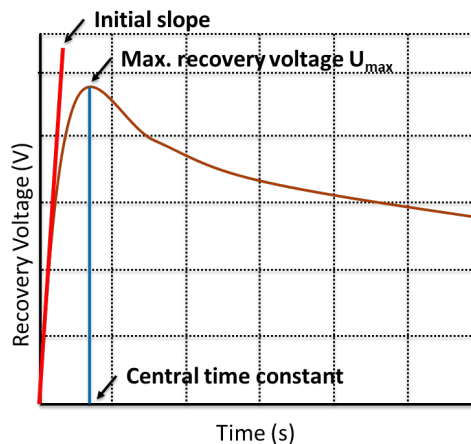


Figure 2.9 Example of RVM polarization spectrum.

In general, an insulation system with a higher moisture content has a relatively shorter charging and discharging time. On the other hand, an insulation system with lower moisture content has a relatively slow polarization response [46]. RVM from factory acceptance testing (FAT) can be used as a reference to monitor the trend of insulation state with future test results.

2.2.7.2 Polarization/Depolarization Currents

The polarization/depolarization currents (PDC) method is a time domain analysis used to evaluate the transformer's insulation condition. PDC measures the polarization and depolarization currents [49]. The basic test circuit is similar to RVM, with the key difference being that PDC measures currents, as illustrated in Figure 2.10 (a). The polarization current i_p is measured when switch S_1 is closed and switch S_2 is open. The depolarization current i_d is measured when S_1 is open and S_2 is closed. Figure 2.10 (b) shows that the test is performed by applying a step DC voltage U_0 , to charge the insulation for a specific period t_p , then short-circuit the insulation for a certain period t_d . Water content and contamination increase the insulation conductivity. Elevated conductivity levels lead to higher polarization and depolarization currents [45, 50]. Figure 2.11 illustrates the variation in the polarization and depolarization currents (i_p and i_d) corresponding to insulation conductivity. Insulation with higher conductivity results in higher PDC values [49]. The advantage of PDC method over RVM and frequency domain spectroscopy is its ability to assess paper and oil's status separately.

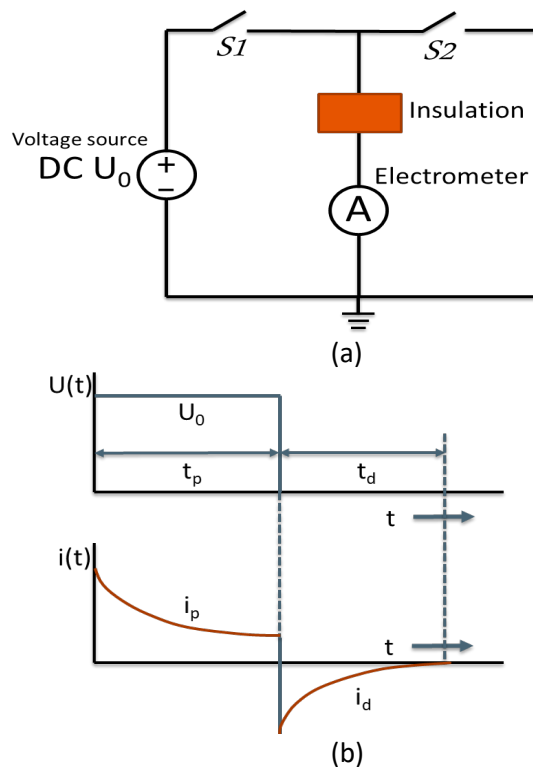


Figure 2.10 (a) Basic PDC measuring circuit and (b) waveform of polarization and depolarization currents.

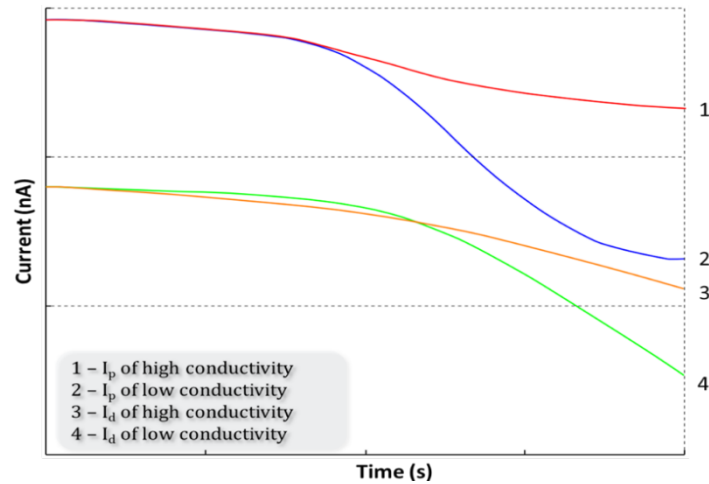


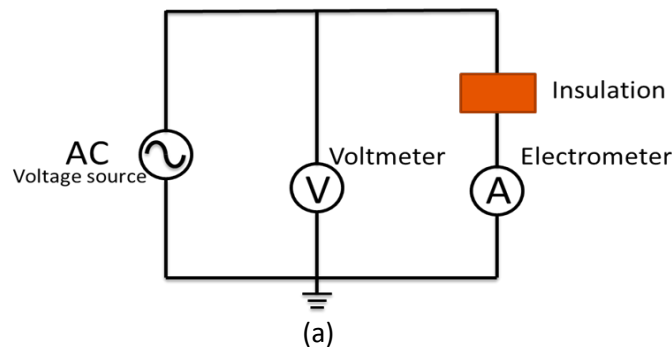
Figure 2.11 Example of relationship between polarization/depolarization currents and insulation conductivity.

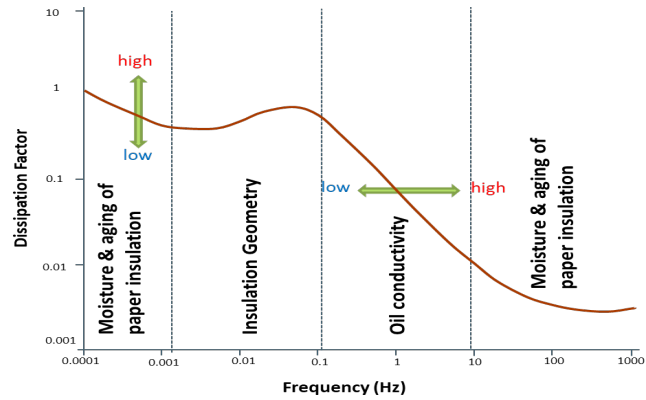
2.2.7.3 Frequency Domain Spectroscopy

In the frequency domain spectroscopy (FDS) method, an AC voltage is applied to the test object with a frequency starts from 1kHz to 1mHz as illustrated in the basic circuit of Figure 2.12 (a). The voltage and current measurements are taken at each of these testing frequency points. Dielectric parameters such as relative complex permittivity, complex capacitance and dissipation factor ($\tan \delta$) can be obtained from this test [51]. These parameters reflect the polarization characteristics of oil-paper insulation system.

In Figure 2.12 (b), a typical dielectric response of oil-paper insulation system is presented as a dielectric dissipation factor ($\tan \delta$) curve. The variation of dissipation factor with frequency indicates the aging and moisture content in both paper and oil insulation. According to the curve, the response for oil insulation dominates the frequency range 0.1Hz to 10Hz, and dissipation factor increases towards the lower frequencies [52].

FDS was found to be of good consistency with other chemical and electrical analysis methods, and hence, it has been a preferred method among the three dielectric response analysis techniques [51]. In addition, FDS detection method exhibits less sensitivity to external noise than PDC [47].



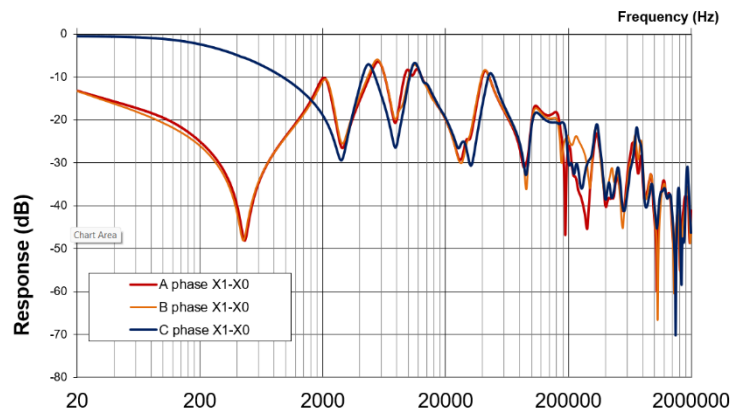


(b)

Figure 2.12 (a) Basic FDS measuring circuit and (b) typical FDS response.

2.2.8 Sweep Frequency Response Analysis

Sweep frequency response analysis (SFRA) is primarily employed to assess the mechanical integrity of power transformers. Ideally, this test should be performed after the installation of the transformer to establish a baseline healthy frequency response signature. This baseline signature can then be compared with future signatures to identify any anomalies or mechanical changes [53]. The measurement is conducted using frequency response analyser, which introduces a low AC voltage (10V) across a wide frequency range (up to 2MHz) into the terminal of each phase while measuring the response at the other terminal. The frequency response signature could be on the form of winding impedance, admittance, or transfer function (in dB) as shown in Figure 2.13 that also shows the phase angle of the three phases of the low voltage windings. The measured response is compared with the reference signature to detect any variations. In cases where a reference signature is unavailable, alternative methods, such as comparing the signature with that of a similar sister transformer or performing a phase-to-phase comparison, can be employed.



(a)

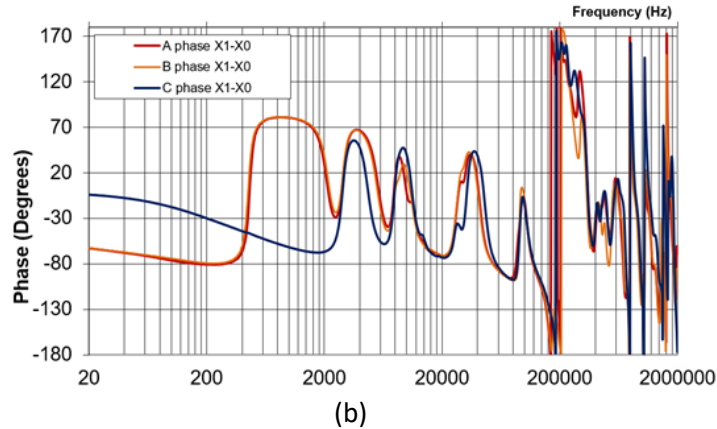


Figure 2.13 FRA measurement example, (a) Transfer function amplitude. (b) Transfer function phase angle.

While the SFRA measurement is well developed and standardized, analysis of the obtained results is still a challenging task. Some attempts have been published in the literatures in order to identify and quantify mechanical faults based on SFRA signature. Most of these techniques are developed based on artificial intelligence [54], statistical coefficients [55] and the estimation of transformer equivalent circuit parameters [56]. While the current industry practice only look at the SFRA magnitude signature, some studies proposed the integration of SFRA magnitude and phase angle plots into one 2D or 3D plots to facilitate the application of digital signal processing techniques and improve the accuracy of the interpretation process [57].

The main drawback of the SFRA measurement technique is its offline nature that calls for taking operating transformers out-of-service. Some attempts were published in the literature for the possibilities of using the natural switching operation, lightning and impulse signal for online SFRA measurements [58, 59]. However, none of these techniques has been implemented in real field applications yet. The main issue of implementing online SFRA measurements is the requirement to impose a signal of a wide frequency range to the electricity grid in which the power frequency should be maintained at 50 or 60 Hz. Some studies proposed the use of transformer I-V Lissajous pattern at the power frequency [60] as an alternative online technique to the offline SFRA method. However, this method has not been tested on real field application yet.

2.2.9 Transformer Turns Ratio Test

The transformer turns ratio (TTR) test can be used to determine insulation failure between turns, core structure insulation failure or inter-winding insulation failure. TTR test is normally performed during commissioning and planned maintenance periods [61].

For comprehensive TTR testing, it is essential to check each tap position and calculate ratios for all three phases. To calculate the voltage ratio V_{ratio} , a reduced voltage V_p is applied to the primary side, resulting in a voltage V_s on the secondary side. The primary and secondary terminal voltages are

proportional to the number of turns on their respective sides, namely, the primary side N_p and the secondary side N_s . Therefore, the ideal turns ratio can be expressed in (2.4)[62].

$$V_{ratio} = \frac{V_p}{V_s} = \frac{N_p}{N_s} \quad (2.4)$$

The measurements are compared to the ratios on the nameplate for all windings and tap positions. A key criterion is ensuring that the difference, denoted as Δ_{ratio} and defined by (2.5), falls within specified limits. Generally, the acceptable tolerance for this difference is set at 0.5%, although for new transformers, a stricter tolerance of 0.1% is often required [39].

$$\% \Delta_{ratio} = \left| \frac{V_{ratio\ measured} - V_{ratio\ nameplate}}{V_{ratio\ measured}} \right| \times 100\% \quad (2.5)$$

The TTR test is a widely employed offline method due to the availability of test devices [63]. It holds particular significance for transformers operating in parallel. When two parallel transformers have unequal turns ratios, disparities in voltage between their outputs can lead to the generation of circulating currents through busbars. Even minor errors in turns ratio can trigger substantial equalization currents, leading to excessive heat generation and increased power losses [63]

2.3. Online Condition Monitoring Methods

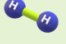

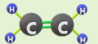
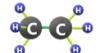
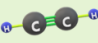
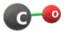

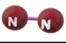

2.3.1 Dissolved gas analysis

Dissolved gas analysis (DGA) stands as one of the widely adopted methods for the detection of internal faults in transformers [64]. This method has been developed based on the fact that under harsh operating conditions, the insulating oil and paper within a transformer decompose and release certain gases that dissolve in the oil, thereby diminishing its dielectric strength [65]. The fault gases include hydrogen (H_2); methane (CH_4); ethane (C_2H_6); ethylene (C_2H_4); acetylene (C_2H_2); carbon monoxide (CO) and carbon dioxide (CO_2). Oxygen (O_2) and nitrogen (N_2), which are not produced by faults, are also included in the measurements. The amount and type of these gases are instrumental in identifying and quantifying various types of faults. Table 2.3 summarizes the fault types and the key gasses corresponding to each fault.

The conventional offline DGA measurements are carried out in a laboratory environment using Gas Chromatography (GC) [66]. While this method is highly precise, it necessitates adherence to several standards, encompassing procedures for collecting oil samples from operational transformers, their transportation, and storage [58]. Moreover, this technique incurs running costs, takes a relatively long time, and has to be conducted by an expert. Consequently, several online DGA sensors have emerged in recent years, including online GC, photo-acoustic spectroscopy (PAS) and online hydrogen detection [67].

For online DGA, the monitoring sensor is directly connected to the transformer and a pump is required to circulate the oil through the measuring unit. The process typically encompasses three steps: gas extraction, gas detection and data analysis.

Table 2.3 Fault types and key gases corresponding to each fault.

Gas - Formula	Molecular	Temperature at Which Gas Forms	Source of Gases
Hydrogen – H ₂		<150°C – corona effect in oil	Partial discharge thermal faults
		>250°C – thermal and electrical faults	Power discharges
Methane – CH ₄		<150°C-300°C	Corona, partial discharge, low to/and medium temperature faults
Ethylene – C ₂ H ₄		300°C - 700°C	High-temperature thermal faults
Ethane – C ₂ H ₆		200°C - 400°C	Low to/and medium temperature faults
Acetylene – C ₂ H ₂		>700°C	High hot spot. Low energy discharge
Carbon Monoxide – CO		105°C - 300°C	Thermal faults involving paper press board, wood and etc.
		>300°C complete decomposition	
Carbon Dioxide – CO ₂		100°C - 300°C	Normal ageing, thermal fault involving cellulose
Nitrogen – N ₂		Vacuum when temperature drops	Indicator of system leaks, over pressurization or changes in temperature
Oxygen – O ₂		Vacuum when temperature drops	Exposure to air, leaky gasket, air breathing through conservator

2.3.1.1 Gas Extraction

For online GC and PAS detection, a gas extraction device is required. The headspace technique is a matured membrane-based dissolved gas-in-oil analysis method. It applies negative pressure to the top space for the dissolved oil extraction [68]. This technology is highly efficient, low risk of gas pollution and easy to maintain. Figure 2.14 illustrates the working principle of Teflon coated membrane (Teflon AF2400) [69, 70]. The membrane serves as a physical barrier, permitting only gas to migrate between the gas phase and liquid phase. A quality membrane should offer excellent gas permeability, oleophobic characteristic, as well as chemical and thermal stability.

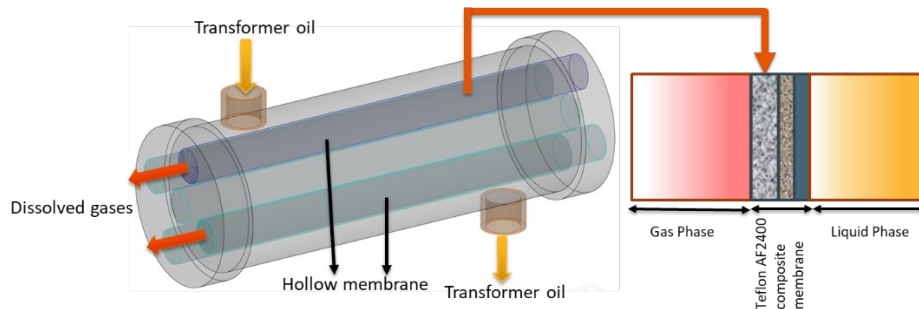


Figure 2.14 Headspace extraction structure diagram and membrane structure.

2.3.1.2 Gas Detection

Gas Chromatographic (GC)

The most common GC detectors are: Thermal Conductivity Detector (TCD) and Flame Ionization Detector (FID). These types of detectors are normally used as a combined method in laboratory environment due to their limitations. For example, TCD sensitivity to detect hydrocarbon gases is low. FID is insensitive to hydrogen and requires several types of carrier/auxiliary gases including hydrogen, which is not allowed to be used inside substations due to its potential flammable hazards. Solid Oxide Fuel Cell (SOFC) sensor is newly developed on-line GC detector [71]. It has high sensitivity and good repeatability to detect H_2 , CO , CH_4 , C_2H_4 , C_2H_6 and C_2H_2 . The sensitivity to detect C_2H_2 is 0.05ppm while it is 0.5ppm in case of FID and TCD sensors.

Figure 2.15 illustrates the basic structure of an online DGA system employing GC with SOFC detector. In this setup, the dissolved gas mixture is initially separated from oil within the gas extraction unit. Since different gases have different adsorption coefficients [72], the gas mixture of H_2 , CO , CH_4 , C_2H_4 , C_2H_6 and C_2H_2 is separated when passing through Chromatographic Column and subsequently detected by the SOFC sensor. The voltage output of the SOFC detector as depicted in Figure 2.16, is then transmitted to the data acquisition unit, where it is converted into digital signals representing the concentration of each gas.

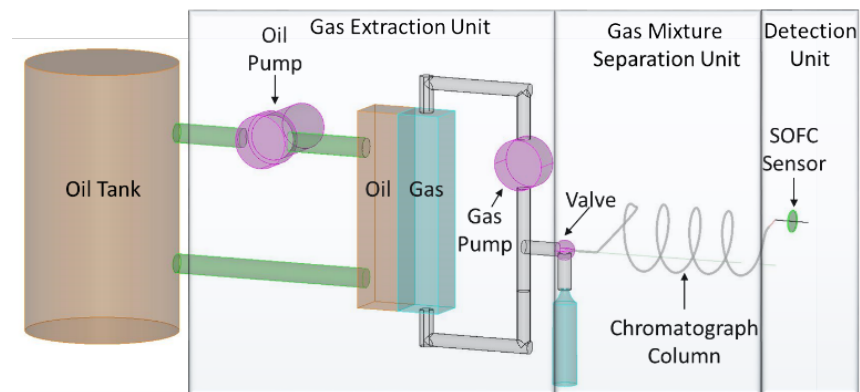


Figure 2.15 Online GC system using SOFC detector.

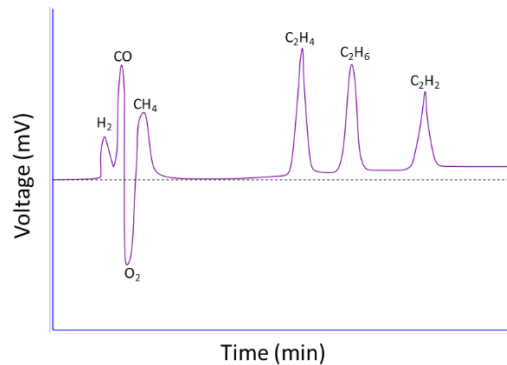


Figure 2.16 Example of voltage signal output of SOFC detector equivalent to gas concentrations.

Photo-acoustic Spectroscopy (PAS)

While GC technique is indeed a highly accurate method for detecting dissolved gases, it has certain drawbacks, including the consumption of carrier gases. Moreover, after extended use, it requires calibration, replacement of chromatographic columns and sensors due to changes in their properties [73]. Photo-acoustic Spectroscopy (PAS) sensor uses indirect absorption spectroscopy and overcomes GC's limitation.

Figure 2.17 illustrates the principle of PAS, which relies on the photo-acoustic effect. The dissolved gases inside an enclosure container absorb light energy and increase the gas molecules' kinetic energy, resulting in temperature increment on the macroscopic level. This heat leads to pressure fluctuations (sound waves) and can be detected by a sensitive microphone. The concentrations of the gases are measured based on the amplitude of the photoacoustic signal detected by the microphone [74-76].



Figure 2.17 The principle of photo-acoustic effect.

The schematic diagram of PAS unit is shown in Figure 2.18 [67]. In this system, light from the laser source passes through the light chopper and is then measured using a photo-acoustic cell. The light chopper wheel rotates and switches the light on and off. The frequency of the light chopper is measured with a photo detector and is used as reference frequency. The performance of the PAS detection unit mainly depends on the characteristics of the laser light source. When the light frequency coincides with the gas absorption band, gas molecules absorb a portion of the light. According to the Beer Lambert Law, the higher the gas concentration in the cell, the more light is absorbed. Figure 2.19 illustrates the electromagnetic spectrum of light. The spectrum includes γ -radiation, X-ray, ultraviolet (UV), visible light, infrared red light, microwaves, and radio waves. The absorption spectrum for gas molecules primarily falls into three regions: Near Infrared (NIR), Middle Infrared (MIR) and Far Infrared (FIR) [77]. The system employs various types of laser light sources to enhance the detection sensitivity. Additionally, it incorporates an optical microphone to mitigate electromagnetic interference from the challenging transformer environment and an optical power meter to monitor and prevent light source power drift during extended operational periods [78].

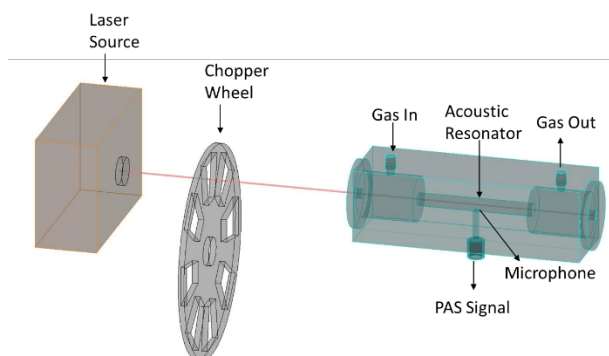


Figure 2.18 Schematic diagram of PAS detection unit.

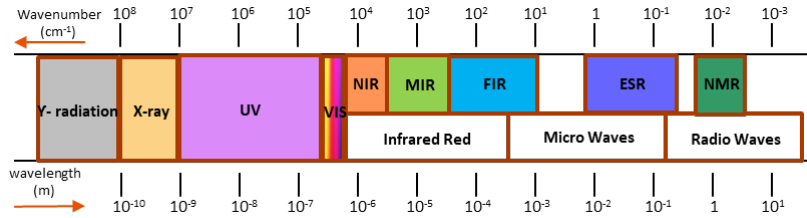


Figure 2.19 The electromagnetic spectrum for various wavelength regions of light.

Online Hydrogen (H₂) Detection

Table 2.4 shows that the presence of dissolved H₂ in transformer oil sample can be attributed to partial discharge, thermal faults and arcing events [79]. According to this table, an increase of H₂ concentration can serve as an indicator for most major faults. During normal transformer operation, the H₂ concentration should ideally remain below 100 ppm [80]. While GC and PAS techniques are capable of detecting hydrogen, these techniques require the gas extraction component. Online hydrogen sensors, on the other hand, come into direct contact with transformer oil without the need for gas and oil separation membranes. Therefore, they require fewer components in their manufacturing, making them a cost-effective option for lower budget condition monitoring.

Table 2.4 Primary faults associated with key gases.

Key Gas	Characteristic Fault
H ₂ , CH ₄ , C ₂ H ₄ , C ₂ H ₆	Thermal fault from 150 to 300°C
H ₂ , CH ₄ , C ₂ H ₄ , C ₂ H ₆	Thermal fault from 300 to 700°C
H ₂ , C ₂ H ₄ , C ₂ H ₂	Over 700°C thermal fault
CO, CO ₂	Decomposition of cellulose
H ₂ , CH ₄	Partial discharge
H ₂ , C ₂ H ₂	Arcing

The use of gas sensitive detection materials is a fundamental principle for H₂ detectors. Over the years, there has been substantial research in metal-hydrogen catalytic effects [81]. In 1868, Thomas Graham discovered the absorption of hydrogen by palladium (Pd) during electrolysis [82]. Studies show that Pd has high hydrogen solubility and is superior as a gate material for small amounts of hydrogen at room temperature [82]. When H₂ molecules become in contact with Pd surface, H₂ atoms diffuse into Pd lattice and forming palladium hydride (PdH_x) as shown in Figure 2.20 [83, 84]. As a results, H₂ absorption causes volume expansion in Pd structure and leads to a change in resistance (ΔR), then the signal conditioning circuit converts the resistance variation into hydrogen concentration [84, 85].

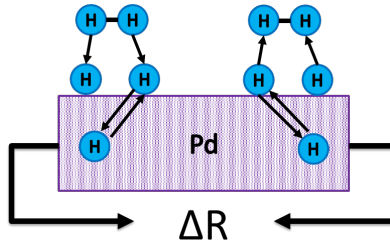


Figure 2.20 Diagram of H₂ atoms react with Pd surface.

In a palladium-hydrogen system, if incorporated H₂ atoms exceed the maximum H₂ solubility within Pd layer, this can cause a hysteretic behaviour in the resistance with irreversible structural changes in the Pd layer [85]. This affects the sensor performance and results in a loss of long-term stability. Hence, a variety of Pd alloys such as Pd-Mg, Pd-Au, Pd-Ag and Pd-Ni have been studied [80]. Pd combined with Ni has already been implemented in industrial hydrogen sensors e.g., Siemens Energy's SITRAM Guard hydrogen sensor.

2.3.1.3 DGA Data Interpretation

Various DGA diagnostic techniques currently used by utilities worldwide include a) Key Gas Method (KGM); b) Rogers Ratio Method (RRM); c) Doernenburg Ratio Method (DRM); and d) Duval Triangle Method (DTM) [7]. As of now, all DGA interpretation guidelines are derived from laboratory results. There is no widely accepted standard for online DGA [7, 86].

a) Key Gas Method

As per IEEE Std C57.104 – 2019, the Key Gas Method (KGM) can be used to diagnose four types of faults: thermal degradation, overheating in oil and cellulose, partial discharge (PD) and arcing as shown in Table 2.5. To diagnose thermal degradation faults, the presence of C₂H₄, along with C₂H₆, CH₄ and H₂, is indicative when the hotspot temperature exceeds 300°C. At temperature surpassing 700°C, the appearance of C₂H₂ is expected. [87].

In the case of overheating in oil and cellulose fault diagnosis, the oil is expected to contain CO, accompanied by C₂H₄, C₂H₆, CH₄ and H₂. For partial discharge fault diagnosis, H₂ along with CH₄, and much smaller amount of C₂H₄ and C₂H₆ will be found in the oil.

In situations involving high energy arcing, temperature can reach the range of 2000°C to 3000°C or even higher [88, 89]. When the temperature exceeds 700°C, the key gas C₂H₂ will be formed along with H₂, CH₄, C₂H₄ and C₂H₆, and CO, which originates from insulating paper breakdown, can be identified in the oil [87].

Table 2.5 The summary of KGM from IEEE C57.104.

Key Gas	Fault type	Typical proportions of generated combustible gases
Ethylene (C ₂ H ₄)	Thermal mineral oil	Predominantly Ethylene with smaller proportions of Ethane, Methane, and Hydrogen. Traces of Acetylene at very high fault temperatures.
Carbon-Monoxide (CO)	Thermal mineral oil and cellulose	Predominantly Carbon Monoxide with much smaller quantities of Hydrocarbon Gases. Predominantly Ethylene with smaller proportions of Ethane, Methane, and Hydrogen.
Hydrogen (H ₂)	Electrical low energy partial discharge (PD)	Predominantly Hydrogen with small quantities of Methane and traces of Ethylene and Ethane.
Hydrogen and Acetylene (H ₂ , C ₂ H ₂)	Electrical high energy (arcing)	Predominantly Hydrogen and Acetylene with minor traces of Methane, Ethylene, and Ethane. Also, Carbon Monoxide if cellulose is involved.

KGM has some limitations, primarily its conservative approach that places more emphasis on the absolute concentration of gases rather than the rate of gas evolution. As a result, KGM has a failure rate of approximately 50% when it comes to inconclusive or incorrect fault identification [7]. Additionally, it's worth noting that CO may not consistently serve as a reliable indicator for detecting thermal faults in insulating paper.

b) Rogers Ratio Method

Roger's ratio method (RRM) relies on three gas ratios: C₂H₂/C₂H₄, CH₄/H₂ and C₂H₄/C₂H₆, to identify five different faults as detailed in Table 2.6. In contrast to KGM, RRM offers the ability to further categorize thermal faults into three levels: low temperature, temperature less than 700°C, and temperature over 700°C. For instance, if the ratio of C₂H₄/C₂H₆ falls between 1.0 to 3.0, and the ratio CH₄/H₂ is greater than 1.0, the transformer's health condition is identified as case 4, indicating a thermal fault less than 700°C. However, it's important to note that RRM may have limitations in detecting certain faults, even when the concentration of specific gases is high [7].

Table 2.6 Rogers Ratio Method (RRM) from IEEE C57.104.

Case	C ₂ H ₂ /C ₂ H ₄	CH ₄ /H ₂	C ₂ H ₄ /C ₂ H ₆	Suggested fault diagnosis
0	< 0.1	0.1 to 1.0	< 0.1	Unit normal
1	< 0.1	< 0.1	< 0.1	Low energy density arcing - PD
2	0.1 to 3.0	0.1 to 1.0	> 0.3	Arcing – High energy discharge
3	< 0.1	0.1 to 1.0	1.0 to 3.0	Low temperature thermal
4	< 0.1	> 0.1	1.0 to 3.0	Thermal < 700°C
5	< 0.1	> 0.1	> 0.3	Thermal > 700°C

c) Doernenburg Ratio Method

The Doernenburg ratio method (DRM) relies on four gas ratios; CH_4/H_2 , C_2H_2/C_2H_4 , C_2H_2/CH_4 , and C_2H_6/C_2H_2 to identify three distinct fault types: thermal decomposition, corona and arcing as shown in Table 2.7.

According to the table, if the ratio CH_4/H_2 is greater than 1.0, further comparisons are made. The ratio C_2H_2/CH_4 is compared with the threshold limit of 0.3, and the ratio C_2H_6/C_2H_2 is compared with the threshold limit of 0.4. If C_2H_2/CH_4 is larger than 0.3, it is more likely to indicate an arcing fault. To apply DRM, at least one of the four key gases used in the ratios (H_2 , CH_4 , C_2H_2 and C_2H_6) needs to exceed twice the relevant L1 concentration shown in Table 2.8 [67]. DRM is an old diagnosis method and due to its low accuracy, it is not commonly used nowadays [7].

Table 2.7 Doernenburg Ratio Method (DRM) from IEEE C57.104.

Suggested fault diagnosis	Ratio 1 (R1) CH_4/H_2 Extracted from mineral oil gas space		Ratio 2 (R2) C_2H_2/C_2H_4 Extracted from mineral oil gas space		Ratio 3 (R3) C_2H_2/CH_4 Extracted from mineral oil gas space		Ratio 4 (R4) C_2H_6/C_2H_2 Extracted from mineral oil gas space	
	1 – Thermal decomposition	>1.0	>0.1	<0.75	<1.0	<0.3	<0.1	>0.4
2 – Corona (low intensity PD)	<0.1	<0.01	Not significant		<0.3	<0.1	>0.4	>0.2
3 – Arcing (high intensity PD)	>0.1, <1.0	>0.01, <0.1	>0.75	>1.0	>0.3	>0.1	<0.4	<0.2

Table 2.8 Limit concentrations of dissolved gases from IEEE C57.104.

Key Gas	Concentrations L1 ($\mu L/L$ ppm v/v)
Hydrogen (H_2)	100
Methane (CH_4)	120
Carbon Monoxide (CO)	350
Acetylene (C_2H_2)	1
Ethylene (C_2H_4)	50
Ethane (C_2H_6)	65

d) Duval Triangle Method

The Duval triangle method (DTM) uses the graphical triangle as depicted in Figure 2.21, to diagnose various fault types. This method employs the concentration of three gases: CH_4 , C_2H_2 and C_2H_4 , which are presented as sides of the triangle with percentages ranging from 0% to 100%. DTM divides the entire triangular area into seven fault regions labelled PD, D1, D2, T1, T2, T3 and DT as given in Table 2.9 [7].

By employing equations (2.6) to (2.8), the gas concentration in percentages can be calculated and utilized within Duval Triangle to determine the fault region. An example is given in Figure 2.21, when % CH_4

is 34.5%, %C₂H₄ is 31% and %C₂H₂ is 34.5%, the possible fault would be categorized as D2, indicating a discharge of high energy, according to Table 2.9.

$$\%CH_4 = \frac{100CH_4}{CH_4+C_2H_4+C_2H_2} \quad (2.6)$$

$$\%C_2H_4 = \frac{100C_2H_4}{CH_4+C_2H_4+C_2H_2} \quad (2.7)$$

$$\%C_2H_2 = \frac{100C_2H_2}{CH_4+C_2H_4+C_2H_2} \quad (2.8)$$

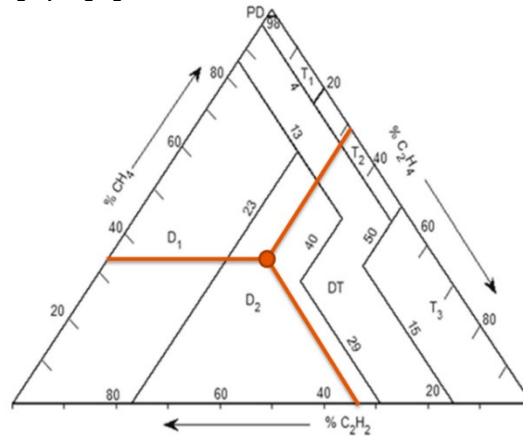


Figure 2.21 Classic Duval Triangle from IEEE C57.104.

Table 2.9 Abbreviations of basic faults.

Symbol	Fault
PD	Partial discharge
D1	Discharge of low energy
D2	Discharge of high energy
T1	Thermal faults of less than 300°C
T2	Thermal faults between 300°C and 700°C
T3	Thermal faults greater than 700°C
DT	Mixture of thermal and electrical faults

Despite the effectiveness of the classic Duval Triangle in diagnosing basic faults, it has limitations when it comes to potential misclassifications near the boundary regions between adjacent sections. Additionally, the Duval Triangle analysis may provide inaccurate results for transformers equipped with load tap changers or containing non-mineral insulating fluids. To address these challenges, various modified Duval Triangles, and alternative geometric shapes, such as the pentagon, have been introduced in the field of transformer fault diagnosis [7, 15, 67, 86].

The Duval pentagon method (DPM) is similar to the DTM but extends its diagnostic capabilities by employing five key gases: H₂, CH₄, C₂H₂, C₂H₄ and C₂H₆. DPM can identify six distinct fault types (PD, D1, D2, T1, T2 and T3), along with a category for stray gassing (S), specifically in mineral oil transformers, as depicted in Figure 2.22. However, it's important to note that DPM may also exhibit misdiagnosing faults that are in proximity to the boundaries between adjacent sections.

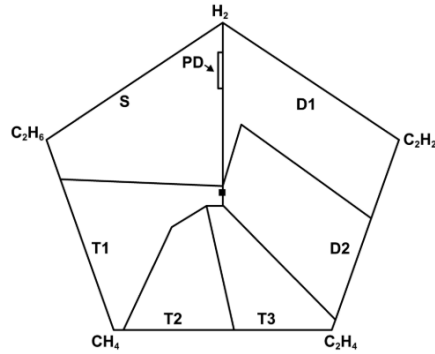


Figure 2.22 Duval pentagon 1 from IEEE C57.104.

The implementation of online DGA method has been significantly advanced online condition monitoring systems. However, traditional diagnostic methods were primarily designed to identify single faults, and they encounter challenges when transformers experience multiple concurrent faults, making definitive identification difficult [7]. To enhance the accuracy of these systems, there is a growing need to develop new diagnostic techniques based on artificial intelligence methods [77, 79].

2.3.2 Partial Discharge

Partial discharge (PD) refers to a localized dielectric discharge that partially bridges the insulation between conductors or between conductors and earth [90]. In oil-immersed transformers, PD can manifest in various locations, including the insulating paper, oil or at the interface of oil-paper insulation. The presence of moisture, gas bubbles, and electrode burrs generated inside the transformer during long-term operation can give rise to PD phenomena [91]. Additionally, insulation defects resulting from overvoltage conditions can cause PD and accelerate the aging of insulation material [91].

PD activity, when left unaddressed, can progressively deteriorate transformer performance and lead to further degradation of the dielectric insulation system. Once PD initiates, it has the potential to spread throughout the insulation until a complete breakdown occurs [92]. Consequently, the early detection of PD during transformer operation is important to avert transformer failures. The accuracy of online PD detection techniques for power transformers relies on various parameters, including electromagnetic emissions, acoustic emissions, and chemical changes [91], as elaborated below.

2.3.2.1 Ultrahigh-frequency (UHF) Detection

PD events generate electromagnetic pulses with frequencies typically falling within the UHF range, which spans from 300 MHz to 3 GHz [93]. In general, the interference signal frequency range on site is below 400MHz [91]. Hence, UHF sensors have gained widespread adoption due to their sensitivity and ability to operate in noisy environments, effectively rejecting interference [94, 95]. Originally developed for use in gas-insulated switchgear (GIS) in 1988, the application of UHF sensors expanded to power transformers in 1997 [96].

UHF sensors can be mounted inside or outside the wall surface of the tank or through an oil drain valve. In order to pinpoint the PD sources, multiple UHF sensors are strategically positioned around the transformer [97]. Localization of the PD source can be achieved by time differences of arrival (TDOA), which measures and compares the captured signals arrival time from different sensor locations [97, 98].

These UHF sensors essentially function as antennas that receive electromagnetic (EM) waves originating from PD sources. The initial UHF signals undergo filtration to eliminate unwanted noise [96, 99]. Following this, an amplifier is connected to the filter to uphold measurement sensitivity. The signals are then transmitted through coaxial cables to a detector and subsequently sampled by a data acquisition (DAQ) system, as illustrated in the process depicted in Figure 2.23.



Figure 2.23 The process of PD measurement.

UHF PD detection employs two common methods: the tuned UHF narrowband or medium band measurement with variable centre frequency; and the UHF broadband measurement with fixed bandwidth [100, 101]. Figure 2.24 (a) shows an example of PD signal measured by tuned the UHF narrowband/medium band method [100]. The lower trace in the figure represents the background noise, while the upper trace represents the actual PD signal. It is worth mentioning that the interference noise disturbs both the upper and lower traces. Figure 2.24 (b) shows a PD signal measured by the broadband UHF method with fixed bandwidth. The setting of this is easy to adapt, however, it has lower signal- to - noise ratio (SNR).

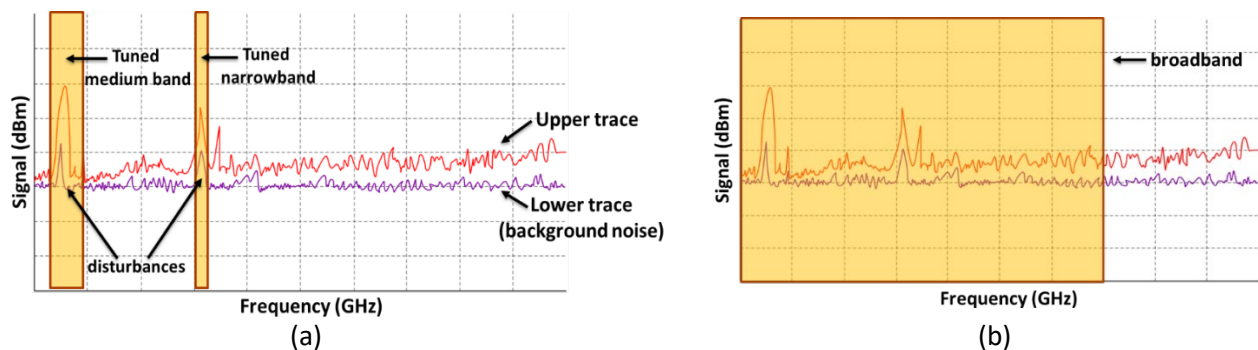


Figure 2.24 (a) Signal of tuned UHF narrowband method and (b) bandwidth of UHF broadband method.

UHF PD detection has several advantages, including its immunity to electromagnetic disturbances when compared to conventional methods outlined in IEC 60270 [96]. As a result, UHF sensors have found use in on-site PD detection. However, it remains uncertain how the magnitude of the UHF signal correlates with the amount of charge in pC, which has led to a lack of appropriate calibration methods [96].

2.3.2.2 Optical Detection

The acoustic emission (AE) method measures the amplitude, attenuation or phase delay of acoustic signals generated by PD events. These ultrasonic AE signals fall within the frequency range of 20 kHz to 500 kHz [93]. The traditional AE sensors' detection element is Lead Zirconate Titanate (PZT)-based material [102]. It is difficult to ensure the sensitivity and accuracy of PD detection, especially if it is highly affected by the electromagnetic interference (EMI) [103, 104]. Optical fibres have advantages of anti-EMI. The traditional optical sensor is designed to detect the light from a PD event. However, this type of optical sensor is unable to localize PD source. To overcome these drawbacks, optical sensors based on AE have gained popularity. Moreover, optical sensors can be installed inside the transformer tank walls due to its compact size and the lack of using metal materials [91, 103]

There are three main types of optical technology: extrinsic Fabry-Perot (FP) based sensor, Dual-Beam Interference based sensor (intrinsic interferometer) and Fibre Bragg Grating (FBG) based sensor. A brief comparison of various optical detection technologies is given in Table 2.10 [91, 102, 104].

Table 2.10 Comparison of different optical detection technologies.

Sensor Type	Comparison
Extrinsic Fabry-Perot Interferometer	<ul style="list-style-type: none"> • Complicate to manufacture • Compact in size
Intrinsic Interferometer (Mach-Zehnder, Michelson and Sagnac Interferometric)	<ul style="list-style-type: none"> • Easy to manufacture • Sensitivity can be improved by using longer optical sensing fibre
Fiber Bragg Gratings	<ul style="list-style-type: none"> • Easy to multiplex • Not sensitive as interferometers to acoustic waves

The Fabry-Perot Interferometer sensor is a typical Fibre Optic Interferometer [104]. In the sensor structure shown in Figure 2.25, the light from a laser light source propagates into the sensing probe through a fibre coupler. The first reflection of the light occurs in the FP cavity which is at the end of the fibre core. A small portion of the incident light returns along the original path of the fibre core. Most of the light undergoes the second reflection at the quartz membrane of the FP cavity. This second reflection also returns back to the fibre coupler. By adjusting the quartz membrane, the two beams of light can be of the same frequency, amplitude, and direction at the fibre coupler. PD event changes quartz membrane shape and phase of the second reflected light and can be detected by a photo-detector, that generates an electrical signal as shown in Figure 2.26 [91, 105].

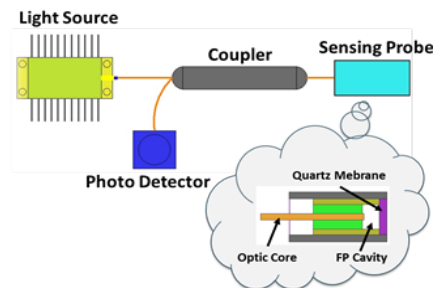


Figure 2.25 Fabry-Perot interference sensor structure.

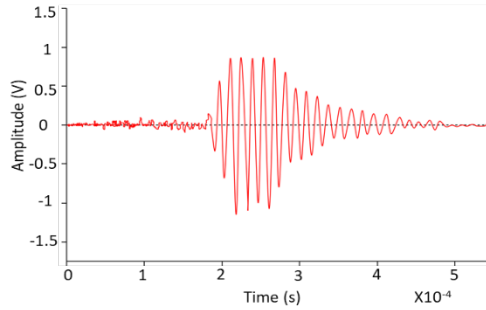


Figure 2.26 Example of output electrical signal from Fabry-Perot optical sensor.

The working principle of dual-beam Interferometers such as Mach-Zehnder sensor, Michelson sensor and Sagnac sensor is similar to Fabry-Perot Interference Sensor as they all have interference optical structure [91]. In the Mach-Zehnder sensor structure, the light in fibre coupler 1 is divided into two beams, through a reference and sensing fibres and interfere again in fibre coupler 2 as shown in Figure 2.27.

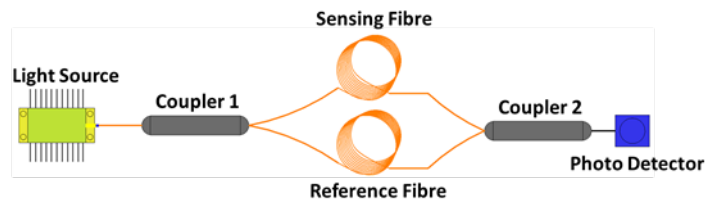


Figure 2.27 Diagram of Mach-Zehnder interferometer structure.

Different from the Mach-Zehnder sensor, in the Michelson sensor structure, the two light beams pass through the reference and sensing fibres, then are reflected by a Faraday rotating mirror back to the previous path as shown in Figure 2.28. So when the sensing fibre is deformed by PD, it causes phase difference between the two light beams [91].

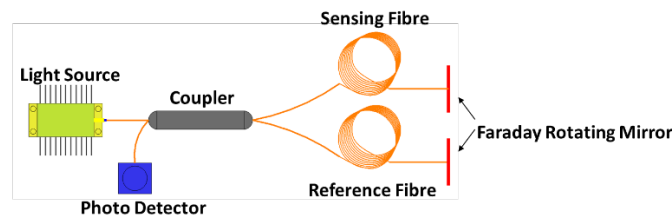


Figure 2.28 Diagram of Michelson interferometer structure.

In the Sagnac sensor structure, the light is divided at the fibre coupler as shown in Figure 2.29. The two beams of light are travelling in opposite directions through the sensing fibre. Then the two light beams interfere at the fibre coupler. PD event results in a phase difference between the two optical signals [91, 106].

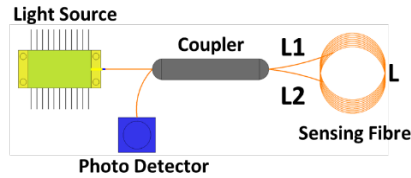


Figure 2.29 Diagram of Sagnac interferometer structure.

Different from interferometers, Fibre Bragg Grating (FBG) sensors have diffraction optical structure. This detection technology is of a reflective structure in the core of an optical fibre as shown in Figure 2.30 [107]. It reflects particular wavelengths of light and transmits all others.

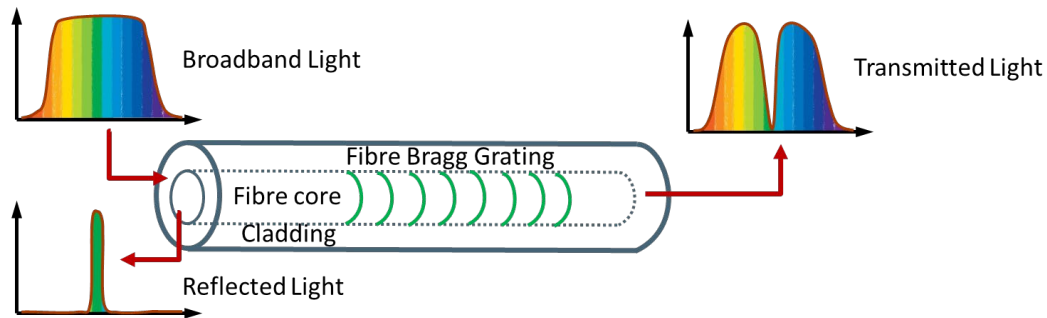


Figure 2.30 Working principle of FBG.

Any change in Bragg wavelength (λ_B) caused by PD is converted into an equivalent change in optical intensity [91]. The optical intensity differences can be detected by photodetector and converted into a voltage signal. The Fibre Bragg Grating sensor structure is shown in Figure 2.31.

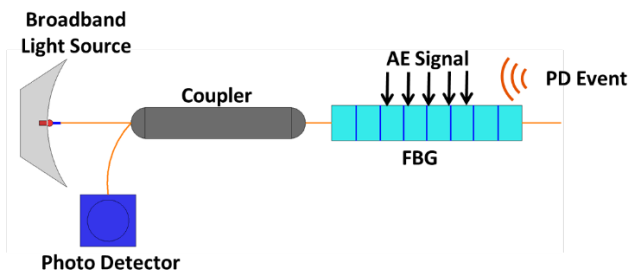


Figure 2.31 Diagram of Fibre Bragg Grating interferometer structure.

Optical sensors present several advantages, including their resilience in harsh environments characterized by high temperatures and chemical corrosion [104]. This robustness allows for the installation of optical sensors within the transformer, mitigating external noise interference. The geometric PD sensors' location can be determined by utilizing multiple optical sensors either around the transformer tank or in a sensor array [108-110]. Overall, optical sensors have been proven to be effective techniques for PD detection.

2.3.2.3 Transient Earth Voltage Detection

Transient Earth Voltage (TEV) represents a relatively recent addition to the PD detection methods [111]. TEV sensors are capable of capturing two frequency ranges: several 100MHz from surface current and several 10MHz from PD current [111].

During a PD event, the lower-frequency component can be detected as current, which flows from the external ground to the TEV sensor. The electromagnetic radiation from PD source also propagates as a surface current on the tank wall. Due to the skin effect, this current travels from inside of the transformer wall, leaks out from joints such as bushings, and is detected by the TEV sensor as shown in Figure 2.32 [111-113].

Although the mechanism and propagation process of the TEV signal are not fully understood yet [114], it is still considered as another online PD detection method. As a non-intrusive method, the major advantage of TEV sensors is that they can be easily attached to the outer surface of the transformer tank wall without any operation interruption.

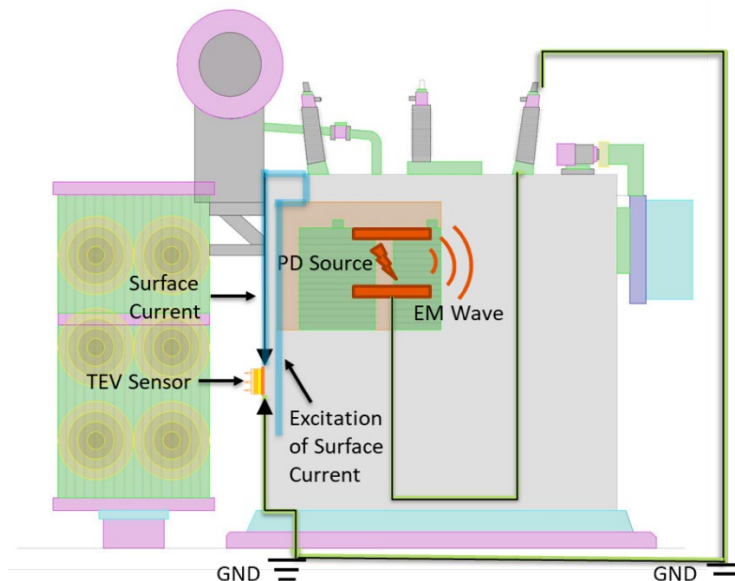


Figure 2.32 Detection principle of TEV signals.

2.3.2.4 High-Frequency Current Transformer

The High-Frequency Current Transformer (HFCT) represents another non-intrusive PD sensor. HFCT devices can be clamped onto the ground connections of a power transformer [115]. They operate by measuring the short transient current pulses flowing through the earth conductor due to PD activity.

A typical HFCT sensor consists of a copper wire wound around a ferrite core, which is connected to a 50Ω BNC connector, as illustrated in Figure 2.33. The transformer earth cable carries transient currents, which pass through the middle of the ferrite core. These currents on the primary side produce an electromagnetic flux around the cable. Subsequently, the flux induces a current and voltage on the secondary winding [107, 116].

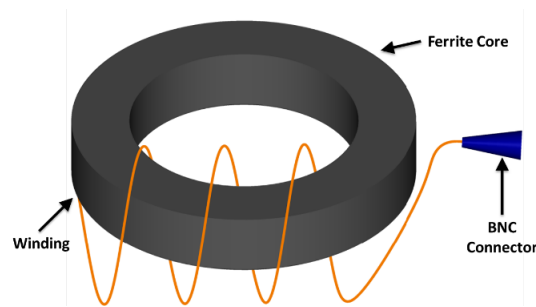


Figure 2.33 Diagram of HFCT structure.

2.3.3 Thermal Measurements

The thermal measurements are used to detect temperature rise in the transformer winding and insulation mediums [117]. During transformer operation, heat generated in the windings and core circulates with oil. The hotter oil rises to the top of the tank, where it cools before descending to the tank bottom. The conventional approach to thermal monitoring involves measuring top oil temperature and estimate the hot-spot temperature (HST) [118].

The temperature of the top oil of the tank can be measured by using resistance thermometer or thermocouple sensor. HST represents the maximum temperature measured from the winding insulation of the transformer. In the case of new transformers, optical sensors can be directly installed in the spacers of winding disks to measure HST [119]. However, for already assembled units, it is not practical to install optical probes inside the winding structure. HST values can be estimated based on the following techniques: thermal equivalent circuits (TECs) [119], stochastic, numerical and practical experiment techniques [117]. TECs are based on thermal-electrical analogy, and widely used due to their simplicity. The most commonly used estimation method is outlined in Clause 7 of IEEE Std C57.91 [18]. The continuous improvement on artificial intelligence technologies will help online thermal analysis become more accurate in order to handle complex applications [120].

An infrared thermograph application is a non-destructive thermal detection method that uses a thermal camera to detect infrared radiation emission. Abnormal conditions such as cooling system fault, short-circuit current, poor joint contact can be monitored online [121]. However, this method only scans the surface radiation and detect the transformer's external temperature as shown in Figure 2.34. Although infrared thermograph method can be used for fast detection of temperature rise, its sensitivity is concerned, especially for detecting HST.

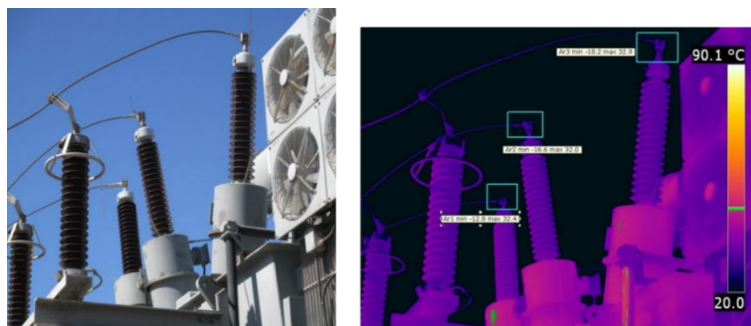


Figure 2.34 An example of thermal image taken by infrared camera.

2.3.4 Vibration Analysis

Vibration analysis is used to detect internal mechanical faults such as deformation or aging of the contacts in transformer based on changes in vibration response [122]. The vibration response can be measured by an accelerometer, which is the most used type. The output of the accelerometer is a voltage signal measured in mV, which contains noise. Therefore, for accurate results, the signal needs to pass through filters [123]. When transformer is in good condition, the measurements can be recorded as fingerprint for future comparisons [124]. Healthy transformers always produce a periodic vibration signal [122].

Vibration response analysis is an online method and can be used as a complement to offline methods such as SFRA [125]. However, vibration response is detected from individual measurement points on the tank, which results in inconsistent signatures.

2.4. Challenges and Opportunities

While several developments have been made to various condition monitoring and fault diagnosis techniques currently used by industry, a lot of challenges still need to be solved through comprehensive research and field trials.

For instance, there is no practical online method to replace the offline SFRA measurements. While some research efforts can be found in the literature to identify and quantify mechanical faults within a transformer through its V-I characteristics at the power frequency [126], the practical feasibility of this technique has not been assessed yet. Also, in the current SFRA method, the analysis of the results is not always a straightforward process due to the lack of widely accepted interpretation codes. The use of artificial intelligence (AI) and effective digital signal processing techniques may result in reliable, consistent and automated code to analyse frequency response analysis signatures [127]. Optimization and digital image processing techniques may also be used to improve the accuracy of the analysis [128, 129].

While measurement and analysis of dissolved gases are well matured for mineral oil, research effort still needs to be conducted to develop reliable DGA codes for biodegradable insulating oil and thermally upgraded insulation paper. The currently used interpretation codes are not consistent and may result in different conclusion to the same oil sample. Combining these techniques in one AI code can improve the detection accuracy of DGA method [130]. The accuracy of current online DGA sensors depend on several environmental and operating conditions, which calls for more research in this area to increase the accuracy of such sensors and enable them to measure other oil parameters such as Furan content, acidity, IFT and BDV [26].

With the global trend to increase the reliance on renewable energy sources, more fluctuation in the generated power and voltage is expected due to the intermittency of such sources. Moreover, the load demand will exhibit uncertainty in magnitude and location with the increased number of plug-in electric vehicles that also result in increased harmonics in the power grids due to the power electronic interface. Such factors will have a significant impact on the transformer condition monitoring and fault diagnosis techniques. For example, if the oil is sampled for DGA measurement during a ramping period in the

generation and/or load, inaccurate values will be revealed [88, 131]. On the other hand, the harmonics in the voltage signal can be employed for online frequency response analysis.

The use of multi-sensors to measure different diagnostic parameters may also call for active research on wireless energy transfer to charge such sensors [124]. While the power required by each individual sensor is small, the use of a large number of online sensors may represent an additional burden to the network.

It is worth mentioning that with the worldwide efforts to reduce greenhouse gas emission and establish more DC and smart grids, the adoption of solid-state transformers and advanced power electronic interfacing systems will be given much attention in the very near future and the use of classical magnetic-core based transformers may be diminished [132, 133].

2.5. Summary

Oil-immersed power transformer is a critical and expensive asset in power systems. Failures of power transformer result in huge repair cost, environment disaster and human injury or death. Therefore, reliable condition monitoring techniques must be adopted to avoid such consequences. Conventional offline condition monitoring techniques have been used for many years. Due to the offline line nature, the tests can only be performed during scheduled maintenance and the opportunity to detect incipient faults could be missed. The online condition monitoring technologies are relatively new and have been given much attention by industry and researchers. In addition, the power industry is moving towards digital operation, which calls for more stable and accurate online condition monitoring system. Over the years, researchers and developers have invented various online monitoring sensors and diagnostic methods such as DGA, PD, thermal measurements, and vibration analysis.

This chapter covers the working principle of commonly used offline and online methods. To design the most suitable condition monitoring system for a power transformer, it is important to understand the functions, measuring ranges, suitable diagnostic methods and advantages and limitations of each technique. The future generations of condition monitoring systems would be comprehensive and could provide users with more precise information. In such systems, it is expected to not only provide information about the health condition of the transformer but also to suggest a reliable asset management scheme and estimating transformer remnant life based on the measured parameters.

Chapter 3 Asset Management Methodologies for Oil-immersed Power Transformers

3.1. Introduction

The traditional concept of operational and maintenance strategies is time-based, involving periodic check-ups on transformers without considering their actual condition. The development of online condition monitoring sensors offers the opportunity to implement condition-based maintenance practices. Real-time condition monitoring increases the likelihood of detecting incipient faults, reducing the probability of failures, improving safety operation, controlling unscheduled maintenance, and assisting in prioritizing the maintenance and replacement schedule based on individual transformers' conditions.

Due to the unavailability of online approaches, some of the condition tests are currently performed offline. Therefore, comprehensive transformer asset management includes both time-based and condition-based maintenance as shown in Figure 3.1 is usually adopted. The maintenance activities consist of economic-based and condition-based assessments. Economic-based assessment employs tools such as cost-benefit analysis. Because individual businesses have different financial plans, the economic assessment would not be discussed in this thesis.

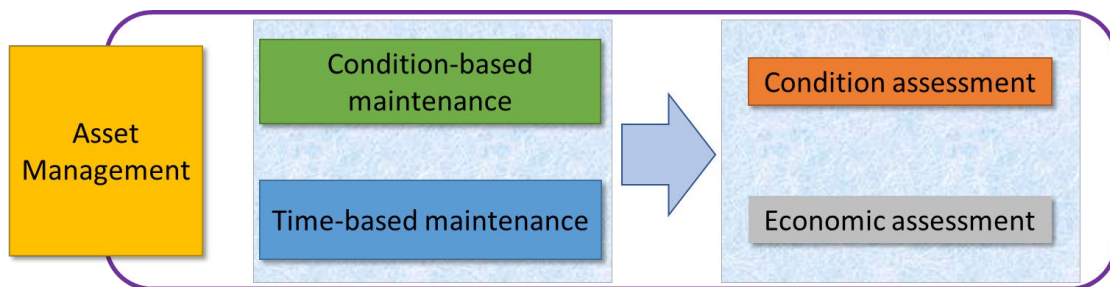


Figure 3.1 Basic structure of asset management.

There has been extensive work on improving and developing condition monitoring methods and data analysis techniques. Advanced monitoring and diagnostic technologies are aimed to improve the accuracy and ease the implementation of condition assessment methods. This chapter presents a state-of-the-art review on the condition assessment techniques published in literature and currently used by industry practice.

The basic structure of the transformer condition-based assessment is shown in Figure 3.2. As shown in the figure, asset management consists of three modules: fault diagnosis, reliability assessment and life management. A fault diagnosis module is utilized to assess the health condition of individual transformer components. Different fault diagnostic methods (presented in Section 2) feed into failure modes, which are the underlying conditions that can lead to failures. In Section 3, reliability assessment methods will be reviewed. Different from fault diagnosis, reliability assessment is utilized to determine the overall health condition of the transformer. The Reliability Index or Health Index (HI) is the overall health score given by the reliability assessment. HI is designed to identify the transformer most in need of the asset manager’s attention and is calculated based on condition monitoring parameters or fault diagnosis data. In Section 4, life management approaches utilized to estimate the transformer aging are presented. The estimated remaining life of power transformer is conducted based on the history and current condition of the transformer. It highlights the priority of the need for replacements for asset managers.

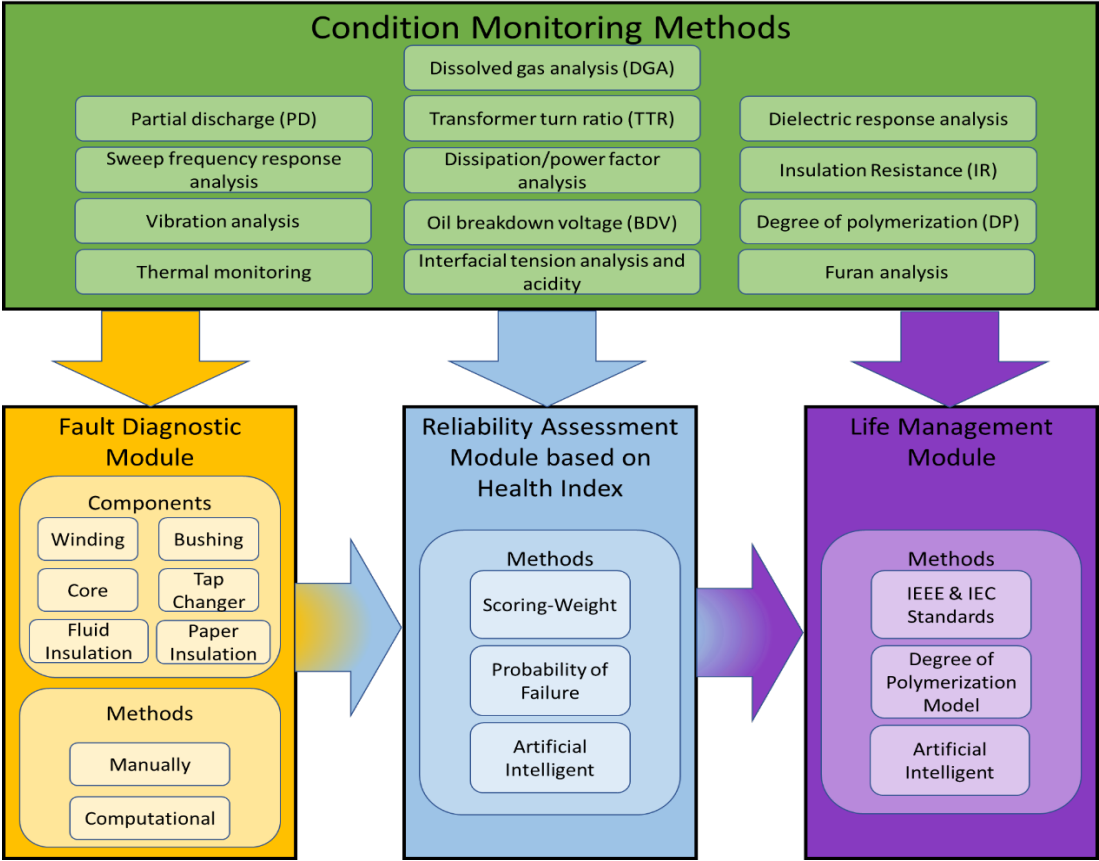


Figure 3.2 The basic structure of condition assessment in asset management.

3.2. Fault Diagnosis

An oil-immersed power transformer is a complicated piece of equipment that comprises many components including bushing, tap changer, insulation, winding, and magnetic core. Through condition monitoring methods, transformer condition data can be analysed according to different failure modes. Due to the wide variety of sizes and types of power transformers, there are no standardized failure modes

for all power transformers. Failure modes can be generally classified based on its location and cause [134-136]. This section presents commonly used condition monitoring methods and their diagnostic techniques.

3.2.1 Condition monitoring methods

Dissolved Gas Analysis (DGA): DGA is one of the most popular fault detection techniques for power transformers [137]. Under harsh operation conditions, both oil and paper insulation decompose and release certain gases that dissolved into the oil and decrease its dielectric strength. The fault gases, namely, hydrogen (H₂), methane (CH₄), ethane (C₂H₆), ethylene (C₂H₄), acetylene (C₂H₂), carbon monoxide (CO) and carbon dioxide (CO₂) can be measured using online or offline methods in parts-per-million (ppm) [7]. By analysing different combinations and proportions of these gases, and their dynamic rates of change, fault type can be identified. The conventional interpretation methods of DGA measurements, as outlined in IEEE Std C57.104, include Rogers Ratios, Doernenburg Ratios, Key gas, Duval Triangle and Pentagon methods. Table 3.1 lists the fault types that can be diagnosed using DGA [7]. Most diagnostic methods only focus on the primary faults, as shown in Table 3.1. Recent research has improved DGA interpretation by introducing Duval Triangle and Pentagon to identify sub-type faults [138, 139]. These new sub-zones within the Triangle method help distinguish between arcing in paper insulation and oil insulation. The sub-zones within the Pentagon method can recognize whether the carbonization of solid insulation has been involved in thermal fault or occurred solely within the oil.

Table 3.1 Primary and sub-types of faults that can be diagnosed using DGA.

Code	Primary Faults	Code	Sub-type Faults
T1	Thermal fault; T < 300 °C	S	Stray gassing; T < 200 °C
T2	Thermal fault; 300 °C < T < 700 °C	O	Overheat; T < 250 °C
T3	Thermal fault; T > 700 °C	C	Possible paper carbonization
D1	Low energy discharge	T3-H	Thermal fault T3 in mineral oil only
D2	High energy discharge	R	Catalytic reaction
PD	Partial discharge		

Partial Discharge (PD): PD refers to a localized dielectric discharge that partially bridges the insulation. During the long-term operation, the presence of moisture, gas bubbles and electrode burrs can lead to the development of PD events. These PD phenomena, if left unaddressed, can contribute to the gradual deterioration of insulation, and accelerate the aging process, ultimately culminating in insulation system breakdown. Thus, early detection of PD is important for reducing potential catastrophic failure and extending the lifespan of transformers. There is a diverse array of techniques and sensors available for the detection of PD, as listed in Table 3.2 [5, 92, 96, 140].

Table 3.2 Partial discharge detection methods

Method	Detection Phenomenon	Sensor
Dissolved gas analysis method	Chemical reactions	Gas Chromatographic (GC)/ Photo-acoustic Spectroscopy (PAS)
Radio frequency (RF) method	Electromagnetic emission	Ultra-High Frequency (UHF) / Very-High Frequency (VHF)
Optical method	Acoustic emission	Optical Sensor
High frequency method	Magnetic field	High Frequency Current Transformer (HFCT)
Transient earth voltage (TEV) method	Transient earth voltage	TEV sensor
Ultraviolet pulse detection method	Electromagnetic emission	Ultraviolet photosensitive sensor
IEC 60270	Current impulse below 1 MHz	Coupling capacitor

PD diagnosis goes beyond mere recognition and encompasses PD classification. There are various well-recognized types of PD, including protruding electrodes, floating electrodes, particles, surface discharges, poor contacts between windings, and void PDs [141].

Frequency Response Analysis (FRA): FRA is an effective offline method that can evaluate the transformer's mechanical integrity. FRA has been proven to be more accurate than the short-circuit impedance (SCI) measurement [14]. The FRA method compares frequency response traces with a transformer's reference data to identify any deviations and determine the internal mechanical defects including winding deformation, which is one of the transformers common mechanical faults, resulting due to large short-circuit currents.

Vibration Analysis: vibration analysis is an online tool used to detect some transformer internal mechanical faults. Hence, it can be employed as a complementary method alongside the offline FRA method. Vibration signatures are typically captured using accelerometers and are instrumental in pinpointing mechanical faults such as clamping structure loosening, misalignment, and imbalance [5, 142, 143]. Various signal process methods have been proposed for feature extraction associated with fault characteristics. Among these techniques, the analysis of the signal's frequency spectrum stands out as the most commonly used method [122].

Thermal Analysis: thermal analysis in transformers often focuses on detecting hot-spot temperature (HST) within the windings. HST measurement is vital for evaluating the performance of the transformer's cooling system and monitoring the insulation degradation rate. Measurements can be conducted through installing internal thermal sensors during transformer manufacturing. For in-service transformers, HST is commonly estimated through top-oil temperature measurements through thermal sensors installed on the top of the transformer tank.

An alternative thermal measurement method is conducted through thermographic testing, which employs infrared cameras to perform non-contact thermal inspection, identifying thermal anomalies. This

method detects infrared energy emissions from the surface of components experiencing excessive heat loss. The output of the thermographic test is an electrical signal presented in color-coded image on a screen. In these images, red and white areas indicate higher temperatures, while blue and black areas represent colder regions [121]. Thermographic test is particularly effective for detecting the exposed areas of the transformer, such as bushings and joints. However, it is not designed for internal temperature measurements.

Transformer Turn Ratio (TTR): TTR test is utilized to detect potential insulation failures occurring between turns within a transformer winding. This test is typically conducted at all the tap positions of each winding. To perform the TTR test, the turn ratio is calculated by the number of turns on the low voltage (LV) and high voltage (HV) sides of the transformer. These measurements are then compared to the specified ratios provided on the transformer's nameplate, and the difference should be within 0.5% for acceptable winding condition [144].

Oil Dissipation Factor (DF) and Power Factor (PF): DF / PF test is conducted to measure the dielectric losses within the transformer's oil. These losses can occur when leakage current flows from active parts to the grounded tank due to the presence of oil-soluble polar contaminations and aging by-products. In this test, the ratio of the capacitance current to the resistive current across the insulation is measured. This ratio is sensitive to even trace amounts of contamination [145].

Therefore, it is generally performed as part of an oil quality testing and is also employed for online bushing condition monitoring. In practical, the assessment is not solely reliant on a single power factor value but takes into consideration the historical trend of measurements over time [118].

Oil Breakdown Voltage (BDV): the dielectric BDV test is employed to assess the dielectric strength of the insulation oil [5]. Dry and clean oil exhibits higher breakdown voltage. The presence of contamination such as moisture, sludge, and other impurities, can lead to an increase in free-ions and ion-forming particles within oil, consequently significantly reducing its oil breakdown voltage.

Oil Interfacial Tension (IFT) and Acidity: the IFT test is a chemical analysis method used to identify degradation products and soluble polar contaminants in the oil. The oil surface tension decreases as hydrophilic components in the insulation oil increase. The acidity test measures the acidic constituents/contaminants in the oil. The acidity is formed due to the acidic oxidation products and causes paper insulation degradation and corrosion of metal parts. Notably, there is a significant correlation between the acidity number and the IFT of the oil. [5].

Dielectric Response Analysis – Recovery Voltage Method (RVM): RVM is a technique for scrutinizing the polarization process within the transformer insulation. The interpretation of RVM results hinges on the assessment of both the magnitude and position of the maximum recovery voltage [14, 45]. In general, increased maximum recovery voltage is an indicator of insulation deterioration.

Dielectric Response Analysis - Polarization and Depolarization Current (PDC): the PDC technique is a time domain analysis for insulation condition evaluation. Oil contamination increases the oil conductivity, and higher conductivity increases the polarization and depolarization currents. PDC measurements are highly sensitive to temperature [14, 47]. Therefore, the test results are more accurate with a reference temperature.

Dielectric Response Analysis - Frequency Domain Spectroscopy (FDS): FDS technique is a frequency domain analysis for insulation condition assessment. The method is based on assessing the dielectric parameters such as relative complex permittivity, complex capacitance, and dissipation factor, which can reflect the insulation polarization characteristics. PDS is commonly used for checking the moisture content in different parts of solid insulation [14]. FDS measurement is also sensitive to temperature [14, 47].

Insulation Resistance (IR): IR test is utilized to assess the insulation conditions affected by contaminations, which can be measured using the leaking current [33]. IR values are measured by a Megger or Megohmmeter at different time intervals. As the magnitude of IR value varies due to environmental conditions such as moisture and temperature, Polarization Index (PI), which uses the IR measurements taken in 1 minute and 10 minutes, has the advantage of eliminating the effect of such parameters on the IR reading [39]. A sharp decline in PI requires urgent attention and further investigation.

Degree of Polymerization (DP): DP is one of the key properties of cellulosic insulation material [146]. The mechanical strength of paper is strongly linked to the length of the cellulose molecules. The cellulose polymer molecules are interconnected through long chains of glucose rings [147]. Under thermal stresses, the glucose chains can break, causing a reduction in the length of the cellulose molecules and a subsequent decrease in the paper's mechanical strength. The average length of these chains is measured in terms of the DP which should be in the range of 1000 – 1200 for new material. Dropping the DP value to 250 is considered the end of paper life [140, 148-150]. The conventional method to measure the DP value is through laboratory tests [151]. This approach requires paper samples to be taken from the transformer, which is impractical for the transformers in operation.

Furan Analysis: Furan analysis is a valuable method for evaluating the paper insulation condition. The degradation of cellulose, primarily caused by factors such as high temperatures, exposure to oxygen, moisture, and acid contents, resulting in the production of various chemical furan compounds. These furan compounds include 2-furaldehyde (2-FAL), 5-methyl-2-furaldehyde (5-M2F), 5-hydroxymethyl-2-furaldehyde (5-H2F), 2-acetyl furan (2-ACF) and 2-furfurol (2-FOL) [152]. The most stable and abundant furan compound is the 2-FAL [153, 154]. The concentration of the furan compounds in ppm can be measured using high-performance liquid chromatography or gas chromatograph-mass spectrometry. There exists a robust correlation between the DP value and the concentration of 2-FAL. More detailed calculations for predicting the DP value using 2-FAL measurements are explained in Section 3.4.

3.2.2 Fault Analysing Methods

Analysing data from oil-immersed power transformers has always posed a challenge. False diagnosis can lead to unnecessary maintenance, and even wrong component replacement, potentially resulting in added costs and operational disruptions. The choice of data analysis methods depends on the characteristics of measured data, with feature extraction in some diagnostic approaches relying on numerical threshold limits, while others focus on recognizing variations in data patterns, as detailed in Table 3.3.

Data analysing methods can be categorized into conventional manual diagnosis and advanced computational techniques such as using artificial intelligence. The distinction between these approaches lies in the process of feature selection and fault diagnosis. Manual diagnosis necessitates the involvement of experienced experts who manually select data features and assess the likelihood of abnormalities. In contrast, advanced computational techniques harness the power of computer science to automatically select relevant data features and conduct fault diagnosis, reducing the reliance on human expertise.

Table 3.3 Conventional fault diagnostic methods.

Condition Monitoring Methods	Refs	Threshold/Ranges/Boundaries	Signal Figures/Plot Graph
Dissolved Gas Analysis (DGA)	[7]	<ul style="list-style-type: none"> ➤ Rogers Ratios ➤ Doernenburg Ratios ➤ Key gas ➤ Duval Triangles and Pentagons 	
Partial Discharge (PD)	[115, 155]		<ul style="list-style-type: none"> ➤ Phase-Resolved Partial Discharge (PRPD) ➤ Time-resolved Partial Discharge (waveform)
Frequency Response Analysis (FRA)	[156]		<ul style="list-style-type: none"> ➤ Frequency response signatures
Vibration Analysis	[122, 123, 157]		<ul style="list-style-type: none"> ➤ Frequency Spectrum ➤ Time domain ➤ Time-frequency domain ➤ Wavelet Transform ➤ Fourier Transform ➤ Hilbert Huang Transform (HHT)
Thermal analysis – Hot-spot temperature		<ul style="list-style-type: none"> ➤ Temperature exceeds normal level 	
Thermal analysis – Thermograph (temperature ΔT above ambient temperature)	[118, 134, 158]	<ul style="list-style-type: none"> ➤ $0\text{ }^{\circ}\text{C} < \Delta T \leq 9\text{ }^{\circ}\text{C}$, attention ➤ $9\text{ }^{\circ}\text{C} < \Delta T \leq 20\text{ }^{\circ}\text{C}$, intermediate ➤ $20\text{ }^{\circ}\text{C} < \Delta T \leq 49\text{ }^{\circ}\text{C}$, serious ➤ $\Delta T > 49\text{ }^{\circ}\text{C}$, critical 	
Transformer Turn Ratio (TTR)	[5]	<ul style="list-style-type: none"> ➤ New transformer $< 0.1\%$ ➤ Upper limitation $< 0.5\%$ 	
Dissipation/Power Factor (PF)	[5]	<ul style="list-style-type: none"> ➤ $\text{PF} \leq 0.5\%$, Normal ➤ $0.5\% < \text{PF} \leq 1\%$, Acceptable ➤ $\text{PF} > 1\%$, Sign of degradation 	
Breakdown Voltage (BDV)	[30]	<ul style="list-style-type: none"> ➤ Minimum level: 20 kV (1 mm gap) and 35 kV (2 mm gap) 	
Interfacial Tension (IFT)	[5]	<ul style="list-style-type: none"> ➤ Transformer size $\leq 69\text{ kV}$, $\text{IFT} \leq 22\text{ dynes/cm}$, End of Life 	

		<ul style="list-style-type: none"> ➤ Transformer size >69 kV, IFT ≤25 dynes/cm, End of Life 	
Acidity (measured in Neutralization Number, NN)	[5]	<ul style="list-style-type: none"> ➤ Transformer size ≤69 kV, NN ≥0.20 mg KOH/gm, Critical ➤ Transformer size 69 – 230 kV, NN ≥0.15 mg KOH/gm, Critical ➤ Transformer size ≥230 kV, NN ≥0.10 mg KOH/gm, Critical 	
Recovery Voltage Measurement	[45, 159]		<ul style="list-style-type: none"> ➤ Compare the maximum recovery voltage.
Polarization and Depolarization Current (PDC)	[5, 159]		<ul style="list-style-type: none"> ➤ Current magnitude in time domain
Frequency Domain Spectroscopy (FDS)	[5, 159]		<ul style="list-style-type: none"> ➤ Capacitance magnitude in frequency domain ➤ Loss factor magnitude in frequency domain
Insulation Resistance (IR) (measured in Polarization Index, PI)	[10]	<ul style="list-style-type: none"> ➤ 1.5 – 2, Dry insulation ➤ 1 – 1.5, Dirty & wet insulation ➤ <1, severe pollution and wet 	
Degree of Polymerization (DP)	[5]	<ul style="list-style-type: none"> ➤ 1200 – 700, Healthy ➤ 700 – 450, Moderate ➤ 450 – 250, Extensive ➤ <250, End of Life 	
Furan analysis (measured in 2-FAL, ppm)	[5]	<ul style="list-style-type: none"> ➤ 0 – 0.1, Healthy ➤ 0.1 – 1.0, Moderate ➤ 1 -10, Extensive ➤ >10, End of Life 	

3.2.2.1 Challenges to conventional interpretation methods

Conventional interpretation methods are still widely adopted by current industry practice to identify and quantify various faults within power transformers based on diagnostic methods listed in Table 3.3. Such methods are facing several challenges that include:

- The use of precise values for ratios and ranges could sometimes lead to misdiagnosed results [87, 160]. For instance, according to Rogers Ratio method used for DGA interpretation, if the ratios for both C_2H_2/C_2H_4 and C_2H_4/C_2H_6 are less than 0.1, then the ratio value of 0.1 for CH_4/H_2 becomes the critical boundary between normal and PD fault.
- The specified ranges can vary across different research papers. For example, some authors suggested DP value below 200 as an indicator of end-of-life, other sources suggest 250 as the threshold [147, 149, 161, 162].
- When measurements fall onto graphical-based methods' boundaries, it is difficult to draw a conclusion [87, 160]. An example of using the DGA Duval Triangle method is shown in Figure 3.3(a). In this case, the marked spot that shows the fault could be D1 or D2. This issue also happens in Duval Pentagon method. In Duval Pentagon, the marked spot shown in Figure 3.3(b) could indicate possible fault T1, T3 or D2. These faults are detailed in Table 3.1.

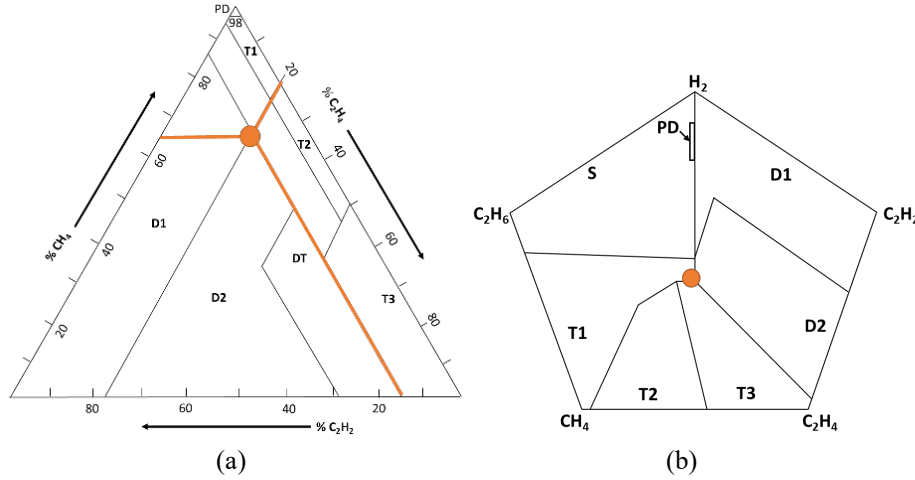


Figure 3.3 (a) Duval Triangle 1. (b) Duval Pentagon 1.

- Data cannot be interpreted unless the measured values surpass the minimum threshold [87, 160]. As an example, according to IEEE 57.104, to apply the DGA Doernenburg Ratio method, at least one of the critical gases (H_2 , CH_4 , C_2H_2 and C_2H_6) concentration used in the ratio must exceed a certain level.
- Different interpretation methods may lead to different conclusions, which can be observed in DGA interpretation [87, 160]. Also, graphical-based interpretation such as frequency response analysis, is not always consistent as it relies on the personnel expertise.

Conventional methods depend heavily on visual inspection, expert knowledge, and judgement. Therefore, other diagnostic methods based on mathematical statistics, equivalent electric models, and artificial intelligence, have been proposed as presented in the following sections.

3.2.2.2 Mathematical statistics method

In this method, statistical indicators are employed to extract features with reference data. The chosen indicator(s) should only be sensitive to the differences in fault conditions [163]. The statistical assessment is used for data comparison, such as FRA data interpretation [158]. In FRA, winding deformation can be identified by statistical indicators such as the Correlation Coefficient (CC) and the Standard Deviation (SD) [14]. CC is used to calculate the variation between data variables while SD is used to assess the deviation of one data set from its mean value. The formulas of CC and SD are given by (3.1) and (3.2), respectively. Other commonly used indicators are Mean Square Error (MSE), Absolute Sum of Logarithmic Error (ASLE) and Maximum Minimum (MM), which have been presented in [55, 156, 164, 165].

$$CC_{(X,Y)} = \frac{\sum_{i=1}^N X_i Y_i}{\sqrt{\sum_{i=1}^N X_i^2 \sum_{i=1}^N Y_i^2}} \quad (3.1)$$

$$SD_{(X,Y)} = \sqrt{\frac{\sum_{i=1}^N [Y_i - X_i]^2}{N - 1}} \quad (3.2)$$

X_i is the i th elements of FRA fingerprint.

Y_i is the i th elements of measured FRA trace.

N is the number of samples.

No general rules define the fault level using statistics indicators [158]. While mathematical statistics method has improved the accuracy of graphical-based interpretation, they fail in quantifying actual fault level.

3.2.2.3 Equivalent electric simulation model method

This method uses software to build a simulation model or equivalent circuit to mimic a real system. The finite element modelling (FEM) is the most popular numerical method that can effectively emulate physical systems [166].

Finite element analysis (FEA) software tools such as COMSOL Multiphysics and Ansys provide coupled physics modelling combined with computational fluid dynamics, thermal, acoustic, electromagnetic and structure simulation capabilities [167]. FEA has been used mainly for thermal and mechanical simulation of power transformer fault diagnosis. In [119, 166, 168-171], FEA is utilized to model thermal equivalent circuits to determine the HST and thermal profiles. In [53, 127, 172, 173], transformer mechanical condition is investigated through FEA. In [174], FEA uses the instantaneous voltage and current signals to identify mechanical deformation.

3.2.2.4 Artificial Intelligence methods

In recent years, artificial intelligence (AI)-based methods have been extensively studied. The significant advantage of using AI is its ability to handle data uncertainty and provide more accurate diagnostic results when compared to conventional methods. Therefore, both knowledge-based and data-driven AI techniques used for condition assessment have been proposed by many scholars as shown in Table 3.4.

Table 3.4 Proposed AI methods for each condition monitoring method.

Condition Monitoring Methods	Artificial Intelligence Methods	Refs
Dissolved Gas Analysis (DGA)	➤ Fuzzy Logic	[158, 160]
	➤ Decision Tree	[137, 175]
	➤ Random Forest	[137, 176]
	➤ KNN	[137, 177, 178]
	➤ Logistic Regression	[179, 180]
	➤ SVM	[177, 181, 182]
	➤ Bayesian Network	[183]
	➤ Naïve Bayes	[137]
	➤ ANN	[160, 184-186]
	➤ ANFIS	[184, 187]
Partial Discharge (PD)	➤ Fuzzy Logic	[188]
	➤ Decision Tree	[188]
	➤ SVM	[2, 14]
	➤ ANN	[141]
	➤ CNN	[141, 189-191]
	➤ ANFIS	[192]

Frequency Response Analysis (FRA)	➤ Fuzzy Logic	[158, 163, 193]
	➤ SVM	[163, 194]
	➤ Bayesian Classifier	[163]
	➤ ANN	[163, 193]
	➤ CNN	[195]
Vibration Analysis	➤ SVM	[196]
	➤ Bayesian Network	[197]
	➤ CNN	[198]
Thermal analysis – Hot-spot temperature	➤ Random Forest	[161]
	➤ SVM	[120, 199]
	➤ ANN	[161, 199]
Thermal analysis – Thermograph	➤ Fuzzy Logic	[158, 200]
	➤ ANN	[200]
	➤ ANFIS	[200]
Dissipation/Power Factor	➤ Fuzzy Logic	[158]
	➤ ANN	[37]
Polarization and Depolarization Current (PDC)	➤ SVM	[201, 202]
	➤ ANN	[203]
Frequency Domain Spectroscopy (FDS)	➤ Fuzzy Logic	[204]
	➤ SVM	[201]
	➤ ANN	[205]
Insulation Resistance (IR)	➤ Fuzzy Logic	[158]
Degree of Polymerization (DP)	➤ ANN	[206]
	➤ ANFIS	[207, 208]
Furan analysis	➤ Fuzzy Logic	[23]
	➤ ANFIS	[209]

3.2.2.4.1 Knowledge-based AI method

Fuzzy Logic: Fuzzy Logic method has been proposed by many authors for data interpretation [210]. When there is no clear definition of classifications to where the data should belong, Fuzzy Logic resolves uncertainty at the boundaries of the defined ranges by adding conditional statements. Fuzzy Logic data analysis structure consists of membership functions, fuzzifier, inference engine, fuzzy rules and defuzzification, as shown in Figure 3.4 [26]. There are many types of membership functions, including triangular, trapezoidal, and Gaussian. Fuzzifier is to allocate input data to the membership function of the fuzzy set. Fuzzy rules are conditional statements which use words statement like “IF-THEN” or “IF-AND-THEN”. These rules are less precise than numerical correlations as they are built based on human experience [211]. The inference engine then converts fuzzy inputs to fuzzy outputs using fuzzy rules. Defuzzifier is to convert the membership functions of the fuzzy set to output data.

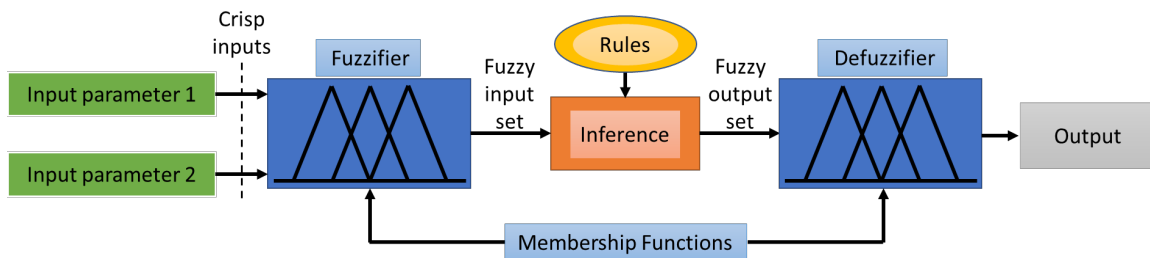


Figure 3.4 Structure of Fuzzy Logic data analysis.

3.2.2.4.2 Data-driven machine learning method

With the development of sensors and communication technologies, the demand for online condition monitoring systems is continually increasing, resulting in substantial data [191]. Pattern recognition or classification models can be trained to learn the data features representing certain transformer conditions. This process is called machine learning (ML) that has two major types: supervised and unsupervised.

Supervised machine learning methods

Supervised ML uses labelled training data sets to study algorithms and statistical models that can classify data and predict outcomes [212]. Classification is a type of supervised ML technique that has been widely implemented in transformer fault diagnostic methods [213, 214]. For example, DGA diagnosis uses labelled data sets containing 7-key gas concentration measurements as inputs and six main fault types as outputs to identify classification patterns.¹ In this section, commonly used classifiers are briefly described. Some of these methods are not only used for fault diagnosis but also employed for transformer reliability assessment and life management.

Decision Tree: A decision Tree is a commonly used method in classification [175]. This method classifies data into branch-like segments, as illustrated in Figure 3.5. A Decision Tree structure contains a root node, decision node and leaf node. In the example of DGA diagnosis, the root node can be used to separate data into thermal-fault and electrical-fault, which is the most relevant attribute/feature of the data sets. Decision nodes represent a possible choice available at that point in the tree structure. Finally, each leaf shows an outcome (T1, T2, T3, D1, D2 and PD are the symbols of DGA fault types, as shown in Table 3.1).

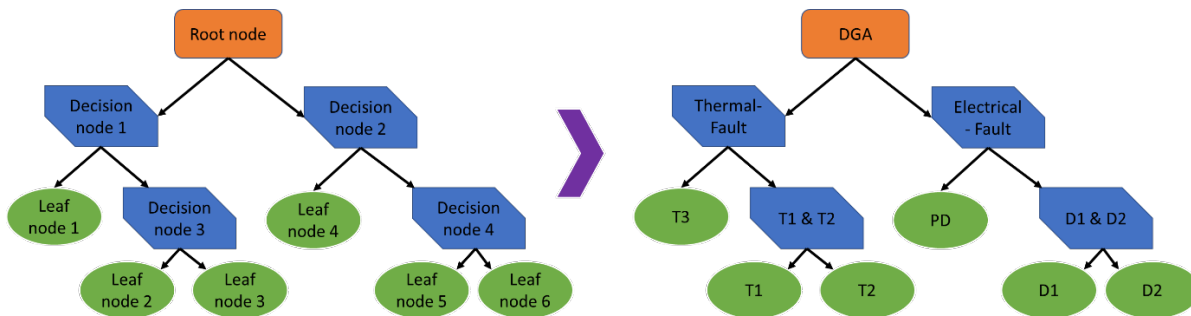


Figure 3.5 An example of Decision Tree structure.

Random Forest: Random Forest is an ensemble learning algorithm that can be viewed as an extension of Decision Tree [215]. The model comprises several individual decision trees, with each tree learning from a random subset of the training dataset [176, 216]. Once all Decision Trees make their predictions, the prediction of Random Forest is determined by aggregating over the ensemble. Unlike a single Decision Tree, Random Forest is able to process multiple classification trees simultaneously; therefore, it is a fast classifier. It also improves the predictive accuracy and controls over-fitting issues by taking the average of various Decision Trees [137, 217].

K-nearest Neighbour (KNN): KNN is a non-parametric classification method. It stores and allocates training data to certain classes, with “K” denoting the number of nearest neighbours considered. The new data will then be classified into one of these classes where its nearest neighbour is located [218]. The concept behind KNN shares similarities with Decision Trees, but instead of using a tree structure, it calculates the distance on the graph. Running KNN is normally faster than a decision tree [217]. There are many different methods to calculate the distance in KNN, such as Euclidean, Chebyshev, Minkowski, city block, Mahalanobis, Spearman correlation, Hamming, Jaccard and cosine [218].

Logistic Regression: Logistic Regression is a machine-learning technique for analysing discrete data [179]. Each set of input $X^i \in R^N$, R^N is an N dimensional feature vector. As an example, if the DGA set comprises 5 gases, then $[X_1^i, X_2^i, X_3^i, X_4^i, X_5^i] = [H_2, CH_4, C_2H_6, C_2H_4, C_2H_2]$ [180]. The output of this model $[Y^i \in \{1, 2, 3, 4\}]$, if there are four possible classified states – normal, thermal fault, low energy discharge and high energy discharge. The inputs can also be the sets of gas ratios and the outputs can be six fault types [179]. Logistic regression can be trained on small data sets; therefore, it is simpler and more efficient. The test results show that logistic regression has an accuracy rate of over 90% and has much better performance than conventional methods such as Rogers Ratios (60%), IEC Ratios (60%) and Duval methods (80%) [180].

Support Vector Machine (SVM): SVM is a binary classifier that constructs an optimal separating decision surface, called a hyperplane, to maximize the margins between the hyperplane and the data set as shown in Figure 3.6 [177]. The support vectors are the data used to find the optimal location of the hyperplane.

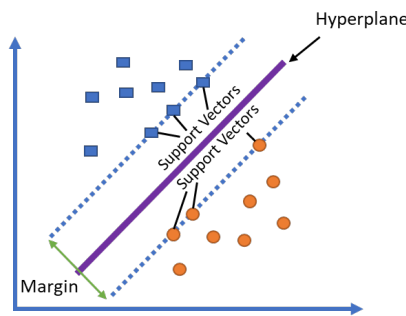


Figure 3.6 Principal diagram of SVM with two classes.

SVM can map non-linear data into higher dimensional feature space and turn it into a linear regression problem [219]. This non-linear relationship can be expressed as a decision function given by (3.3) [220]. The training data set is $\{X_i, Y_i\}_{i=1}^m$, where Y_i is the label of the input vector X_i . $X_i \in R^N$, R^N is the N dimension of input vectors. $K(X_i, X)$ is the Kernel function, which maps low-dimensional space into high-dimension. The popular kernel functions are Linear kernel, Polynomial kernel, Gaussian kernel, Sigmoid and Radial Basic Function (RBF) [177]. The hyperplane can be found when $f(x) = 0$. The two groups of data that are separated by boundaries are negative $f(x) = -1$ and positive $f(x) = +1$. SVM is a popular technique used in transformer fault diagnosis in which the function $f(x)$ is used to classify the conditions such as discharge fault ($f(x) = +1$) and thermal fault ($f(x) = -1$).

$$f(x) = \text{sign} \left[\sum_{i=1}^m \alpha_i Y_i K(X_i, X) + b \right] \quad (3.3)$$

$K(X_i, X)$ is Kernel function.

$f(x)$ is a linear combination of kernel functions centred at the m training data samples X , with their corresponding label Y .

α_i is the Lagrange multiplier corresponding to each sample.

b is the bias term.

SVM has the advantage of using a small amount of training data, hence, less training time [220, 221]. The SVM technique's accuracy depends on its parameters and the used kernel function [222].

Bayesian Network: Bayesian Network, also known as Belief Network, is a probabilistic graphical model based on Bayes theorem [223]. The Bayesian Network model consists of a directed acyclic graph with probability table(s), as shown in Figure 3.7 [183, 224]. In the directed acyclic graph, the variables such as condition monitoring and fault type data are presented in nodes. These variables in the network are linked through edges to indicate the dependencies between variables. Using the DGA method as an example, measured C_2H_2 gas concentration is used to calculate the probability of arcing fault. The top table in Figure 3.7 gives the probability of C_2H_2 ; ($P(C_2H_2)$) existing in the measurement. The bottom conditional probability table gives the probability of having arcing fault based on C_2H_2 ; ($P(\text{Arcing} | C_2H_2)$). The probability of arcing fault can be calculated using (3.4); in this case, $P(\text{Arcing} = T)$ is 0.26.

$$P(\text{Arcing} = T) = P(\text{Arcing} = T | C_2H_2 = T) \times P(C_2H_2 = T) + P(\text{Arcing} = T | C_2H_2 = F) \times P(C_2H_2 = F) = 0.1 \times 0.8 + 0.9 \times 0.2 = 0.26 \quad (3.4)$$

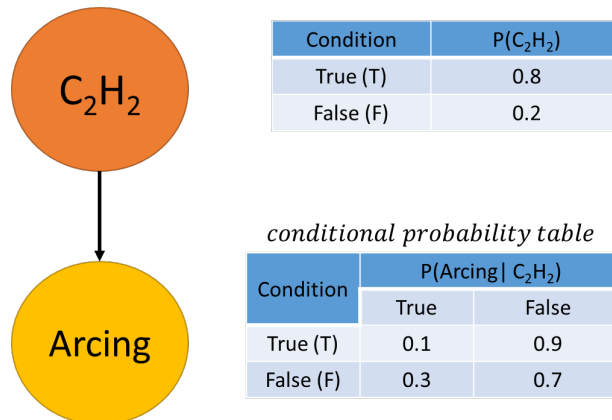


Figure 3.7 An example of Bayesian Network model.

The Bayesian Network replaces the crisp decision bounds with probabilities and enables the integration of expert's knowledge [183].

Naïve Bayes: Naïve Bayes is a probability classification algorithm that is also based on Bayes theorem [137]. It assumes all features conditionally independent of each other [217]. The Naïve Bayes equation used for DGA arcing fault detection can be expressed by (3.5), where the conditional probability of each

feature is calculated and multiplied [225]. Naïve Bayes is easy to model and suitable for large data sets [217].

$$P(Arcing|H_2, C_2H_2) = P(H_2|Arcing) \times P(C_2H_2|Arcing) \times P(Arcing) \quad (3.5)$$

Artificial Neural Network (ANN): The fundamental of ANN is to imitate human brain neural networks, using interconnected neurons to process condition monitoring parameters and determine the transformer condition. The basic architecture of ANN is based on three main layers: an input layer, a hidden layer and an output layer as shown in Figure 3.8 [186]. The input signals feed-forward the network and adjust the weight twice using w_{ij} , w_{jk} . If the output is different from the actual output, the signal can propagate backward through the network to re-adjust the weights. In some papers, ANN is referred to only feed-forward network. With back-propagation algorithm, it is called Back-propagation Neural Network (BPNN) [205] [226] [227].

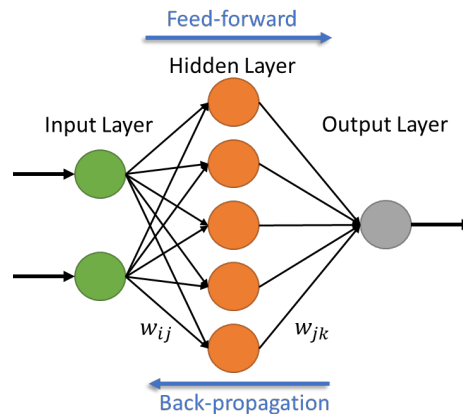


Figure 3.8 Basic structure of Artificial Neural Network.

In recent years, deep learning methods, which are based on neural networks, have attracted the attention of many researchers. One typical method is called Convolutional Neural Network (CNN), in which only some neurons in a layer are connected to the next layer [141, 228, 229]. Another commonly known deep learning method is the Adaptive Neuro Fuzzy Inference System (ANFIS) that combines ANN with Fuzzy Logic. ANFIS model combines the calculational capability of ANN and the logic capability of Fuzzy Logic [184]. The typical architecture of ANFIS comprises five layers as shown in Figure 3.9 [230-232]. Layer 1 is the fuzzy layer, which uses membership functions (MFs) to fuzzifier the input variables [233, 234]. Layer 2 is the product layer, which calculates the firing strengths of the fuzzy rules that is calculated by multiplying all MFs. Layer 3 is the normalized layer, which normalizes the firing strengths by calculating the ratio of a rule's firing power to the sum of all rules' firing strength. Layer 4 is the de-fuzzy layer, and layer 5 gives the overall output.

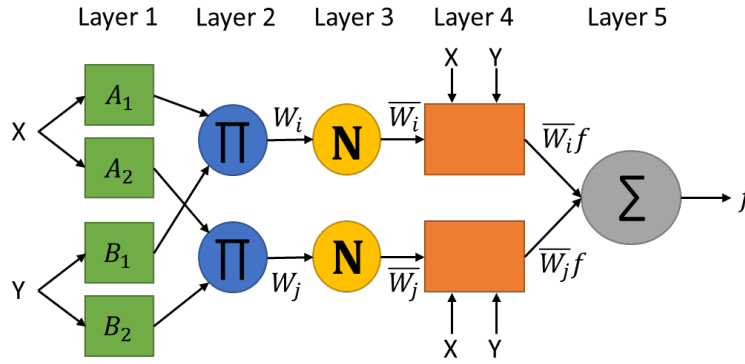


Figure 3.9 Basic structure of ANFIS model.

Neural networks (NNs) used for fault diagnosis have grown substantially in recent years. According to Table 3.4, NNs can be implemented for different condition monitoring methods. Although the hidden layers are not visible to users, NNs are able to develop complex non-linear relationships between condition parameters and fault types.

AI algorithms developed for power transformer fault detection are designed to analyse the condition monitoring data automatically. The fault diagnostic module is able to pick up possible fault signals and offers opportunities for early intervention through patterns found in previously trained data. However, the major limitation of AI methods focuses on the availability of training and testing data. Balanced training and testing data need to include not only the normal condition but also all types of fault condition. Practically all these data are not always available, which can be the main barrier for engineers to implement AI methods.

3.3. Reliability Assessment

In the previous section, the fault diagnostic module was introduced as a crucial part of asset management. The fault diagnosis function assesses the condition of individual transformer components. Information provided by fault diagnosis is not enough for maintenance plans, and the asset management team needs to evaluate hundreds and thousands of pieces of equipment. The reliability assessment module becomes another important part of asset management to ensure a certain level of power system reliability within an economic platform. Unlike fault diagnosis, reliability assessment examines the transformer's overall health and delivers a maintenance priority list. The most common practice in the power industry is to use the health index (HI) to define the overall health condition of power transformers [235].

3.3.1 Health Index

HI is a powerful tool which has been employed to assess the technical and operating state of the transformer [236]. HI integrates data from inspection, operating conditions and condition monitoring into a quantitative index to provide an overall health information to asset managers [235]. HI applied in reliability assessment is used to assess the long-term degradation level, prioritize critical equipment, and propose a maintenance plan through condition parameters data.

3.3.1.1 Health Index input parameters

The overall transformer health condition can be measured through different features. In the Current industry practice for HI algorithms, emphasis is placed on insulation system testing [4, 237]. The three major HI factors, namely, DGA factor (DGAF), Oil Quality factor (OQF) and Paper Insulation factor (PIF) collect data through routine oil sampling tests [218, 238, 239]. As depicted in Figure 3.10, the seven input parameters from the DGA test are the concentration of H₂, CH₄, C₂H₂, C₂H₄, C₂H₆, CO and CO₂. The typical input parameters from an Oil Quality test are breakdown voltage (BDV), interfacial tension (IFT), acidity, water content, colour and dissipation factor (DF) [239]. The Paper insulation factor is generally determined by 2-FAL furan compound.

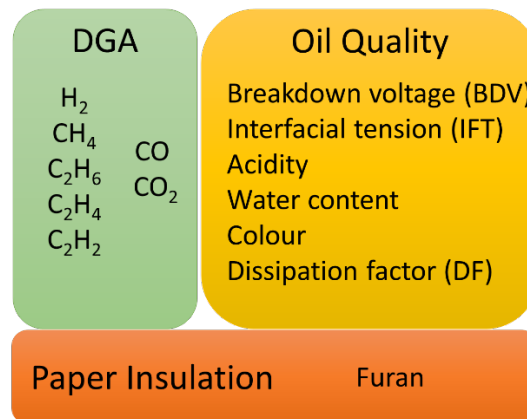


Figure 3.10 HI model used by current industry practice.

Prior research has seen the proposal of numerous features for the implementation of HI model by various authors. In [4], a total of 24 features have been listed. The load history has also been recognized as a critical feature in HI modelling. In [135], the condition of the tap changer was incorporated into the HI index and in [235, 240], the condition of the bushing has been added. Furthermore, data elements such as maintenance history and age, have been also leveraged as HI features [240, 241].

The process of selecting features for the HI model necessitates careful consideration of the failure modes relevant to a specific transformer assessment. This involves the utilization of various condition assessment techniques to evaluate a failure mode. The failure modes can be categorized based on their criticality, including oil criticality, paper criticality, and electrical criticality, as elucidated in the following sections.

3.3.1.2 Health index output scores

The majority HI scores are typically depicted within the range of 0 – 100 (or 0% - 100%), where “0” means the highest probability of a failure event and “100” means the transformer is in optimal health with the lowest failure probability [242-246]. Some scholars adopt a numerical rating ranging from 0 to 1, where 0 means optimal health with the lowest failure probability [247]. Based on HI score, the overall transformer condition can be classified into different states such as “Very poor”, “Poor”, “Fair”, “Good” and “Very Good”.

3.3.2 Health index algorithms

So far, various HI algorithms such as the scoring-weighting method, probability of failure method, AI-based methods, and Markov method have been presented in the literature. These methods are explained below.

3.3.2.1 Summation of individual failure mode scores with weighting factor

The basic HI calculation method is to score individual failure modes and then sum up all failure modes scores to give an overall health condition rating. This scoring-weighting method can be presented by a normalized equation as given by (3.6) [134]. The purpose of using weight factors here is to highlight the priority of some failure modes. For example, according to CIGRE WG 12-05, unexpected failure of OLTC can lead to catastrophic consequence [248]. By assigning 40% weight to the OLTC condition and 60% weight to the condition of remaining components within the transformer, the importance of possible failures in OLTC can be emphasized [4].

$$HI = \frac{\sum_{i=1}^N W_{FM_i} \times S_{FM_i}}{\sum_{i=1}^N W_{FM_i}} \quad (3.6)$$

N is the total number of failure modes.

S_{FM} is the score of an individual failure mode.

W_{FM} is the weighting per failure mode.

As previously mentioned, given the crucial significance of oil and paper conditions, HI algorithm is scored based on DGAF, OQF, and sometimes PIF, as illustrated in Figure 3.11. These parameters are scored based on IEEE, IEC and CIGRE standards such as IEEE C57.104 and IEEE C57.106. The weight assigned to each parameter W_i and the respective test WF_i are determined through a combination of survey reports, statistical analysis, and expert knowledge.

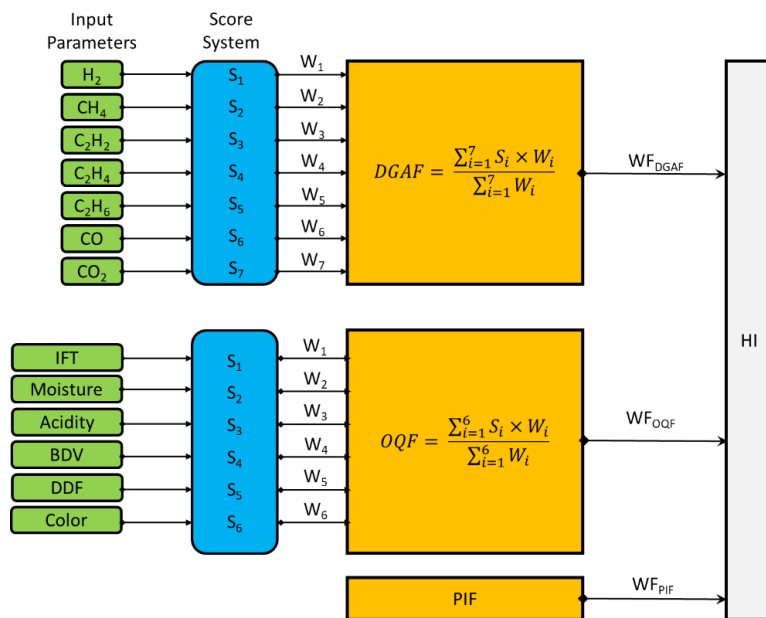


Figure 3.11 Scoring-weighting method used in industry.

The overall HI rating in percentage is calculated as a cumulative sum of the three factors with their corresponding weights as given by (3.7) [136, 245].

$$HI = \frac{\sum_{i=1}^N (S_i \times WF_i)}{\sum_{i=1}^N (S_{i-max} \times WF_i)} \times 100\% = \frac{(DGAF \times WF_{DGAF}) + (OQF \times WF_{OQF}) + (PIF \times WF_{PIF})}{4 \times (WF_{DGAF} + WF_{OQF} + WF_{PIF})} \times 100\% \quad (3.7)$$

S_{i-max} is the maximum score of each test.

The scoring-weighting method is a simple algorithm as it allows weighting factors to highlight common failure modes. However, the weights may not be updated regularly according to changes in operating, aging, and health condition of power transformers. Furthermore, scoring tables from different standards may result in different HI ratings. Another major limitation of this method is that accuracy is heavily dependent on the data availability.

3.3.2.2 Probability of failure

The probability of failure method is worth mentioning here due to its simplicity. If the probability of each failure mode is known from the fault diagnostic module and historical data, this method can provide approximate failure probability using (3.8) [134, 249].

$$HI = 1 - ((1 - est. PoF_{FM1}) \times (1 - est. PoF_{FM2}) \times (1 - est. PoF_{FM3}) \times \dots (1 - est. PoF_{FMn})) \quad (3.8)$$

n is the total number of failure modes.

$est. PoF_{FMi}$ ($i = 1 \sim n$) is the estimated probability of each failure mode.

Assuming that DGA and Furan tests have been used for failure modes 1 and 2, respectively, then $est. PoF_{FM1}$ is the estimated probability of DGA failure mode and $est. PoF_{FM2}$ is the estimated probability of Furan failure mode. If $est. PoF_{FM1}$ is approximately 10% and $est. PoF_{FM2}$ is approximately 20%, then according to (3.8), HI is 0.28 or 28%. If DGA result shows an increased failure rate from 10% to 60%, then HI value also increases to 68%. Although this method provides only approximate probability of HI, it has the advantage of not masking any failure mode over the scoring-weighting method.

3.3.2.3 Artificial intelligence methods

AI-based HI algorithm does not require a pre-defined formula. It uses analytic data techniques to find a new correlation between transformer condition indicators and HI classes: Very poor, Poor, Fair, Good, and Very Good. Many scholars have proposed several AI-based methods to enhance the HI algorithm. Table 3.5 lists some of the proposed AI methods used to build HI algorithms.

Table 3.5 AI methods used for HI algorithm.

AI methods	Input Variables	References	Remarks
Logistic Regression	DGA, DF, Moisture, Acidity, BDV, 2-FAL	[250]	<ul style="list-style-type: none"> Provides explicit probability of HI giving feature vector.
General Regression Neural Network (GRNN)	DGA, DF, 2-FAL, Dielectric strength, Moisture, Acidity	[236]	<ul style="list-style-type: none"> Multi-dimensional measurements combine through an optimal scoring-weighting system.
	DGA, 2-FAL, Acidity, IFT, Moisture, BVD, Insulation Resistance, PF, Turn Ratio, winding resistance, short circuit impedance, excitation current, Bushing – age, DDF, tap changer type and operations per month, loading and maintenance history	[240]	<ul style="list-style-type: none"> Allow using small training sets. Simpler algorithm to implement than SVM. Condition of transformer subsystems estimated using GRNN. Condition scores for each subsystem are delivered by using GRNN. Overall HI is non-linear combination of condition scores for each subsystem by using additive and multiplicative means.
Fuzzy Logic	DGA, Furan (2-FAL), moisture, acidity, BDV, DF	[251]	<ul style="list-style-type: none"> Results highly closer to experts' diagnosis. Hard to determine the membership functions.
	DGA, Furan, DF, Moisture, Acidity	[252]	
Fuzzy C-Means	Inaccurate and uncertain data	[237]	<ul style="list-style-type: none"> Help with database construction, assigning oil characteristic record with weight to a particular HI level.
Decision Tree	DGA, BDV, IFT, Acidity, Moisture, Colour, DF, 2-FAL	[218]	<ul style="list-style-type: none"> In general, it has lower accuracy than SVM and KNN.
KNN	DGA, BDV, IFT, Acidity, Moisture, Colour, DF, 2-FAL	[218, 253]	<ul style="list-style-type: none"> Easy to implement, but poor performance if the predictor variables increase or the number of relevant attributes is low. Non-parametric method, its performance doesn't vary significantly depending on distribution pattern of data. Robust to noise. Can be time-consuming during the classification phase.
SVM	DGA, BDV, IFT, Moisture, DF, 2-FAL	[254] [255]	<ul style="list-style-type: none"> Non-linear classifier for large dimension of independent variable. Possible deterioration if dimension is too large relative to the size of training data. SVM works better with optimization techniques.
ANN	DGA, IFT, Moisture, Acidity, BDV, DDF, Colour, Furan	[239]	<ul style="list-style-type: none"> Simplify the process of data training. Fast diagnosing speed. Performance depends on the completeness of the training sample. The process is not visible. Oscillation easily occurs in the identification.
ANFIS	DGA, BDV, DF, Acidity, IFT, Moisture in oil and paper, 2-FAL	[256]	<ul style="list-style-type: none"> ANFIS provides more accurate results than ANN.

The advantage of using AI algorithms for HI classification can avoid the direct calculation of HI scores based on empirical weighting factors. Therefore, this can increase the accuracy by not applying crisply defined ranges to determine HI classes.

3.3.2.4 Markov model

The above HI methodologies focus on calculating HI score/classification based on the transformers measured conditions. In some research papers [244, 257, 258], the Markov model has been proposed to predict the future HI state based on the current HI state. The future state of HI can be expressed by (3.9). The transition probability P denotes the probability of transitions to the next state.

$$HI(t + 1) = HI(t) \times P^{(t)} \quad (3.9)$$

$HI(t)$ is the current state HI at time t .

$P^{(t)}$ is the transition probability matrix at time t .

3.4. Life Management

The designed lifespan for oil-immersed power transformer is generally 25 - 40 years [259]. Due to the harsh operating conditions of in-service power transformers, the aging degradation rate increases, causing earlier retirement. Life management, as one of asset management's significant tasks, is designed to recognize the level of degradation and estimate the remaining lifespan of the transformer under current conditions. The remaining lifespan calculation predicts time intervals between fleets' service life, allowing businesses to replace them gradually [260].

From the business point of view, the definition of End of Life (EoL) can be divided into three categories: economical EoL, strategic EoL and technical EoL [261]. An example of economical EoL is when maintenance cost is too high, i.e., economically, it is no longer worth maintaining the transformer. Examples of strategic EoL could be power network upgrades or the obsolescence of critical components. This section will focus on technical assessment, and the methods used to estimate the degree of deterioration of power transformers. When the deterioration reaches a level where the transformer is too risky to be in operation, it is defined as technical EoL.

The degradation of components such as bushings, tap-changers, tank, cooling systems, and active parts (magnetic core, windings, and insulation) can cause gradual reduction in the dielectric, mechanical and thermal strength. Even under normal operating conditions, losing strength may eventually end the transformer's life. Without economic considerations, replacing or refurbishing the above-mentioned components, apart from the active parts, is possible. Therefore, in previous studies, calculating the remnant life of oil-immersed power transformers is mainly focused on winding solid insulation. The solid insulations including paper, pressboard and wood are made of cellulosic materials [262]. The chemical decomposition of cellulose is caused by oxidation, hydrolysis and pyrolysis mechanism [148, 263]. Hence, the degradation of cellulose is strongly influenced by the level of oxygen, water content and thermal conditions. The oxygen and water contents are considered to be controllable by using modern oil

preservation systems with improved sealing systems [264]. The thermal stress is considered to dominate the degradation process [265]. The hotspot temperature inside the transformer can cause the most significant aging. Therefore, the winding hot-spot temperature (HST) is the main factor determining the insulation lifespan.

3.4.1 Thermal-based Method

The thermal methods introduced in IEEE Std C57.91 and IEC 60076.7 can be used to estimate the percentage loss of life (% Loss of Life) of the insulation through calculating the aging acceleration factor F_{AA} [18, 266]. The calculation of the aging acceleration factor is based on the winding HST and the Arrhenius reaction rate theory [264].

Equation (3.10), which is presented in IEEE Std C57.91 is practically applied for thermally upgraded paper. It commonly uses a reference HST of 110 °C for 65 °C average winding rises [18, 267]. It means the value of the accelerated aging factor is greater than 1 for a winding reference HST over 110 °C; and less than 1 for a temperature below 110 °C.

Equation (3.11) that is presented in IEC 60076.7 (AS/NZS 60076.7) is practically applied for non-thermally upgraded paper (Kraft paper). The reference HST is 98 °C when the aging acceleration factor F_{AA} is equal to 1 according to Table 2 in the standard. The IEC standard also defines that the relative aging rate is doubled for every 6 °C increase in HST.

$$\begin{array}{l} \text{For thermally upgraded} \\ \text{paper} \end{array} \quad F_{AA}(t) = e^{\left[\frac{15000}{110+273} - \frac{15000}{\theta_{HST}(t)+273} \right]} \quad (3.10)$$

$$\begin{array}{l} \text{For non-thermally upgraded} \\ \text{paper} \end{array} \quad F_{AA}(t) = 2^{\frac{\theta_{HST}(t)-98}{6}} \quad (3.11)$$

$\theta_{HST}(t)$ is the winding hottest-spot temperature (C°) at time t .

The equivalent aging factor of the transformer for the total time is calculated by (3.12) according to IEEE Std C57.91. Usually, it uses a total period of 24-hour cycle, then $\sum_{n=1}^N \Delta t_n$ is 24.

$$F_{EQA} = \frac{\sum_{n=1}^N F_{AA,n} \Delta t_n}{\sum_{n=1}^N \Delta t_n} \quad (3.12)$$

F_{EQA} is the equivalent aging factor for the entire period.

n is the index of the time interval Δt .

N is the total number of time intervals.

Δt_n is the time interval.

$F_{AA,n}$ is aging acceleration factor for the temperature that exists during the time interval Δt_n .

% Loss of Life is the lifetime of cellulose lost over time, which is calculated using the equivalent aging factor given by (3.13). The % Loss of Life is to be subtracted from the normal insulation life to estimate the remaining life of cellulosic paper. According to both IEEE (Table I.2 of IEEE C57.91) and IEC (IEC

60076.7, Table 3) standards, the minimum Normal Insulation Life is 180,000 hours (20.5 years) for a thermally upgraded insulation system at reference temperature of 110 °C.

$$\% \text{ Loss of Life} = \frac{F_{EQA} \times t \times 100}{\text{Normal Insulation Life}} = \frac{F_{EQA} \times 24 \times 100}{180\,000} \quad (3.13)$$

F_{EQA} is the equivalent aging factor for the total time-period.

The remaining useful life (RUL) at time t can be determined by using the previous state of the insulation paper and its current condition along with the process noise as given by (3.14) [161, 268, 269].

$$RUL(t) = RUL(t - 1) - F_{AA}(t) + w(t) \quad (3.14)$$

$w(t)$ is the process noise at time t .

The thermal models defined in the standards offer straightforward approaches for gauging insulation aging. Nevertheless, directly measuring the winding HST through sensors often proves to be cost-prohibitive. Instead, it is typically estimated using other measurements and relevant factors. In accordance with IEEE Std C57.91, the HST θ_{HST} can be calculated using top-oil temperature (TOT) θ_{top} measurement. The TOT can also be estimated through the ambient temperature as per equation (3.15).

$$\theta_{HST} = \theta_{top} + \Delta\theta_{HST} = \theta_{amb} + \Delta\theta_{top} + \Delta\theta_{HST} \quad (3.15)$$

θ_{top} is the top-oil temperature (°C).

θ_{HST} is the winding hotspot temperature (°C).

θ_{amb} is the average ambient temperature during the load cycle to be studied (°C).

$\Delta\theta_{top}$ is the top-oil rise over ambient temperature (°C).

$\Delta\theta_{HST}$ is the winding hotspot rise over top-oil temperature (°C).

In practice, the calculation of HST can be much more complex as the thermal conditions depend on the load, environmental and transformer conditions [161, 270]. All these uncertainties will result in errors in the TOT estimation, HST calculation and RUL prediction. It is worth mentioning that even a slight error like 2 °C in HST calculation can make about 20% difference in acceleration aging factor. Dynamic thermal models have been used to increase the accuracy of monitoring continuous temperature changes.

Kalman Filter: some research suggests a state estimation tool called Kalman filter for thermal modelling [270-272]. Kalman filter is an optimal recursive data-processing algorithm, which can optimally estimate the temperature. The principle of this mathematical model is shown in Figure 3.12. The thermal dynamics present the actual system and ambient temperature, and TOT can be measured in the real system. The thermal model aims to have the estimated HST value as close as possible to the actual HST value by comparing the estimated and measured TOT values. The controller gain K is to control the decay rate of the error function, which means offering a faster elimination of the error [272].

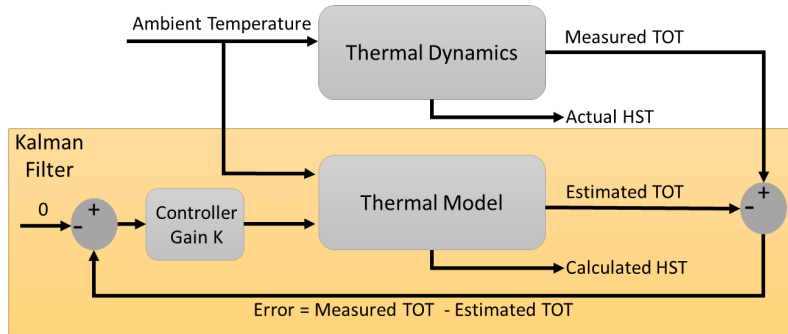


Figure 3.12 Using Kalman filter for thermal model.

The standard Kalman filter is only designed to model linear relationships with Gaussian noise, which does not change with time [272]. However, the correlation of the TOT with its relevant parameters, such as temperature and load is non-linear [161]. To address non-linear conditions, the Extended Kalman Filter (EKF) and Unscented Kalman Filter (UKF) have been developed. The drawback of this recursive algorithm is the problem of handling long-term predictions by accumulating prediction errors.

Although computational methods can improve the accuracy of the thermal model, the function of temperature and time from IEEE or IEC is based on a well-dried and oxygen-free insulation system [148]. Alternatively, the transformer's water and oxygen content remain constant, and in reality, most in-service transformers are not operating under such perfect condition [268]. The following section introduces another thermal method considering moisture and oxygen contents in oil.

3.4.2 DP-value method

3.4.2.1 Kinetic Model to predict DP-value

The thermal aging process of paper can also be assessed by measuring the Degree of Polymerization (DP). As mentioned, it is difficult to measure DP value directly. Therefore, the Kinetic model method assesses the degradation of cellulose using estimated DP value with consideration of the effects of moisture and oxygen contents [268]. The kinetics of cellulose degradation is calculated using (16) based on the pseudo-zero-order kinetic equation and Arrhenius reaction rate theory [153, 273]. The value “A” in the equation is decided by environmental factors like moisture content of the paper and dissolved oxygen in oil. While the value of A can be experimentally measured, it is not constant through the transformer life [162, 274]. Δt is the aging period. The value of “ E_a ” depends on the type of cellulose and chemical reaction [162]. From the International System of Units (SI), the gas constant R is $8.314 \text{ J.mol}^{-1}\text{K}^{-1}$. The temperature of the paper typically refers to the HST of winding as the hottest temperature causes the most degradation.

$$\frac{1}{DP(t)} - \frac{1}{DP(t-1)} = A_{(t-1)} \times \Delta t \times e^{\frac{-E_a}{R \times T(t-1)}} \quad (3.16)$$

$DP(t-1)$ and $DP(t)$ are the DP values at the start and the end of the period.

A is the environmental factor, which can depend on the moisture and oxygen content in oil at (t-1) where (t-1) is the previous state and t can be hours, days, or years.

Δt is the aging period.

E_a is the activation energy of the aging reaction (J.mol^{-1}).

R is the gas constant ($\text{J}\cdot\text{mol}^{-1}\cdot\text{K}^{-1}$).
 T is the temperature of the paper (K).

Rearranging (3.16), the expected life of the paper can be calculated as below equation (3.17) [265].

$$\text{Expected Life } \Delta t = \frac{1}{\frac{DP(t)}{A_{(t-1)}} - \frac{1}{DP(t-1)}} \times e^{\frac{E_a}{R \times T(t-1)}} \quad (3.17)$$

Compared to the thermal models from IEEE/IEC standards, this model has the advantage of considering moisture and oxygen involvement. However, both the values of A and HST are complicated to be determined.

During paper degradation, cellulose breakdown also generates by-products; water, furan compounds and carbon oxides (CO , CO_2) [275]. These by-products dissolve into oil and can be measured through an oil sample testing. Equation (3.18) is the general formula used to calculate the DP-value based on condition monitoring data $M(t)$ including furan concentrations or the ratio of CO and CO_2 [273].

$$DP(t) = \frac{a - \log_{10}M(t)}{b} \quad (3.18)$$

a and b are constants that describe the linear relationship.

Extensive research has shown a correlation between the DP-value and the concentration of the 2-FAL furan compound [276]. Therefore, the 2-FAL analysis can also be utilized to determine the deterioration of the cellulosic insulation system.

Various methods have been developed to model the correlation between DP-value and 2-FAL. Equations (3.19) and (3.20) are the most widely used models [277]. Chendong model applies to non-thermally upgraded paper whereas Stebbins model is applied for thermally upgraded paper. However, the generation of 2-FAL is also depended on the type and quantity of the paper, and these two models do not consider the amount of degraded paper at any time [277]. In 1999, De Pablo developed a degradation model which can overcome the limitation of other models. Based on experimental laboratory data reported by De Pablo, every three cellulose chain scissions generate one 2-FAL molecule. This model is represented by (3.21) which was later validated and improved by Serena [278]. Another improved model given by (3.22) is called De Pablo model 2 or the Pahlavanpour model [154]. The advantage of this model is that it can consider the different degradation rates of winding paper, i.e., effect of hot spots. These models are summarized in Table 3.6.

Table 3.6 various DP-Furan correlational models.

Chendong model: For non-thermally upgraded paper	$DP = \frac{\log_{10}(2\sim\text{FAL}_{\text{ppm}}) - 1.51}{-0.0035}$	(3.19)
Stebbins model: For thermally upgraded paper	$DP = \frac{\log_{10}(2\sim\text{FAL}_{\text{ppm}} \times 0.88) - 4.51}{-0.0035}$	(3.20)

De Pablo model: consider the quantity of the paper	$DP = \frac{7100}{8.88 + (2 \sim FAL_{ppm})} \quad (3.21)$
---	--

Pahlavanpour model: consider the different degradation rate for winding paper at different locations	$DP = \frac{800}{0.186 \times (2 \sim FAL_{ppm}) + 1} \quad (3.22)$
---	---

Furan analysis is one of the most popular methods for thermal aging estimation [279]. However, over the years, many cases prove that the concentrations of 2-FAL in the operating transformer oil samples are much lower than laboratory data for the same DP-value [279]. The correlation between furan compounds and DP depends on many other factors, such as the type and quality of oil/paper and ambient conditions (e.g., moisture) [265, 276, 279]. The above models have been established in the laboratory environment. Therefore, instead of performing sole furan analysis, combining such models with other oil diagnostic methods is more useful.

3.4.2.2 AI methods to predict DP-value

AI methods have also been used in predicting DP. New models employing data from realistic conditions have been presented in recent studies [149, 280]. The new general formula given by (3.23) can be established using regression analysis. In [207], ANFIS was employed to estimate DP-value based on 2-FAL, CO and CO₂ measurements.

$$DP = a \times \ln(2 \sim FAL_{ppb}) + b \quad (3.23)$$

a and *b* are constant developed in regression analysis.
 1 ppb = 0.001 ppm

3.4.2.3 RUL calculation based on DP-value

According to IEEE C57.91 Table I.2, the End-of-Life Criteria recommended that if DP-value is 200, it is considered the end of paper insulation life. The remaining life of paper insulation in percentage (%RUL) can be calculated using retained DP value as given by (3.24) [147, 281] and (3.25) [147]. In (3.24), it is assumed that the degradation starts when DP is 622; while this value is changed to 820 when using (3.25).

$$\% RUL = 1 + 88.1 \ln \left(\frac{DP}{622} \right) \quad (3.24)$$

$$\% RUL = 1 + \frac{[\log_{10}(DP) - 2.903]}{-0.006021} \quad (3.25)$$

Some scholars have proposed using AI methods directly to predict the transformer age from condition monitoring sensors. For example, in [150] [282], RUL can be estimated using ANFIS and ANN based on oil testing results.

3.5. Future Improvement areas

Current industry practice in the field of asset condition monitoring and fault diagnosis still relies on personnel expertise, which may result in inconsistent interpretation and recommended asset management actions. AI methods are the future tools to automate and standardize asset management methods of oil-immersed power transformer. However, there are two areas that call for further development. One is to develop a suitable failure mode analysis method for the power transformers, and the second is to develop a proper hybrid AI-based mode that can provide proven accuracy regardless of the size and operating conditions of the transformer. These two areas are briefly elaborated below.

3.5.1 Failure modes definition

As mentioned above, no standardized failure modes are used for power transformer condition assessment. The failure modes can be constructed based on the source of fault, as shown in Figure 3.13 [283, 284]. However, implementation for such failure mode structure could be confusing. For example, thermal and electrical faults are closely related. Hence, it is hard to determine whether the fault is thermal or electrical originated. The failure mode structure can also be built based on location – winding, oil insulation, paper insulation, core, bushing, tap changer, cooling system and tank [134-136, 224, 285, 286]. It seems clear to choose the condition monitoring method for individual components and locate the fault. However, this calls for an extensive number of sensors to be installed. In most cases, this is not a cost-benefit for businesses. Some research efforts have been conducted to identify various faults in the transformer oil and paper insulation using fuzzy logic, ANFIS, and gene expression programming [64, 65, 287]. However, feasibility of these models has not been assessed in field application yet.

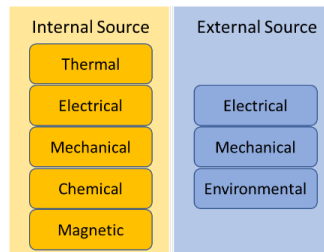


Figure 3.13 Sources of faults.

3.5.2 Hybrid models

In the above sections, only individual AI algorithms have been summarized. Due to significant measurements and history, using AI and minimizing human intervention seem to be the future for big data analysis. Researchers are continuously exploring the optimal AI methods, including hybrid models. Hybrid models integrate different AI algorithms into a single model, which can bring benefits from these algorithms and avoid their downsides. Some examples of the hybrid model are listed in Table 3.7. Although researchers have claimed, their new models improved the accuracy, such models do not seem to be a standard model that can work for all different datasets.

Table 3.7 Examples of hybrid model used in condition assessment.

References	Hybrid models	Remarks
[259]	Bayesian ordered regression & ANN	<ul style="list-style-type: none"> ➤ Classify HI into 5 classes (very bad, bad, moderate, good, very good) without calculating HI score. ➤ Easily adapted. ➤ Improved accuracy compared to some single AI methods. ➤ Full quantized uncertainty of its parameters and predictions. ➤ More efficient use of unsymmetrical datasets.
[288]	Unsupervised Clustering & supervised classification	<ul style="list-style-type: none"> ➤ Unsupervised ML Clustering used for feature extraction. ➤ Reduce the size of data and processing time.
[188]	Fuzzy Logic & decision tree	<ul style="list-style-type: none"> ➤ Avoid crisp decision tree rules
[289, 290]	Principal Component Analysis (PCA) & Particle Swarm Optimization (PSO) & SVM	<ul style="list-style-type: none"> ➤ PCA is used to reduce the dimension of data sets. ➤ PSO is used to obtain the optimal parameters for SVM algorithm.
[291]	Relevance vector machine (RVM) & ANFIS	<ul style="list-style-type: none"> ➤ RVM performs binary separation. ➤ ANFIS performs further fault diagnosis. ➤ Higher accuracy than single ANFIS, SVM and ANN.

3.6. Summary

Cost-effective and reliable transformer asset management techniques are essential to design strategic maintenance and replacement plans. Continuously improved technologies in condition monitoring and computational methods increase the opportunity to use condition-based maintenance. This chapter reviewed various methods used in condition assessment major modules: fault diagnostic module, reliability assessment module and life management module. In the fault diagnostic module, fault diagnostic methods according to individual transformer components have been introduced. However, the transformer condition could often be between normal and faulty conditions, which means that the measurements are not in the normal range but still acceptable in practice. Therefore, reliability assessment using HI is utilized to evaluate the overall health condition of the transformer. Calculating HI is commonly used in scoring-weighting and enhanced through Artificial Intelligence methods. In the life management module, the degradation of the insulation system has been a major indicator of End-of-Life for power transformers. The remaining service life of a transformer can be estimated through the degradation factors and other indicators.

Chapter 4 Deep Machine Learning-based Asset Management Approach for Oil-Immersed Power transformers using Dissolved Gas Analysis

4.1. Introduction

The reliable operation of a power system is largely dependent on the health condition and performance of its key equipment, particularly power transformers. Faults or malfunctions in a power transformer can directly impact the safety and reliability of the entire power grid. Therefore, it is essential to develop cost-effective asset management methods to assess its health condition and provide a timely decision to rectify emerging faults and avoid any potential catastrophic consequences. Over decades, many condition monitoring methods have been evolved to detect various faults in power transformers [5]. In industry practice, one of the most widely used methods for analysing power transformer oil to detect incipient faults is the Dissolved Gas Analysis (DGA) method [6]. This technique has been proven to be effective in identifying potential issues in power transformers and has become an essential asset management tool.

The fundamental principle of DGA is to measure the levels of various dissolved gases in the transformer oil. These gases are generated as a result of overheating, arcing and partial discharge events [7]. By analysing the type and concentrations of dissolved gases in transformer oil samples, potential faults can be identified, and rate of insulation degradation can be assessed, allowing timely maintenance and repair plans to prevent potential severe damages to the transformer. The measured dissolved gases in transformer oil include Hydrogen (H_2), Methane (CH_4), Ethylene (C_2H_4), Ethane (C_2H_6), Acetylene (C_2H_2), Carbon Monoxide (CO) and Carbon Dioxide (CO_2). These gases have been considered as key indicators of potential transformer faults, and their concentration can provide valuable insights into the overall health condition of the transformer.

Several conventional DGA interpretation methods, derived from ANSI/IEEE standard and IEC publication 599, have been extensively utilized in the power industry [7, 8]. These methods include Key gas method, Rogers Ratios, Doernenburg Ratios, Duval Triangles and Pentagons graphical methods. However, each of these methods exhibits certain limitations such as out-of-code ratios, distinct boundaries, and the exclusion of gas evolution, which may lead to incorrect and inconsistent fault diagnoses [9]. As a result, the accuracy of diagnostic results relies more on the level of experience of the professionals conducting the test. To overcome such subjective interpretations, researchers have developed several artificial intelligence (AI)-based methods to improve the diagnostic accuracy. In [9], various AI-based methods for DGA interpretation have been presented. One of the methods is Fuzzy Logic, which replaces the precise values of input-output variables with a range of values to handle the uncertainties and imprecisions in the DGA data [79, 158]. Other AI methods such as Decision Tree [175], Random Forest [176], k-Nearest neighbours (KNN) [177, 178], Logistic Regression [179, 180],

Support Vector Machine (SVM) [181, 182], Bayesian Network [183], Artificial Neural Network(ANN) [160, 185, 186], Adaptive Neural Fuzzy Inference System (ANFIS) [184, 187] have also shown promising results in enhancing the analysis of DGA data. These methods are designed for various levels of data complexity, often requiring the use of multiple training models to analyse DGA data comprehensively. For example, ANFIS model encounters difficulties and may get stuck in the training process. On the other hand, fuzzy logic requires ample number of fuzzy rules, which complicate and reduce the accuracy of the DGA models of multiple input and output parameters.

In recent years, another powerful AI tool called Deep Machine Learning algorithm has emerged to solve complex problems that were previously challenging for traditional AI methods. Deep learning is modelled to mimic the hierarchical structure of the human brain and is designed to process data in a similar way, starting with lower-level features and gradually building up to higher-level concepts [292]. By doing so, deep learning models are able to handle complex problems with large data sets. This has made them highly effective for a wide range of applications, including image and sound recognition.

As the concept of future smart grids continues to evolve, the online monitoring of key assets including power transformers has become more prevalent. This will lead to a substantial rise in the amount of sophisticated data being collected and analysed. Some of these raw data are presented in numerical form, while others may take the form of images or sound signals, such as vibration signals [141, 198]. This requires adaptable diagnostic methods with enhanced learning and feature extraction capabilities to effectively reflect meaningful insights from the measured data. In [325, 326], a specific type of deep machine learning called the probabilistic neural network with optimizer was developed to provide fault diagnosis in power transformers based on five DGA gas measurements. The output of the method identifies four potential fault conditions, including high/low temperature fault, partial discharge, and arc discharge.

This paper aims to provide a more comprehensive asset management solution for mineral oil-immersed power transformers. In addition to the fault diagnostic module, the developed asset management system also comprises a life management module to provide asset managers with the deterioration level of the solid insulation based on the amount of CO₂ and CO gases obtained from online DGA measurement sensors. The fault diagnostic module encompasses “no fault” condition, in addition to identifying thermal fault, arc discharge and partial discharge as will be elaborated below.

4.2. Methodologies Utilized in Developing the Asset Management Model

A. Data Pre-processing – Normalization

The aim of data normalization in the data pre-processing stage is to bring features onto a comparable scale to enhance the model performance and improve the training stability [293]. In the training datasets, the gas concentration exhibits a wide range from 0 to 100,000s ppm. To prevent the dominance of large values on training weights, which could potentially distort the training results [294], a commonly utilized normalization method called Minimum-Maximum normalization as given by (4.1) is employed [295]. The Minimum-Maximum normalization technique scales the data into a range between 0 and 1, based on the

minimum and maximum values in the datasets. Figure 4.1 (a) depicts the raw data distribution of H₂ gas measurements (in ppm) collected from an online DGA sensor, while Figure 4.1 (b) illustrates the data distribution after normalization. Comparison of the two figures shows that the normalization process does not alter the essential features of the collected data.

$$X_{nor} = \frac{X - X_{min}}{X_{max} - X_{min}} \quad (4.1)$$

where X , is the original value before normalization.

X_{nor} is the X value after normalization.

X_{max} and X_{min} represent the maximum and minimum of values of X value, respectively.

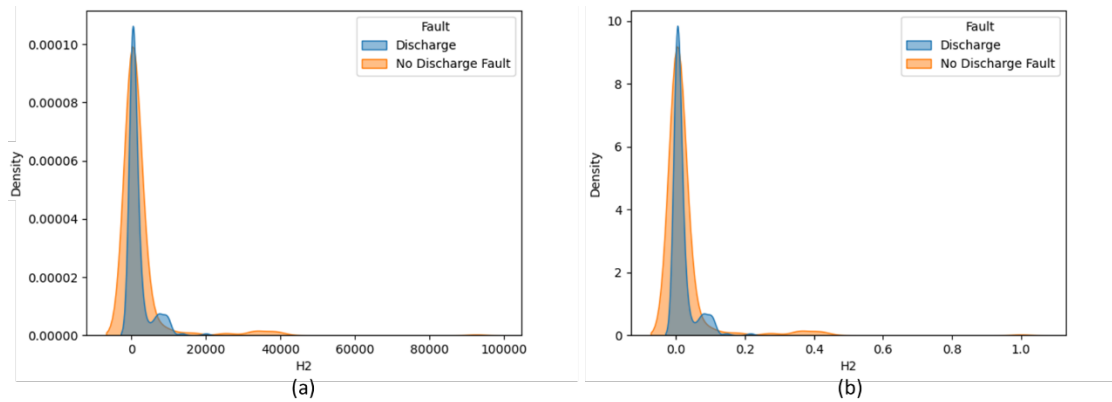


Figure 4.1 (a) Raw H₂ Data (in ppm) collected from DGA sensor. (b) Data processed using Minimum-Maximum normalization.

B. Data Pre-processing – Balance Datasets

The training datasets often exhibit uneven distribution, where minority classes are vastly outnumbered by majority classes. When the model is trained using such imbalanced dataset, machine learning algorithms tend to favour the majority classes, leading to potential misclassification of the minority classes [296]. Based on the datasets presented in Table 4.1, it can be observed that the various transformer conditions are not evenly distributed. Specifically, the occurrence of partial discharge faults constitutes a relatively small percentage of all conditions (accounting for only 8.7%). On the other hand, energy discharge faults and thermal faults are much more prevalent, comprising approximately 35% and 41.3% of the total conditions, respectively. Interestingly, the normal condition makes up 15.7% of the conditions, which is noteworthy given that in real-world scenarios, normal conditions tend to be the most commonly observed results [297]. The imbalance nature of the datasets could potentially have a significant impact on the outcomes of machine learning algorithms.

Another crucial issue that must be considered when utilizing machine learning algorithms is their ability to generalize beyond the training datasets. In the construction of the training datasets, the transformer fault types of transformers are typically identified based on the expert judgements, which are often derived from conventional interpretation methods such as IEEE/IEC ratio and Duval Triangles/Pentagons.

However, the heuristic nature of expert judgments, coupled with the fact that transformers may exhibit multiple faults simultaneously, can lead to varying degrees of inconsistency between datasets collected from different sources. This inconsistency in the training data can pose a significant challenge to the generalization capability of machine learning algorithms and may ultimately undermine their effectiveness in practical applications.

Table 4.1 Datasets for Fault Diagnostic module training.

Reference	Energy Discharge	No fault	Partial Discharge	Thermal Fault	Total # of samples
[178]	6	0	5	9	20
[184]	3	0	1	3	6
[158]	3	0	2	6	11
[230]	4	0	0	6	10
[290]	4	0	2	4	10
[234]	6	12	4	12	34
[87]	2	0	1	3	6
[298]	2	0	1	3	6
[299]	8	0	4	12	24
[300]	6	13	3	11	33
[301]	10	5	3	7	25
[302]	28	9	0	38	75
[303]	8	1	1	12	22
[186]	15	8	0	8	31
[291]	3	0	1	4	7
[167]	4	2	0	10	16
[183]	1	2	1	2	6
[304]	10	0	3	23	36
[305]	4	0	7	9	20
[306]	3	1	1	5	10
[307]	4	0	1	6	8
[308]	2	2	0	0	4
[309]	0	4	1	5	10
[310]	4	0	3	2	9
[8]	74	34	9	34	151
[311]	8	6	1	15	30
[6]	5	2	0	13	20
[312]	6	3	3	12	24
Total	233	104	58	274	664
Percentage	35%	15.7%	8.7%	41.3%	

(Note: In references [184], [291], and [307], the discrepancy between the total number of samples and the total number of conditions arises from some samples containing multiple conditions, resulting in overlapping counts.)

To overcome the above-mentioned issues of imbalanced data, Synthetic Minority Over-sampling Technique (SMOTE) has been implemented [313, 314]. The principle of SMOTE is to generate synthetic samples for minority classes. It begins by randomly selecting a data point from the minority class and identifying its k nearest neighbours. SMOTE then places a synthetic point along the line connecting the chosen data point and one of its nearest neighbours. These steps are repeated until the dataset is balanced, thereby ensuring a more even representation of all classes in the training data. Figure 4.2

presents a comparative histogram illustrating the effect of data balancing through SMOTE processing. Figure 4.2(a) provides an overview of the distribution of multi-class targets within the initial training dataset before the application of SMOTE. Each bin within the histogram corresponds to a distinct label. Specifically, the x-axis denotes the labels associated with the dataset. In this context, label “1” pertains to Thermal fault, label “2” signifies partial discharge (PD) fault, label “4” indicates No Fault, label “8” represents Discharge fault, and label “9” corresponds to a combination of Discharge and Thermal faults. The y-axis represents the frequency (number of instances) that belong to each label. On the other hand, Figure 4.2(b) shows the distribution of labels in the training data after applying SMOTE. As can be observed, the frequency of labels “2”, “4”, “8”, and “9” have been changed due to the introduction of synthetic samples.

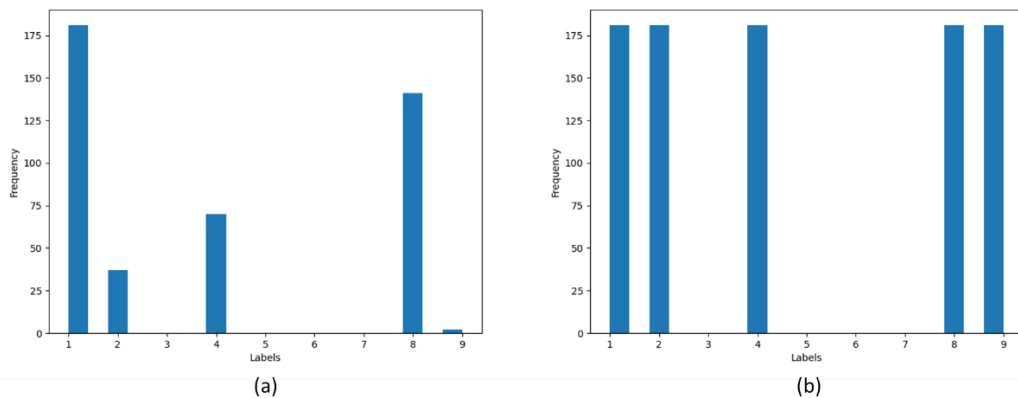


Figure 4.2 (a) Data distribution before SMOTE and (b) Data distribution after SMOTE. (for reference to label numbers, see Table 3)

C. Convolution Neural Network

Convolution Neural Network (CNN) has emerged as a popular and effective deep learning technique, particularly for analysing visual data [141]. In recent years, there has been growing interest in leveraging CNN for condition monitoring applications. A study published in [141] has utilized CNN to identify six types of PD faults in power transformers by analysing Phase-Resolved Partial Discharge (PRPD) signals captured by Ultrahigh Frequency (UFH) sensors. Another investigation in [198] focused on using CNN to assess transformer winding conditions through the analysis of vibration signatures. Furthermore, [315] explored the application of CNN in assessing oil quality based on oil aging images. Considering the future advancements and ongoing developments of online condition monitoring methods, CNN holds a great potential as a powerful tool that can provide more comprehensive condition assessment of power transformers in real-time. This will provide a more accurate and holistic understanding of transformer performance, facilitate timely maintenance interventions, and extend the operational lifespan of power transformers.

The structure of a CNN comprises two primary components: feature selection and neural network as shown in Figure 4.3. The feature selection layers encompass convolutional layers, pooling layers, batch

normalization layers, and flattened layers [316]. The convolutional layers play a significant role in feature extraction, applying filters or kernels to the input data to capture patterns and spatial dependencies. The pooling layers reduce the spatial dimensions of the resulting feature maps, effectively summarizing the learned features. The batch normalization layers normalize the outputs of the previous layers to enhance training stability and accelerating convergence. Finally, the flattened layers transform the multidimensional feature maps into a one-dimensional vector. This process prepares the extracted features for further processing in neural network. The feature selection process in CNN provides the key advantage over traditional machine learning algorithms, such as Support Vector Machine (SVM). CNN can autonomously learn intricate features and patterns directly from the raw input data, eliminating the need for manual feature engineering. This capability significantly reduces the burden of feature extraction and enhances the overall efficiency of the model.

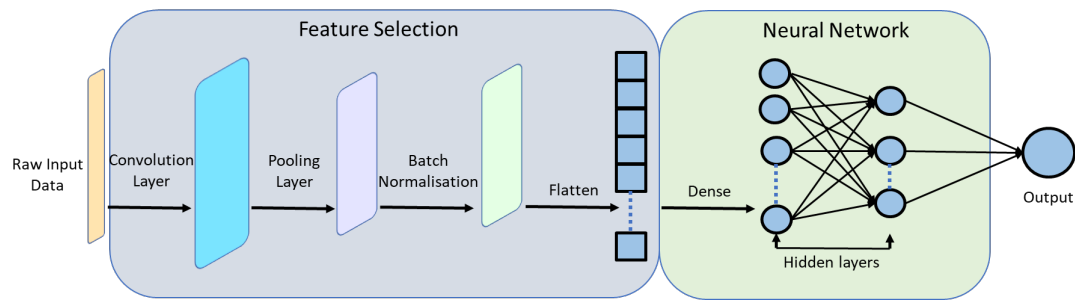


Figure 4.3 The structure of Convolution Neural Network.

The neural network component comprises fully connected layers, which integrate the extracted features and make predictions based on the learned representations. In Figure 4.4, a neural network with 2 hidden layers is depicted. The inputs $x_1 \dots x_i$, contain the features of the input data that are fed into the network. Within the hidden layers, each neuron takes input from the previous layer, applies a weight (i.e., w_{ij} or w_{jk}) and a bias (i.e., b_j or B_k), and passes the results through an activation function as presented by (2). During the training process, the backpropagation algorithm determines the weights along with biases of the neural network to minimize the error of difference between the predicted output and the target or desired output. This adjustment is performed using an optimization algorithm, such as Adaptive Moment Estimation. The optimization algorithm updates the weights based on the calculated error and the network's learning rate, which controls the step size of the weights updates.

Activation functions play a critical role in transforming the weighted sum of inputs and bias into an output value. For example, the Rectified Linear Unit (ReLU) activation function is commonly used in neural networks which results in the input value if it is positive, and zero otherwise. Another example is Sigmoid function, which squashes the input value into a range between 0 and 1, in case output needs to be interpreted as probabilities.

$$Y_j = f_1\left(\sum_{j=1}^i (w_{ij} \times x_i + b_j)\right) \quad (4.2)$$

where, Y_j is the output of the first hidden layer.

x_i is the input.

f_1 is the activation function.

w_{ij} is the weight.
 b_j is the bias.

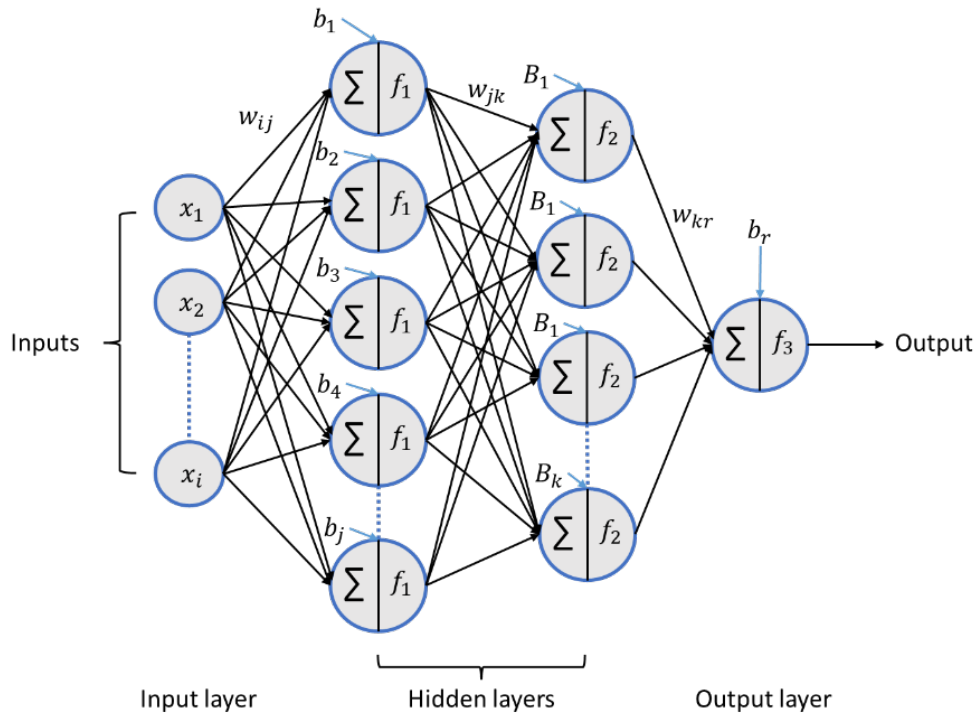


Figure 4.4 General structure of neural networks with 2 hidden layers.

4.3. Proposed Asset Management Model

The asset management approach proposed, as depicted in Figure 4.5, utilizes gas measurements acquired from an online DGA sensor. This model consists of two distinct sub-modules: a Fault Diagnostic module and a Life Management module.

In this section, a detailed explanation of the training process for each module is presented, along with insights into the possible outputs derived from these modules.

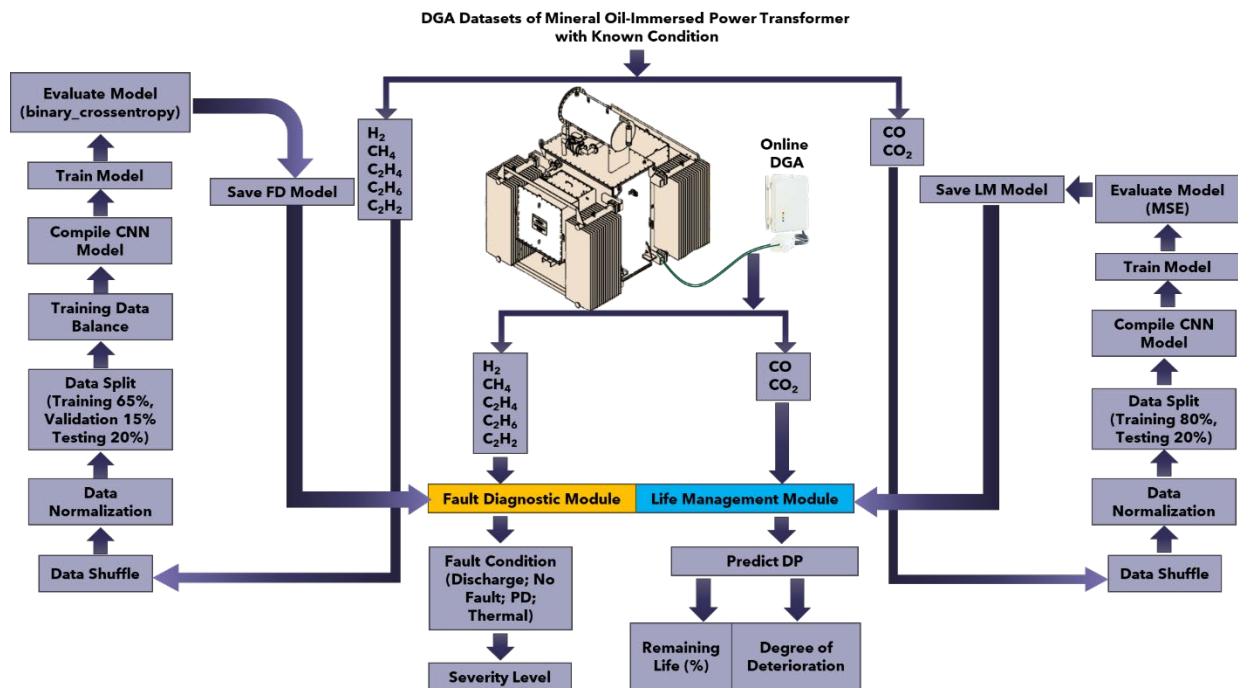


Figure 4.5 Proposed workflow for the oil-immersed power transformer asset management model.

A. Fault Diagnostic module

There are six primary types of faults that can be identified using DGA method, as outlined in Table 4.2 based on the IEC 60599 and IEEE57.104 [3]. Due to the limited information available in the datasets, fault types have been classified into three broader categories: Partial Discharge (PD), Energy Discharges and Thermal Faults.

Table 4.2 Six fundamental types of faults diagnosed using DGA.

Code	Primary Faults
T1	Thermal fault; $T < 300^{\circ}\text{C}$
T2	Thermal fault; $300^{\circ}\text{C} < T < 700^{\circ}\text{C}$
T3	Thermal fault; $T > 700^{\circ}\text{C}$
D1	Low energy discharge
D2	High energy discharge
PD	Corona Partial Discharge

Partial Discharge occurs when a localized area of solid or fluid insulation material, exposed to high voltage stress, undergoes a partial breakdown without fully bridging the gap between two conductive materials [7, 137, 317]. In this context, PD specifically refers to corona-type PD that transpire within gas bubbles or

voids. During PD activities, air or nitrogen in the gas phase undergoes ionization, forming a plasma of ionized oxygen and nitrogen atoms. This plasma interacts with the surrounding oil or cellulose, leading to the generation of hydrogen as the primary by-product.

Energy Discharges in oil-immersed power transformers occur when there is an energy discharge that creates a localized conducting path or short circuit between conductive materials [7, 137, 317]. This leads to sparking around loose connections within the transformer. When low energy arcs, denoted as D1 in Table 4.2, occur in transformer oil, only a thin layer of the oil makes contact with the path of the arc. The high temperature of the arc, exceeding 3000°C, causes decomposition of this small oil layer. The decomposition primarily yields acetylene, with traceable amounts of ethylene being produced. In contrast, high energy arcs, referred to as D2 in Table 4.2, involve a greater current flowing through the arc path, resulting in a longer duration. The extended duration allows for a larger volume of oil to be heated by the arc. The convective flow of cooler surrounding oil contributes to this process. Consequently, a significant temperature gradient is established in the oil surrounding the arc path, ranging from around 3000°C to 500°C. Interestingly, despite the higher energy content of D2 arcs, their average oil temperature is lower compared to D1 arcs. However, D2 arcs generate a substantial amount of ethylene in addition to acetylene due to the temperature gradient and longer duration of the arc.

Thermal Faults in oil-immersed power transformers arise from the circulation of electric current within the insulating paper due to excessive dielectric losses [7, 137, 317]. Thermal faults can be classified into three categories: T1, T2 and T3. T1 fault occurs when there is an increase in the average winding temperature, typically caused by increased load or ambient temperature. T2 fault, on the other hand, involves localized hotspots within the winding, resulting from electrical contact or excessive current density. Localized hotspots generate higher temperatures, which accelerate the insulation aging and compromise the transformer's overall performance. Lastly, T3 fault encompasses more severe conditions, such as arcing or short circuits, which cause significant temperature rise and pose an immediate risk to the transformer's operation and safety.

The proposed Fault Diagnostic module shown in Figure 4.5 employs CNN to analyse the measurements of five gases: H₂, CH₄, C₂H₄, C₂H₆, and C₂H₂. As introduced in the previous section, CNN has proven to be highly effective in processing complex data, making it ideal candidate for fault diagnosis in power transformers. Based on the concentrations of these gases, the module classifies the transformer's condition into four fundamental categories: "Discharge", "No Fault", "PD", and "Thermal". Moreover, the module is capable of diagnosing combined fault conditions, such as "Discharge and Thermal Faults", adding further versatility to improve diagnostic accuracy.

In the context of enabling the module for multi-label classification tasks, a binary representation, as shown in Table 4.3 has been adopted. The proposed approach utilizes a four-digit binary representation based on 2ⁿ, where 'n' is set to four in this application, accommodating the representation of up to sixteen possible cases.

Table 4.3 Possible conditions represented using binary numbers.

Case	Discharge	No Fault	PD	Thermal	Diagnosis
0	0	0	0	0	No Fault
1	0	0	0	1	Thermal Fault
2	0	0	1	0	PD Fault
3	0	0	1	1	PD, Thermal Fault
4	0	1	0	0	No Fault
5	0	1	0	1	Thermal Fault
6	0	1	1	0	PD Fault
7	0	1	1	1	PD, Thermal Fault
8	1	0	0	0	Discharge Fault
9	1	0	0	1	Discharge, Thermal Fault
10	1	0	1	0	Discharge, PD Fault
11	1	0	1	1	Discharge, PD and Thermal Fault
12	1	1	0	0	Discharge Fault
13	1	1	0	1	Discharge, Thermal Fault
14	1	1	1	0	Discharge, PD Fault
15	1	1	1	1	Discharge, PD and Thermal Fault

Based on the output of the Fault Diagnostic module, an asset management decision will be provided to users with the severity level as listed in Table 4.4.

Table 4.4 Fault Diagnostic module outputs and corresponding Asset Management statement.

Fault Diagnostic Module Output	Asset Management Statement – severity level
No Fault	“No Fault detected, very low likelihood of failure.”
PD	“Sign of Partial Discharge fault, low risk of failure.”
Thermal Fault	“Sign of Thermal fault, moderate risk of failure”
PD and Thermal Faults	“Sign of Thermal fault, moderate risk of failure”
Discharge Fault	“Sign of Discharge fault, very high risk of failure.”
Discharge and Thermal Faults	“Sign of Discharge fault, very high risk of failure.”
Discharge and PD Faults	“Sign of Discharge fault, very high risk of failure.”
Discharge, PD and Thermal Faults	“Sign of Discharge fault, very high risk of failure.”

B. Life Management module.

The life expectancy of power transformers predominantly relies on their paper insulation [5]. The composition of transformer paper is primarily comprised of 90% cellulose by weight. Cellulose is an

organic compound characterized by lengthy chains of glucose rings, typically ranging between 1000 to 1200 per chain for new paper [5]. The Degree of Polymerization (DP) refers to the average number of glucose rings present within each chain. Based on experience, it is commonly considered that transformers reach their end-of-life when the DP of paper declines to 200, which means the tensile strength decreases to approximately 40% of its initial value [58, 59]. However, measuring DP requires a paper sample from the transformer, which is not feasible for in-service transformers.

The life expectancy of power transformers predominantly relies on their paper insulation [9]. The composition of transformer paper is primarily comprised of 90% cellulose by weight. Cellulose is an organic compound characterized by lengthy chains of glucose rings, typically ranging between 1000 to 1200 per chain for new paper [9]. The Degree of Polymerization (DP) refers to the average number of glucose rings present within each chain. Based on experience, it is commonly considered that transformer reaches their end-of-life when the DP of paper declines to 200, which means the tensile strength decreases to approximately 40% of its initial value [318, 319]. However, measuring DP requires a paper sample from the transformer, which is not feasible for in-service transformers.

In the present industry practice, the estimation of DP value is often conducted through the analysis of furan compounds. Furans are generated as by-products during the degradation of paper insulation impregnated with oil. Among the five furan compounds, 2-furfural (2-FAL) is commonly utilized as a predictor of DP due to its higher stability compared to other compounds [318]. However, the development of online furan measuring methods is still an ongoing research area.

Previous research has revealed a correlation coefficient of 0.87 between 2-FAL and DP [318]. Notably, the ratio of carbon dioxide to carbon monoxide (CO_2/CO) exhibits the highest correlation coefficient of 0.97 [318], emphasizing its superior stability as an indicator for assessing the condition of insulation paper. It is important to highlight that CO_2 and CO are also generated through the oxidation of oil [318]. The utilization of this ratio is justified by the fact that in situations of high thermal fault and arcing faults, CO shows a much more rapid increase compared to CO_2 [320]. Conversely, during significant heat generation in normal operation conditions, CO_2 increases at a faster rate than CO .

Unlike conventional machine learning approaches, deep learning has the capability to directly incorporate measurements of CO_2 and CO as input features, thereby eliminating the requirement for extra features such as CO_2/CO ratio.

The proposed Life Management module, also depicted in Figure 4.5, utilizes a CNN regression approach, incorporating simply two-gas measurements CO_2 and CO to forecast the DP value.

Based on the DP value, the Life Management module delivers an evaluation of the paper insulation condition and categorize it into four levels: “Healthy insulation”, “Moderate deterioration”, “Extensive deterioration”, and “End of insulation life”.

Table 4.5 DP values and their associated significance [150].

DP Value	Significance
1200-700	Healthy Insulation
700-450	Moderate Deterioration
450-250	Extensive Deterioration
<250	End of Life

The inclusion of the estimated percentage of remaining life within the asset management framework does not only enhance the precision of the assessments but also provide a dynamic understanding of the insulation condition. An estimation for the percentage of remaining life based on the DP value can be conducted using (4.3) [149]. Upon review of Table 4.5, “Healthy Insulation” category corresponds to DP values ranging from 700 to 1200. In order to align the model with real-world applications more effectively, a DP value of 800 is considered to be corresponding to 100% transformer remaining life as per (4.3).

$$\% \text{ of remaining life} = 166.1 \times \log_{10}(DP) - 382.2 \quad (4.3)$$

4.4. Results and Discussion

A. Fault Diagnostic module

The database comprises a collection of 1083 DGA samples incorporated from the 29 literatures listed in Table 4.1. 65% of the samples were randomly selected for the training phase, with an additional 15% allocated for the validation phase while the remaining 20% were designated for the testing phase.

The Fault Diagnostic module employs the capabilities of a one-dimensional CNN, which has an architecture adept at processing sequential data. Within this framework, several adjustable parameters play crucial roles in shaping the model’s performance. These parameters include the filter size, which determines the width of the convolutional filters employed to extract features from the input data. Additionally, the kernel size dictates the scope of each convolutional operation, influencing the receptive field of the network. The choice of padding, whether ‘valid’ or ‘same’, modifies the dimensions of the output feature maps. Lastly, the activation function, a vital component, governs the non-linearity introduced within the network, contributing to its ability to capture complex patterns and relationships within the data.

The module training process involves an exhaustive exploration of various configuration settings. Different options were tested at filter sizes: 32, 64, and 128, along with varying numbers of neural network layers. Through these experiments, layers have been systematically added to assess their impact on the model’s performance. Despite the array of layer configurations tested, the final set of layers and parameters that yielded optimal results are as shown in Table 4.6.

Table 4.6 Optimal parameters of the developed Fault Diagnostic module.

Layer	Parameter	Setting
Convolutional layer	Filter size	64
	Kernel size	3
	Padding	'same'
	Activation function	'ReLU'
Dense layer	The number of neurons	16
	Activation function	'ReLU'
Dense_1 layer	Activation function	'sigmoid'

The ReLU activation function transforms negative input values to zero while leaving positive values unchanged. The ReLU function finds extensive application in neural networks across diverse domains owing to its efficient computation and improved gradient propagation, thus facilitating the extraction of significant features from the input data.

The sigmoid activation function possesses the ability to condense input values within a range between 0 and 1, as depicted by (4.4).

$$f(x) = \frac{1}{1 + e^{-x}} \quad (4.4)$$

The sigmoid function exhibits an S-shaped curve is capable of transforming both positive and negative input values into probabilities. Thus, binary classification will be provided. For example, if both “Discharge” and “Thermal” faults are present, the predicted probabilities might be presented as [0.8, 0.2, 0.4, 0.7] ([“Discharge”, “No Fault”, “PD”, “Thermal”]); with more probability assigned to the present faults. It’s noteworthy that each output probability is determined independently, meaning the prediction for one condition does not influence the prediction of another.

During the model compilation phase, the ‘Nadam’ optimizer, which is a combination of the Nesterov Accelerated Gradient (NAG), and Adam optimizers has been applied. The selection of ‘binary_crossentropy’ as the loss function, as given by (4.5), is a common choice for binary classification problems. It measures the dissimilarity between predicted probabilities and true labels (0 or 1), thus optimizing the model to achieve accurate binary predictions.

$$\text{Binary Cross – Entropy Loss} = -[y_i \times \log(\hat{y}_i) + (1 - y_i) \times \log(1 - \hat{y}_i)] \quad (4.5)$$

where, y_i is the actual target value (0 or 1) of the i -th data point.

\hat{y}_i is the predicted value of the i -th data point generated by the model.

Lastly, 'accuracy', a standard evaluation metric, is used for classification tasks. It calculates the ratio of correctly predicted instances to the total number of instances to provide insight into the model's overall performance.

During the last phase of model training, the model's weights are updated based on the provided training data. The training process involves passing the training data through the network, computing predictions, comparing them with the actual targets, and then backpropagating the error to update the model's weights. 'Epochs' defines the number of times the model will iterate over the entire training dataset, which is 1000 times in this case. The batch size determines the number of training examples the model processes in each update of the gradient. Smaller batch sizes may lead to more frequent updates, while larger batch sizes can speed up the training process. A batch size of 16 has been chosen for the developed model based on running through many simulations with different batch sizes.

The training process of the model randomly runs due to the random initial weights, leading to varying results in accuracy and loss. Following parameters adjustments, the training model has been executed several times, and the run producing the highest accuracy and lowest loss is selected. The generated plots shown in Figure 4.6 provide valuable insights into the training process and the performance of the developed CNN model. The alignment or divergence of the curves reveals the overfitting or underfitting phenomena and guide potential adjustments in the model architecture or hyperparameters for optimal performance. In Figure 4.6(a), the 'Training loss' curve, depicted in yellow, shows how the model's loss decreases as it learns to better fit the training data. The 'Validation loss' curve, depicted in red, demonstrates the model's performance on unseen validation data. A decreasing validation loss over epochs indicates successful generalization of the model. In some runs, it was noticed the validation loss started to rise after a certain number of epochs while the training loss curve was stable. This overfitting phenomenon indicates that the model has started to memorize the training data instead of capturing underlying patterns. In Figure 4.6(b), the 'Training acc' curve in yellow illustrates the model's accuracy using the training data, showing the performance of predicting the training samples. The 'Validation acc' curve in red showcases the model's performance using validation data. As epochs progress, observed increasing validation accuracy that aligned with the training accuracy reflects the model's ability to generalize and predict unseen data accurately.

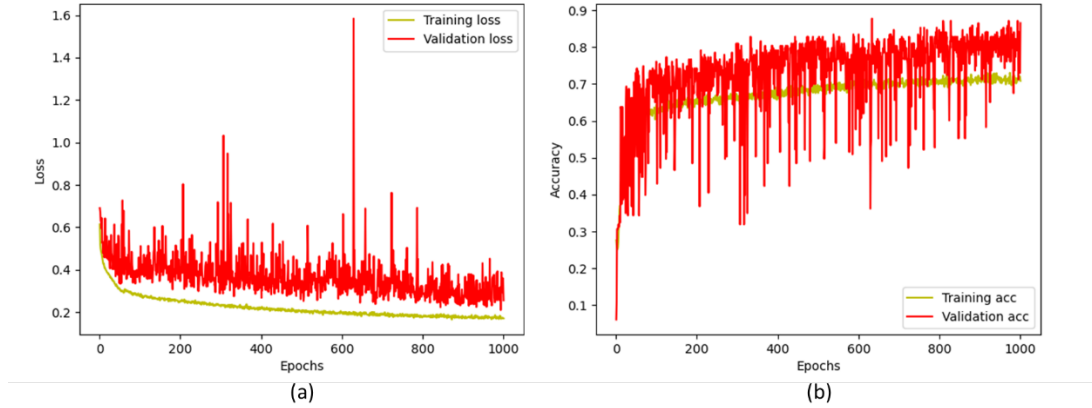


Figure 4.6 Fault Diagnostic module: (a) Training and validation loss plot. (b) Training and validation accuracy plot.

The satisfied model performance was achieved with an accuracy of 0.8479 and a corresponding loss of 0.2989 using the test dataset. This model was subsequently saved for the Fault Diagnostic module. To operate the Fault Diagnostic module, new gas measurements were fed into the module, enabling the prediction of outputs through its learned capabilities.

In order to evaluate the performance of the Fault Diagnostic module, a dataset comprising 151 samples from the IEC TC10 database was used [4]. Subsequently, a thorough assessment of misdiagnoses within each class was carried out. Notably, the analysis revealed that misdiagnosis predominantly occurred within the “No Fault” condition as revealed by confusion matrix of the Fault Diagnostic module shown in Figure 4.7. This may be attributed to the fact that the majority of the collected datasets were predominantly geared towards the identification of fault conditions.

		Actual condition				
		Discharge	No Fault	PD	Thermal	
Predicted condition	Discharge	70 46.36%	8 5.30%	0 0%	2 1.32%	87.50% 12.50%
	No Fault	4 2.65%	23 15.23%	0 0%	3 1.99%	76.70% 23.30%
	PD	0 0%	0 0%	9 5.96%	0 0%	100% 0%
	Thermal	0 0%	3 1.99%	0 0%	29 19.20%	90.60% 9.40%
		94.60% 5.40%	67.60% 32.40%	100% 0%	85.30% 14.70%	86.75% 13.25%

Figure 4.7 Confusion matrix of the proposed Fault Diagnostic module.

The samples presented in Table 4.7 originate from the IEC TC 10 database (samples 1-151) and Table 4.8 from Korea Electric Power Corporation (KEPCO) historical data [8, 321]. The second last column in the table shows the actual condition of the transformers as determined through physical inspection while the last column lists the diagnostic results generated from the proposed Fault Diagnostic module. Certain discrepancies have been identified in the samples #21, #51, #60, #80, #87, #90, #91, #97, #107, #120-#122, #125, #127, #132, #141, #142, #144, #150, #151 and KEPCO's samples. In Table 4.9 & Table 4.10, traditional IEEE and IEC DGA interpretation methods are used to analyse all samples and compare the results with those obtained from the module. The following observations can be drawn out of these comparisons:

- In the case of sample #21, the actual condition is described as “Traces of discharges in paper of cone junction of HV cable”, categorized as low energy discharge. Traditional methods such as Duval Triangle 1, Roger ratio and IEC ratio methods can identify this discharge fault. However, the developed module did not capture this specific fault.
- For samples #51, #60, and #80, the observed reveal instances of high energy discharge, detectable through IEEE and IEC ratios as well as Duval Triangle 1 methods. Surprisingly, the developed module failed to identify these faults.
- In the case of samples #87, #90, and #91, the inspection findings indicate “Thermal runaway in thick paper insulation”, classified as a low thermal fault. Both the IEC ratio method and Duval Triangle 1 successfully identified this fault. However, the proposed module encountered a misdiagnosis in these instances.
- For sample #97, the actual condition is described as “Low temperature overheating of clamping beams of yokes by stray flux”, categorized as a low thermal fault. It is noteworthy that both the IEC ratio and Duval Triangle 1 methods indicate a PD fault. The proposed module diagnosed it as a discharge fault.
- For sample #107, the inspection outcome shows “Defects on contacts of tap changer selector”, categorized as high thermal fault. While both the Roger ratio method and the proposed module diagnose a discharge fault, the Duval Triangle 1 method identifies it as a thermal fault.
- In the cases of #120, #121, #122, #125, #127, #132, #141, #142, #144, #150, #151, the inspection result denoted no fault. Notably, all other methods, including the proposed approach, failed to correctly indicate the condition.
- Observations reveal that the module occasionally indicated the presence of multiple faults, as seen in samples #3, #31 and #86. In the case of sample #3, the module detected a PD fault in addition to a thermal fault. Notably, when the Duval Triangle 1 was applied to analyse sample #3, the result aligned with the inspection outcome. Similarly, for sample #31, the module detected a discharge fault along with a PD fault. The application of the Duval Triangle 1 method to sample #31 also produced the result consistent with the inspection finding. For sample #86, in contrast to the inspection result which revealed a thermal fault, the proposed module indicated a thermal fault along with a discharge fault. Other traditional methods, on the other hand, aligned with the inspection result.

- Another assessment was conducted on four KEPCO transformers based on their annual DGA measurements. The results exhibited the capability of the developed module in early fault detection for transformers 1, 2 and 3, which enables proactive maintenance measures to be taken. In the case of transformer 4, the module not only detected the thermal fault but also identified a potential discharge fault.
- In the overall assessment of diagnostic accuracy using IEC TC10 data, the developed module consistently demonstrates a better accuracy when compared to traditional methods. It's worth noting that the Doernenburg ratio method appears to have higher accuracy when applied to KEPCO data. This discrepancy can be attributed to a specific requirement outlined in IEEE C57.104 [3], which mandates a minimum concentration limit for at least one key gas used in the ratios before the Doernenburg ratio method can be applied. In the KEPCO dataset, the "No Fault" cases appear to have very low gas concentration levels, therefore, identified as "No Fault". On the other hand, in the IEC TC10 data, for samples #120, #121, #122, #125, #127, #132 #141, #142, #144, #150, and #151, the gas measurements exceed the concentration limit, resulting in incorrect outcomes when utilizing the Doernenburg ratio method. This issue also manifests in the KEPCO data, producing inconclusive results for 12 or 24 months before the actual failures may really happen.

Table 4.7 Comparison between the diagnostic result from the Fault Diagnostic module and actual condition from inspection. (All gases are measured in PPM)

IEC TC10 Samples	H ₂	CH ₄	C ₂ H ₄	C ₂ H ₆	C ₂ H ₂	Actual condition from inspection	Module's result
1	32930	2397	0	157	0	PD	PD
2	37800	1740	8	249	8	PD	PD
3	92600	10200	0	0	0	PD	PD; Thermal
4	8266	1061	0	22	0	PD	PD
5	9340	995	6	60	7	PD	PD
6	36036	4704	5	554	10	PD	PD
7	33046	619	2	58	0	PD	PD
8	40280	1069	1	1060	1	PD	PD
9	26788	18342	27	2111	0	PD	PD
10	78	20	13	11	28	Discharge	Discharge
11	305	100	161	33	541	Discharge	Discharge
12	35	6	26	3	482	Discharge	Discharge
13	543	120	411	41	1880	Discharge	Discharge
14	1230	163	233	27	692	Discharge	Discharge
15	645	86	110	13	317	Discharge	Discharge
16	60	10	4	4	4	Discharge	Discharge
17	95	10	11	0	39	Discharge	Discharge
18	6870	1028	900	79	5500	Discharge	Discharge

19	10092	5399	6500	530	37565	Discharge	Discharge
20	650	81	51	170	270	Discharge	Discharge
21	210	22	6	6	7	Discharge	No Fault
22	385	60	53	8	159	Discharge	Discharge
23	4230	690	196	5	1180	Discharge	Discharge
24	7600	1230	836	318	1560	Discharge	Discharge
25	595	80	89	9	244	Discharge	Discharge
26	120	25	8	1	40	Discharge	Discharge
27	8	0	43	0	101	Discharge	Discharge
28	6454	2313	2159	121	6432	Discharge	Discharge
29	2177	1049	440	207	705	Discharge	Discharge
30	1790	580	336	321	619	Discharge	Discharge
31	1330	10	66	20	182	Discharge	Discharge; PD
32	4	1	7	2	52	Discharge	Discharge
33	1900	285	957	31	7730	Discharge	Discharge
34	57	24	27	2	30	Discharge	Discharge
35	1000	500	400	1	500	Discharge	Discharge
36	440	89	304	19	757	Discharge	Discharge
37	210	43	102	12	187	Discharge	Discharge
38	2850	1115	1987	138	3675	Discharge	Discharge
39	7020	1850	2960	0	4410	Discharge	Discharge
40	545	130	153	16	239	Discharge	Discharge
41	7150	1440	1210	97	1760	Discharge	Discharge
42	620	325	181	38	244	Discharge	Discharge
43	120	31	66	0	94	Discharge	Discharge
44	755	229	404	32	460	Discharge	Discharge
45	5100	1430	1140	0	1010	Discharge	Discharge
46	13500	6110	4510	212	4040	Discharge	Discharge
47	1570	1110	1780	175	1830	Discharge	Discharge
48	3090	5020	3800	323	2540	Discharge	Discharge
49	1820	405	365	35	634	Discharge	Discharge
50	535	160	305	16	680	Discharge	Discharge
51	13	3	3	1	6	Discharge	No Fault
52	137	67	53	7	104	Discharge	Discharge
53	1084	188	166	8	769	Discharge	Discharge
54	34	21	49	4	56	Discharge	Discharge
55	7940	2000	3120	355	5390	Discharge	Discharge
56	150	130	55	9	30	Discharge	Discharge
57	8200	3790	4620	250	5830	Discharge	Discharge
58	260	215	334	35	277	Discharge	Discharge
59	75	15	14	7	26	Discharge	Discharge
60	530	345	266	85	250	Discharge	No Fault
61	60	5	21	2	21	Discharge	Discharge

62	90	28	31	8	32	Discharge	Discharge
63	220	77	170	22	240	Discharge	Discharge
64	5900	1500	1200	68	2300	Discharge	Discharge
65	420	250	530	41	800	Discharge	Discharge
66	2800	2800	3500	234	3600	Discharge	Discharge
67	99	170	200	20	190	Discharge	Discharge
68	310	230	610	54	760	Discharge	Discharge
69	800	160	260	23	600	Discharge	Discharge
70	1500	395	395	28	323	Discharge	Discharge
71	20000	13000	29000	1850	57000	Discharge	Discharge
72	305	85	197	25	130	Discharge	Discharge
73	1900	530	383	35	434	Discharge	Discharge
74	110	62	140	90	250	Discharge	Discharge
75	3700	1690	2810	128	3270	Discharge	Discharge
76	2770	660	712	54	763	Discharge	Discharge
77	245	120	131	18	167	Discharge	Discharge
78	1170	255	312	18	325	Discharge	Discharge
79	4419	3564	2861	668	2025	Discharge	Discharge
80	810	580	570	111	490	Discharge	No Fault
81	5000	1200	1000	83	1100	Discharge	Discharge
82	10000	6730	7330	345	10400	Discharge	Discharge
83	1570	735	1330	87	1740	Discharge	Discharge
84	1270	3450	1390	520	8	Thermal	Thermal
85	3420	7870	6990	1500	33	Thermal	Thermal
86	360	610	260	259	9	Thermal	Discharge; Thermal
87	1	27	4	49	1	Thermal	No Fault
88	3675	6392	7691	2500	5	Thermal	Thermal
89	48	610	10	29	0	Thermal	Thermal
90	12	18	4	4	0	Thermal	No Fault
91	66	60	7	2	0	Thermal	No Fault
92	1450	940	322	211	61	Thermal	Thermal
93	0	18900	540	410	330	Thermal	Thermal
94	960	4000	1560	1290	6	Thermal	Thermal
95	24700	61000	42100	26300	1560	Thermal	Thermal
96	14	44	7	124	1	Thermal	Thermal
97	2031	149	3	20	0	Thermal	Discharge
98	480	1075	1132	298	0	Thermal	Thermal
99	40000	400	600	70	6	Thermal	Thermal
100	8800	64064	95650	72128	0	Thermal	Thermal
101	6709	10500	17700	1400	750	Thermal	Thermal
102	1100	1600	2010	221	26	Thermal	Thermal
103	290	966	1810	299	57	Thermal	Thermal
104	2500	10500	13500	4790	6	Thermal	Thermal

105	1860	4980	10700	0	1600	Thermal	Thermal
106	860	1670	2050	30	40	Thermal	Thermal
107	150	22	60	9	11	Thermal	Discharge
108	400	940	820	210	24	Thermal	Thermal
109	6	2990	26076	29990	67	Thermal	Thermal
110	100	200	670	110	11	Thermal	Thermal
111	290	1260	820	231	8	Thermal	Thermal
112	1550	2740	5450	816	184	Thermal	Thermal
113	3910	4290	6040	626	1230	Thermal	Thermal
114	12705	23498	34257	6047	5188	Thermal	Thermal
115	1	8	100	8	6	Thermal	Thermal
116	300	700	1700	280	36	Thermal	Thermal
117	107	143	222	34	2	Thermal	Thermal
118	134	134	45	157	0	No Fault	No Fault
119	100	200	200	200	20	No Fault	No Fault
120	0	225	110	225	3	No Fault	Thermal
121	105	125	166	71	10	No Fault	Thermal
122	100	50	50	65	15	No Fault	Discharge
123	100	70	170	70	10	No Fault	No Fault
124	150	0	220	0	8	No Fault	No Fault
125	0	224	112	224	5	No Fault	Thermal
126	200	50	200	50	3	No Fault	No Fault
127	85	0	35	80	70	No Fault	Discharge
128	175	0	375	100	3	No Fault	No Fault
129	80	0	100	200	4	No Fault	No Fault
130	150	0	100	200	15	No Fault	No Fault
131	125	100	150	100	20	No Fault	No Fault
132	200	3	200	50	0	No Fault	Discharge
133	50	30	0	0	5	No Fault	No Fault
134	100	70	170	70	10	No Fault	No Fault
135	95	280	150	250	10	No Fault	No Fault
136	60	40	60	50	3	No Fault	No Fault
137	84	79	166	52	56	No Fault	No Fault
138	66	111	110	90	15	No Fault	No Fault
139	235	180	145	270	336	No Fault	No Fault
140	250	150	250	150	150	No Fault	No Fault
141	150	0	220	0	150	No Fault	Discharge
142	200	50	200	50	30	No Fault	Discharge
143	134	224	224	550	154	No Fault	No Fault
144	250	0	150	15	280	No Fault	Discharge
145	150	0	320	80	22	No Fault	No Fault
146	0	150	200	550	150	No Fault	No Fault
147	150	0	200	200	150	No Fault	No Fault

148	200	100	100	100	50	No Fault	No Fault
149	250	190	250	180	180	No Fault	No Fault
150	75	35	110	50	80	No Fault	Discharge
151	151	131	250	73	266	No Fault	Discharge

Table 4.8 Comparison between the diagnostic results from the Fault Diagnostic module and actual condition during inspection for Korea Electric Power Corporation (KEPCO) historical data. (All gases are measured in PPM)

KEPCO Samples	H ₂	CH ₄	C ₂ H ₄	C ₂ H ₆	C ₂ H ₂	KEPCO Health State	Module's result	
Transformer 1	1999	0	6	2	2	0	No Fault	No Fault
	2000	0	25	13	9	0	No Fault	No Fault
	2001	0	35	37	31	0	No Fault	Thermal
	2002	0	44	28	85	0	No Fault	Thermal
	2003	251	139	256	123	1064	Electrical Fault	Discharge
Transformer 2	2011	10	7	2	5	0	No Fault	No Fault
	2012	13	11	3	26	0	No Fault	No Fault
	2013	48	24	12	63	14	No Fault	Discharge
	2015	335	246	1324	150	1123	Electrical Fault	Discharge
Transformer 3	2000	0	1	5	0	0	No Fault	No Fault
	2002	0	7	11	14	0	No Fault	No Fault
	2003	0	64	150	99	0	No Fault	Thermal
	2004	218	744	1743	264	7	Thermal fault	Thermal
Transformer 4	2000	5	44	4	9	0	No Fault	No Fault
	2001	6	42	10	9	0	No Fault	No Fault
	2002	6	44	12	10	0	No Fault	No Fault
	2003	7	56	12	10	0	No Fault	No Fault
	2004	628	1381	1873	351	2.8	Thermal Fault	Discharge; Thermal

Table 4.9 Comparison of diagnostic results: proposed module vs. the traditional methods for the IEC TC 10 database. (All gases are measured in PPM)

IEC TC10 Sample #	Actual condition from inspection	Roger Ratio Method	Doernenburg Ratio Method	IEC Ratio Method	Duval Triangle	Module's result
1	PD	N/A	N/A	N/A	PD	PD
2	PD	N/A	N/A	PD	PD	PD
3	PD	N/A	N/A	N/A	PD	PD; Thermal
4	PD	N/A	N/A	N/A	PD	PD
5	PD	N/A	N/A	N/A	PD	PD
6	PD	N/A	N/A	N/A	PD	PD
7	PD	PD	N/A	PD	PD	PD
8	PD	N/A	PD	PD	PD	PD
9	PD	No Fault	N/A	N/A	PD	PD

10	Discharge	Discharge	Discharge	Discharge	Discharge	Discharge
11	Discharge	N/A	Discharge	Discharge	Discharge	Discharge
12	Discharge	N/A	Discharge	Discharge	Discharge	Discharge
13	Discharge	N/A	Discharge	Discharge	Discharge	Discharge
14	Discharge	Discharge	Discharge	Discharge	Discharge	Discharge
15	Discharge	Discharge	Discharge	Discharge	Discharge	Discharge
16	Discharge	Discharge	N/A	N/A	Discharge	Discharge
17	Discharge	N/A	Discharge	N/A	Discharge	Discharge
18	Discharge	N/A	Discharge	Discharge	Discharge	Discharge
19	Discharge	N/A	Discharge	N/A	Discharge	Discharge
20	Discharge	N/A	N/A	N/A	Discharge	Discharge
21	Discharge	Discharge	N/A	Discharge	Discharge	No Fault
22	Discharge	Discharge	Discharge	Discharge	Discharge	Discharge
23	Discharge	N/A	Discharge	Discharge	Discharge	Discharge
24	Discharge	Discharge	Discharge	Discharge	Discharge	Discharge
25	Discharge	Discharge	Discharge	Discharge	Discharge	Discharge
26	Discharge	N/A	Discharge	Discharge	Discharge	Discharge
27	Discharge	N/A	N/A	N/A	Discharge	Discharge
28	Discharge	Discharge	Discharge	Discharge	Discharge	Discharge
29	Discharge	Discharge	Discharge	Discharge	Discharge	Discharge
30	Discharge	Discharge	N/A	Discharge	Discharge	Discharge
31	Discharge	N/A	N/A	N/A	Discharge	Discharge; PD
32	Discharge	N/A	Discharge	Discharge	Discharge	Discharge
33	Discharge	N/A	Discharge	Discharge	Discharge	Discharge
34	Discharge	Discharge	Discharge	Discharge	Discharge	Discharge
35	Discharge	Discharge	Discharge	Discharge	Discharge	Discharge
36	Discharge	Discharge	Discharge	Discharge	Discharge	Discharge
37	Discharge	Discharge	Discharge	Discharge	Discharge	Discharge
38	Discharge	Discharge	Discharge	Discharge	Discharge	Discharge
39	Discharge	N/A	Discharge	N/A	Discharge	Discharge
40	Discharge	Discharge	Discharge	Discharge	Discharge	Discharge
41	Discharge	Discharge	Discharge	Discharge	Discharge	Discharge
42	Discharge	Discharge	Discharge	Discharge	Discharge	Discharge
43	Discharge	N/A	Discharge	N/A	Discharge	Discharge
44	Discharge	Discharge	Discharge	Discharge	Discharge	Discharge
45	Discharge	N/A	Discharge	N/A	Discharge	Discharge
46	Discharge	Discharge	Discharge	Discharge	Discharge	Discharge
47	Discharge	Discharge	Discharge	Discharge	Discharge	Discharge
48	Discharge	N/A	N/A	N/A	Discharge	Discharge
49	Discharge	N/A	Discharge	Discharge	Discharge	Discharge
50	Discharge	Discharge	Discharge	Discharge	Discharge	Discharge
51	Discharge	Discharge	Discharge	Discharge	Discharge	No Fault
52	Discharge	Discharge	Discharge	Discharge	Discharge	Discharge

53	Discharge	N/A	Discharge	Discharge	Discharge	Discharge
54	Discharge	Discharge	Discharge	Discharge	Discharge	Discharge
55	Discharge	Discharge	Discharge	Discharge	Discharge	Discharge
56	Discharge	Discharge	N/A	N/A	Discharge	Discharge
57	Discharge	Discharge	Discharge	Discharge	Discharge	Discharge
58	Discharge	Discharge	Discharge	Discharge	Discharge	Discharge
59	Discharge	Discharge	Discharge	Discharge	Discharge	Discharge
60	Discharge	Discharge	Discharge	Discharge	Discharge	No Fault
61	Discharge	N/A	N/A	N/A	Discharge	Discharge
62	Discharge	Discharge	Discharge	Discharge	Discharge	Discharge
63	Discharge	Discharge	Discharge	Discharge	Discharge	Discharge
64	Discharge	Discharge	Discharge	Discharge	Discharge	Discharge
65	Discharge	Discharge	Discharge	Discharge	Discharge	Discharge
66	Discharge	Discharge	Discharge	Discharge	Discharge	Discharge
67	Discharge	N/A	N/A	N/A	Discharge	Discharge
68	Discharge	Discharge	Discharge	Discharge	Discharge	Discharge
69	Discharge	Discharge	Discharge	Discharge	Discharge	Discharge
70	Discharge	Discharge	Discharge	Discharge	Discharge	Discharge
71	Discharge	Discharge	Discharge	Discharge	Discharge	Discharge
72	Discharge	Discharge	N/A	Discharge	Discharge	Discharge
73	Discharge	Discharge	Discharge	Discharge	Discharge	Discharge
74	Discharge	Discharge	Discharge	N/A	Discharge	Discharge
75	Discharge	Discharge	Discharge	Discharge	Discharge	Discharge
76	Discharge	Discharge	Discharge	Discharge	Discharge	Discharge
77	Discharge	Discharge	Discharge	Discharge	Discharge	Discharge
78	Discharge	Discharge	Discharge	Discharge	Discharge	Discharge
79	Discharge	Discharge	Discharge	Discharge	Discharge	Discharge
80	Discharge	Discharge	Discharge	Discharge	Discharge	No Fault
81	Discharge	Discharge	Discharge	Discharge	Discharge	Discharge
82	Discharge	Discharge	Discharge	Discharge	Discharge	Discharge
83	Discharge	Discharge	Discharge	Discharge	Discharge	Discharge
84	Thermal	Thermal	Thermal	Thermal	Thermal	Thermal
85	Thermal	Thermal	Thermal	Thermal	Thermal	Thermal
86	Thermal	Thermal	Thermal	Thermal	Thermal	Discharge; Thermal
87	Thermal	N/A	No Fault	Thermal	Discharge; Thermal	No Fault
88	Thermal	Thermal	Thermal	Thermal	Thermal	Thermal
89	Thermal	Thermal	N/A	Thermal	PD	Thermal
90	Thermal	Thermal	No Fault	Thermal	Discharge	No Fault
91	Thermal	Thermal	No Fault	N/A	Discharge	No Fault
92	Thermal	Discharge	N/A	N/A	Thermal	Thermal
93	Thermal	N/A	N/A	N/A	Thermal	Thermal
94	Thermal	Discharge	Thermal	Thermal	Thermal	Thermal

95	Thermal	Thermal	Thermal	Thermal	Thermal	Thermal
96	Thermal	N/A	No Fault	Thermal	Thermal	Thermal
97	Thermal	N/A	N/A	PD	PD	Discharge
98	Thermal	Thermal	N/A	Thermal	Thermal	Thermal
99	Thermal	N/A	PD	N/A	Thermal	Thermal
100	Thermal	Thermal	N/A	Thermal	Thermal	Thermal
101	Thermal	Thermal	Thermal	Thermal	Thermal	Thermal
102	Thermal	Thermal	Thermal	Thermal	Thermal	Thermal
103	Thermal	Thermal	Thermal	Thermal	Thermal	Thermal
104	Thermal	Thermal	Thermal	Thermal	Thermal	Thermal
105	Thermal	N/A	N/A	N/A	Thermal	Thermal
106	Thermal	Thermal	Thermal	Thermal	Thermal	Thermal
107	Thermal	Discharge	N/A	N/A	Thermal	Discharge
108	Thermal	Thermal	Thermal	Thermal	Thermal	Thermal
109	Thermal	Thermal	Thermal	Thermal	Thermal	Thermal
110	Thermal	Thermal	Thermal	Thermal	Thermal	Thermal
111	Thermal	Thermal	Thermal	Thermal	Thermal	Thermal
112	Thermal	Thermal	Thermal	Thermal	Thermal	Thermal
113	Thermal	N/A	Thermal	N/A	Thermal	Thermal
114	Thermal	N/A	Thermal	Thermal	Thermal	Thermal
115	Thermal	Thermal	N/A	Thermal	Thermal	Thermal
116	Thermal	Thermal	Thermal	Thermal	Thermal	Thermal
117	Thermal	Thermal	Thermal	Thermal	Thermal	Thermal
118	No Fault	N/A	No Fault	Thermal	Thermal	No Fault
119	No Fault	Thermal	Thermal	Thermal	Discharge; Thermal	No Fault
120	No Fault	N/A	N/A	N/A	Thermal	Thermal
121	No Fault	Thermal	Thermal	Thermal	Thermal	Thermal
122	No Fault	Discharge	N/A	N/A	Discharge; Thermal	Discharge
123	No Fault	Thermal	N/A	N/A	Thermal	No Fault
124	No Fault	N/A	N/A	N/A	Thermal	No Fault
125	No Fault	N/A	N/A	N/A	Thermal	Thermal
126	No Fault	Thermal	N/A	N/A	Thermal	No Fault
127	No Fault	N/A	N/A	N/A	Discharge	Discharge
128	No Fault	N/A	N/A	N/A	Thermal	No Fault
129	No Fault	N/A	N/A	Thermal	Thermal	No Fault
130	No Fault	N/A	N/A	N/A	Thermal	No Fault
131	No Fault	Discharge	N/A	N/A	Thermal	No Fault
132	No Fault	N/A	N/A	N/A	Thermal	Discharge
133	No Fault	N/A	N/A	N/A	Discharge	No Fault
134	No Fault	Discharge	N/A	N/A	Thermal	No Fault
135	No Fault	Thermal	Thermal	Thermal	Thermal	No Fault
136	No Fault	Thermal	N/A	N/A	Thermal	No Fault

137	No Fault	Discharge	N/A	N/A	Discharge; Thermal	No Fault
138	No Fault	N/A	Thermal	N/A	Discharge; Thermal	No Fault
139	No Fault	Discharge	N/A	N/A	Discharge	No Fault
140	No Fault	Discharge	N/A	N/A	Discharge; Thermal	No Fault
141	No Fault	N/A	N/A	N/A	Discharge	Discharge
142	No Fault	Discharge	N/A	N/A	Thermal	Discharge
143	No Fault	N/A	N/A	N/A	Discharge	No Fault
144	No Fault	N/A	N/A	N/A	Discharge	Discharge
145	No Fault	N/A	N/A	N/A	Thermal	No Fault
146	No Fault	N/A	N/A	N/A	Discharge	No Fault
147	No Fault	N/A	N/A	N/A	Discharge	No Fault
148	No Fault	Discharge	N/A	N/A	Discharge; Thermal	No Fault
149	No Fault	Discharge	N/A	N/A	Discharge; Thermal	No Fault
150	No Fault	Discharge	N/A	Discharge	Discharge	Discharge
151	No Fault	Discharge	Discharge	Discharge	Discharge	Discharge

Table 4.10 Comparison of diagnostic results: proposed module vs. the traditional methods for Korea Electric Power Corporation (KEPCO) historical data. (All gases are measured in PPM)

KEPCO Samples		KEPCO Health State	Roger Ratio Method	Doernenburg Ratio Method	IEC Ratio Method	Duval Triangle	Module's result
Transformer 1	1999	No Fault	N/A	No Fault	N/A	Thermal	No Fault
	2000	No Fault	N/A	No Fault	N/A	Thermal	No Fault
	2001	No Fault	N/A	No Fault	N/A	Thermal	Thermal
	2002	No Fault	N/A	N/A	N/A	Thermal	Thermal
	2003	Electrical Fault	N/A	Discharge	N/A	Discharge	Discharge
Transformer 2	2011	No Fault	Thermal	No Fault	N/A	Thermal	No Fault
	2012	No Fault	N/A	No Fault	N/A	Thermal	No Fault
	2013	No Fault	N/A	N/A	N/A	Discharge	Discharge
	2015	Electrical Fault	Discharge	Discharge	Discharge	Discharge	Discharge
Transformer 3	2000	No Fault	N/A	No Fault	N/A	Thermal	No Fault
	2002	No Fault	N/A	No Fault	N/A	Thermal	No Fault
	2003	No Fault	N/A	N/A	N/A	Thermal	Thermal
	2004	Thermal fault	Thermal	Thermal	Thermal	Thermal	Thermal
Transformer 4	2000	No Fault	Thermal	No Fault	N/A	Thermal	No Fault
	2001	No Fault	Thermal	No Fault	Thermal	Thermal	No Fault
	2002	No Fault	Thermal	No Fault	Thermal	Thermal	No Fault
	2003	No Fault	Thermal	No Fault	Thermal	Thermal	No Fault
	2004	Thermal Fault	Thermal	Thermal	Thermal	Thermal	Discharge; Thermal

From the above analysis, it can be concluded that the developed CNN-based fault diagnostic module comprises the following unique features:

- *Ability to identify multi-label classification:* Conventional DGA interpretation techniques like Duval Triangle 1, IEEE, and IEC ratios methods predominantly pinpointed singular faults. Among them, Duval Triangle 1 method can only identify a combined discharge and thermal fault. In contrast, the CNN model exhibits the ability to discern distinct features across all four different conditions.
- *Using a single training model:* To distinguish three pivotal faults; Discharge, Partial Discharge, and Thermal faults, the conventional machine learning methods require three distinct training models to collectively assess the transformer’s overall condition. However, CNN method streamlines this process by utilizing a single training model, which minimizes the training duration substantially. This simplified approach not only expedites the training phase but also produces a remarkable level of accuracy.
- *Avoiding data manipulation:* The CNN model possesses inherent feature selection capabilities, which facilitates the use of raw data directly and independently. This mechanism circumvents the need for manually engineered features like gas ratios or gas percentage. Additionally, this intrinsic capability contributes to reduce execution time, making it particularly suitable for real-time condition monitoring.

B. Life Management module

The training of the Life Management module employed 47 datasets sourced from three distinct literatures as listed in Table 4.11 [207, 322, 323]. These datasets were divided into a training set comprising 80% of the data and a testing set constituting the remaining 20%.

Table 4.11 Training datasets for Life Management module

Sample #	CO ₂	CO	DP
1	5315	662	329
2	3089	405	570
3	1936	97	1055
4	5004	935	343
5	229	10	1024
6	2500	350	484
7	7800	1050	296
8	1600	145	965
9	2600	360	465
10	12000	1650	146
11	218	34	1150
12	4150	592	392
13	877	98	727
14	4465	1062	300
15	16500	1750	152
16	809	64	1304

17	2631	368	490
18	1493	135	963
19	4404	595	266
20	2490	148	846
21	2584	391	500
22	2509	359	654
23	4342	577	362
24	4200	580	268
25	2980	502	600
26	1817	209	785
27	4210	580	276
28	2514	376	652
29	700	5495	705
30	189	2011	467
31	697	3685	1015
32	8197	22789	229
33	582	4567	502
34	892	7038	725
35	1843	2492	110
36	1582	12371	263
37	669	6764	514
38	299	2348	235
39	297	2323	725
40	162	1139	725
41	242	1883	993
42	356	3347	725
43	902	7135	725
44	1695	13345	217
45	964	4002	1015
46	102	1274	525
47	542	2346	1015

The training model in this context also incorporated a one-dimensional CNN architecture. The specific parameters utilized in configuring the CNN architecture are detailed in Table 4.12.

Table 4.12 Optimal parameters of the developed Life Management module.

Layer	Parameter	Setting
Convolutional layer	Filter size	128
	Kernel size	1
	Activation function	'ReLU'
Dense layer	The number of neurons	64
	Activation function	'ReLU'
Dense_1 layer	The number of neurons	1

In the phase of compiling the model, the Adaptive Moment Estimation ‘adam’ optimizer and ‘mse’ loss function are adopted. As stated above, ‘adam’ enhances optimization by independently adjusting learning rates for each parameter based on the historical gradients. The Mean Squared Error ‘mse’ loss function as given by (4.6), quantifies the average squared difference between the predicted values generated by a model and the target values in the dataset. It is often used as a loss function for regression models to guide the optimization process.

$$MSE = \frac{1}{n} \times \sum (y_i - \hat{y}_i)^2 \quad (4.6)$$

where, n is the total number of samples in the dataset used to evaluate the model performance.

y_i is the actual observed value of the i -th data point.

\hat{y}_i is the corresponding predicted value by the model of the i -th data point.

By setting the number of epochs to 5000 and the batch size to 16, an optimal model performance has been observed. The progression of the training process is visually depicted in Figure 4.8. A substantial reduction in both the training and validation losses over the course of training can be observed from the figure.

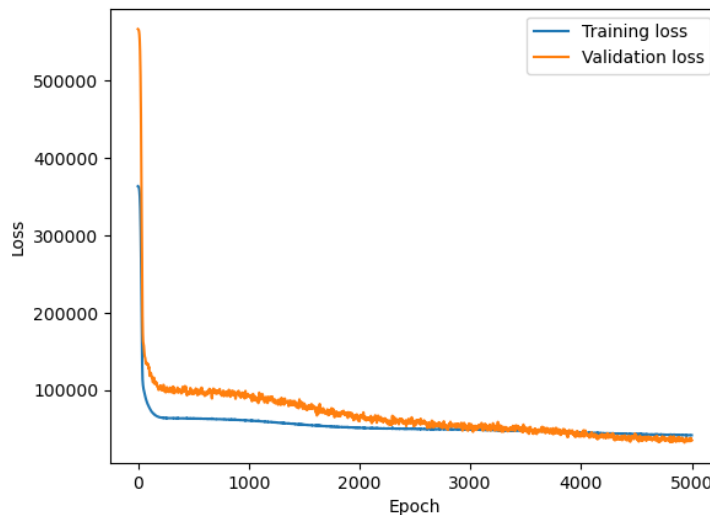


Figure 4.8 The training and validation loss plot for the Life management module.

To assess the accuracy of the developed module, a database that was not included in the training process was analysed as outlined in Table 4.13 [324]. As can be seen in the Table, only two samples (#5 and #7) out of the total 15 results deviate from the expected target values. This reflects an accuracy level of 86.7% for the developed model.

Table 4.13 Comparison between the predicted result from the Life Management module and actual condition from dataset.

Sample #	CO ₂	CO	Targeted DP	Condition based on targeted DP	Predicted DP	Condition based on predicted DP (using CO, CO ₂)
1	812	62	1304	Healthy	1020	Healthy
2	2628	370	490	Moderate	540	Moderate
3	1498	132	963	Healthy	984	Healthy
4	1878	164	1189	Healthy	727	Healthy
5	2298	214	1149	Healthy	596	Moderate
6	4400	594	266	Extensive	338	Extensive
7	2562	146	846	Healthy	565	Moderate
8	2587	387	500	Moderate	544	Moderate
9	2502	353	654	Moderate	556	Moderate
10	4348	576	362	Extensive	339	Extensive
11	4206	586	268	Extensive	341	Extensive
12	2984	503	600	Moderate	489	Moderate
13	1815	211	785	Healthy	748	Healthy
14	4217	566	276	Extensive	342	Extensive
15	2421	372	652	Moderate	564	Moderate

In the past, there was a lack of records connecting CO₂ and CO measurements with the degree of deterioration of insulating paper. To pursue further module testing, an additional 131 CO₂ and CO measurements have been collected from diverse sources of the literature. Table 4.14 presents the degree of deterioration corresponding to CO₂ and CO measurements [207]. Subsequently, the CO₂ and CO measurements are fed into the life management module for processing. Upon comparing the module's outcomes with the estimated results, a variance was observed in 20 out of 131 cases, shown in Table 4.15, demonstrating an approximate 85% concurrence rate.

Table 4.14 CO₂ and CO concentration ranges and the corresponding levels of deterioration [207].

CO ₂	CO	Significance
0 - 2500	0 - 350	Health Insulation
2500 - 4000	350 - 570	Moderate Deterioration
4000 - 10000	570 - 1400	Extensive Deterioration
≥ 10000	≥ 1400	End of Life

Table 4.15 Comparison between the predicted result from the Life Management module and estimated condition according to Table 4.14

Samples #	CO2	CO	Condition based on Table 4.14 ranges	Predicted DP	Condition based on predicted DP
1	4310	586	Extensive	340	Extensive
2	8713	951	Extensive	252	Extensive
3	3144	400	Moderate	479	Moderate
4	4463	576	Extensive	338	Extensive
5	9778	971	Extensive	234	End of Life
6	7310	1128	Extensive	268	Extensive
7	3468	389	Moderate	442	Extensive
8	6171	881	Extensive	297	Extensive
9	5777	614	Extensive	314	Extensive
10	6447	603	Extensive	304	Extensive
11	4832	1018	Extensive	314	Extensive
12	3625	516	Moderate	414	Extensive
13	6691	1062	Extensive	281	Extensive
14	5184	858	Extensive	314	Extensive
15	5337	604	Extensive	322	Extensive
16	1856	145	Healthy	736	Healthy
17	1819	129	Healthy	755	Healthy
18	1255	82	Healthy	1164	Healthy
19	2345	195	Healthy	586	Moderate
20	262	97	Healthy	696	Moderate
21	2480	158	Healthy	574	Moderate
22	1577	137	Healthy	926	Healthy
23	592	213	Healthy	886	Healthy
24	384	21	Healthy	770	Healthy
25	405	21	Healthy	782	Healthy
26	685	33	Healthy	947	Healthy
27	872	53	Healthy	1056	Healthy
28	612	25	Healthy	904	Healthy
29	475	14	Healthy	824	Healthy
30	560	23	Healthy	874	Healthy
31	588	24	Healthy	890	Healthy
32	505	205	Healthy	835	Healthy
33	549	193	Healthy	861	Healthy
34	1145	104	Healthy	1204	Healthy
35	1013	65	Healthy	1138	Healthy
36	1117	76	Healthy	1196	Healthy
37	913.9	66.71	Healthy	1080	Healthy

38	860	32	Healthy	1050	Healthy
39	758	37	Healthy	989	Healthy
40	528	36	Healthy	854	Healthy
41	306	109	Healthy	721	Healthy
42	3137	436	Moderate	477	Moderate
43	1420	56	Healthy	1049	Healthy
44	1698	124	Healthy	841	Healthy
45	3795	353	Moderate	407	Extensive
46	6760	614.4	Extensive	298	Extensive
47	1859	126	Healthy	738	Healthy
48	1917	177	Healthy	714	Healthy
49	1454	140.3	Healthy	1014	Healthy
50	5498	701	Extensive	315	Extensive
51	2012	190	Healthy	683	Moderate
52	3686	700	Extensive	393	Extensive
53	22790	8200	End of Life	191	End of Life
54	4568	585	Extensive	335	Extensive
55	7040	900	Extensive	282	Extensive
56	12372	1585	End of Life	167	End of Life
57	6765	670	Extensive	296	Extensive
58	2350	300	Healthy	577	Moderate
59	2325	295	Healthy	581	Moderate
60	1140	298	Healthy	1190	Healthy
61	1885	163	Healthy	725	Healthy
62	7136	680	Extensive	289	Extensive
63	4992	675	Extensive	325	Extensive
64	13346	1700	End of Life	162	End of Life
65	715	195	Healthy	959	Healthy
66	452.12	152.44	Healthy	806	Healthy
67	41.42	55.9	Healthy	544	Moderate
68	1458.83	255.75	Healthy	998	Healthy
69	711.18	771.67	Healthy	936	Healthy
70	611.92	885.87	Healthy	874	Healthy
71	218	34	Healthy	670	Moderate
72	265	40	Healthy	700	Healthy
73	318	47	Healthy	730	Healthy
74	381	55	Healthy	767	Healthy
75	452	65	Healthy	809	Healthy
76	533	75	Healthy	856	Healthy
77	624	86	Healthy	909	Healthy
78	726	98	Healthy	968	Healthy
79	838	112	Healthy	1034	Healthy
80	960	126	Healthy	1105	Healthy

81	1093	142	Healthy	1180	Healthy
82	1236	158	Healthy	1169	Healthy
83	1388	176	Healthy	1058	Healthy
84	1548	194	Healthy	941	Healthy
85	1714	212	Healthy	819	Healthy
86	1884	231	Healthy	718	Healthy
87	2058	250	Healthy	662	Moderate
88	2231	269	Healthy	608	Moderate
89	2402	289	Healthy	572	Moderate
90	2878	355	Moderate	513	Moderate
91	1983	189	Healthy	692	Moderate
92	1283	157	Healthy	1136	Healthy
93	1903	192	Healthy	716	Healthy
94	1734	83	Healthy	820	Healthy
95	1666	159	Healthy	860	Healthy
96	1504	192	Healthy	972	Healthy
97	1720	152	Healthy	822	Healthy
98	1867	194	Healthy	727	Healthy
99	1351	183	Healthy	1084	Healthy
100	2460	155	Healthy	576	Moderate
101	1669	126	Healthy	861	Healthy
102	1979	117	Healthy	702	Healthy
103	1808	227	Healthy	750	Healthy
104	1319	120	Healthy	1114	Healthy
105	762	114	Healthy	989	Healthy
106	1819	129	Healthy	755	Healthy
107	3797	496	Moderate	396	Extensive
108	1761	244	Healthy	782	Healthy
109	2247	264	Healthy	604	Moderate
110	4778	1062	Extensive	313	Extensive
111	7310	1128	Extensive	268	Extensive
112	1261	139	Healthy	1153	Healthy
113	1752	235	Healthy	789	Healthy
114	1296	255	Healthy	1115	Healthy
115	1335	110	Healthy	1104	Healthy
116	2131	220	Healthy	643	Moderate
117	3144	400	Moderate	479	Moderate
118	1812	151	Healthy	757	Healthy
119	5002	893	Extensive	316	Extensive
120	6440	902	Extensive	292	Extensive
121	5029	737	Extensive	322	Extensive
122	4962	679	Extensive	325	Extensive
123	6256	762	Extensive	300	Extensive

124	5495	700	Extensive	315	Extensive
125	9751	913	Extensive	236	End of Life
126	13289	1671	End of Life	162	End of Life
127	24996	3052	End of Life	210	End of Life
128	25007	2304	End of Life	215	End of Life
129	11780	1489	End of Life	180	End of Life
130	22789	8197	End of Life	191	End of Life
131	23691	11281	End of Life	197	End of Life

C. Contribution and significance

Results show that the developed asset management module offers a generalized approach to evaluate power transformer condition. Constructed using diverse datasets from reputable literature sources, this model emerges as a comprehensive tool for users at all stages. The model features a continuous learning capacity, progressively enhancing its performance as it encounters new data, thus ensuring its adaptability to specific requirements, including power transformers operating within distinct conditions and environments.

The model's foundation lies in the employment of CNN deep machine learning algorithms, empowering it to assimilate fresh information and fine-tune its predictions accordingly. By harnessing this innovative model, users can access invaluable insights into the well-being of their power transformers, facilitating well-informed decisions regarding maintenance and potential replacements.

While the model was developed mainly for mineral oil immersed-power transformers due to the availability of required data, same concepts can be used to modify the model to other transformer types once sufficient data are available to train the model.

Overall, key advancements and contributions highlighted in this study include:

- Developed transformer asset management solely relying on measurements obtained from online DGA sensors.
- Empowerment of the model to interpret online DGA measurements accurately and diagnose multiple faults to provide more insights into transformer health condition.
- Estimating the DP value based on CO and CO₂ measurements and hence eliminating the need to measure furan compounds offline. This feature facilitates the online implementation of the developed asset management model.
- Employing CNN, which utilizes a single training model and requires minimal input features.

4.5. Summary

This chapter presents a comprehensive approach for transformer asset management through the integration of two modules: Fault Diagnostics and Life Management. Both modules have undergone training utilizing deep CNN machine learning technique. This technique empowers the model to harness

the potential of online DGA measurements, providing asset managers with a streamlined means to obtain highly accurate insights into the health condition of power transformers. Furthermore, the model offers indication of paper insulation deterioration in real time using the measurements of CO and CO₂ that can be obtained using online DGA sensors. The feature is crucial information for effective real time asset management schemes. The adoption of CNN not only simplifies the process, but it utilizes a single training model and requires minimal input features. The proposed approach enhances the precision of predictions, hence facilitating informed decision-making for asset managers. This comprehensive strategy, encompassing fault diagnostics and life assessment, demonstrates the integration of cutting-edge technology into asset management practices, and contributes to the enhanced reliability and longevity of power transformer.

Chapter 5 Conclusions and Future Work

5.1. Conclusions

This thesis represents a dedicated effort toward the development of a comprehensive online asset management model for oil-immersed power transformers.

Commencing with an exhaustive exploration into contemporary condition monitoring methodologies applicable to oil-immersed power transformers, this study navigated through a thorough investigation. Following Chapter 1 introduction, Chapter 2 meticulously examined 15 distinct condition monitoring methods, encompassing 11 offline methodologies and 4 online approaches. Of particular focus within these online methods, Chapter 2 intricately dissected the technologies integral to the DGA method. Detailed insights were provided into the operational functionality of prevalent DGA units, elucidating their capacity to extract gases present in insulation oil within power transformers. Among the diverse technologies available, GC and PAS emerged as the most prevalent and widely adopted techniques in the current market landscape. Moreover, the chapter encapsulated the realm of DGA data interpretation. Predominantly, the industry standard involves the application of ratios and graphical methods derived from esteemed IEEE and IEC standards, often complemented by the expertise of seasoned professionals. This combined approach has demonstrated reasonably accurate DGA analyses within the industry. However, it is imperative to acknowledge the limitations of these practices in achieving real-time, online condition monitoring. Despite their reliability, these methodologies fall short in providing instantaneous and continuous monitoring capabilities, prompting the need for a paradigm shift towards developing an advanced online asset management model.

Chapter 3 of this thesis constitutes a pivotal segment wherein a comprehensive review of methods employed in the management of oil-immersed power transformers, primarily focusing on condition-based assessment, is meticulously presented. Within the framework of asset management, this chapter intricately dissects three fundamental modules: fault diagnosis, reliability assessment, and life management, delineating the diverse methods utilized within each. Specifically, this section delves into an exploration of cutting-edge methodologies deployed in recent years, notably emphasizing the burgeoning advancements in AI techniques. Among these AI techniques, data-driven machine learning methods have garnered substantial attention and scrutiny for their potential applications in augmenting the efficiency and accuracy of condition-based assessment strategies for oil-immersed power transformers.

In Chapter 4, a pivotal stride was taken towards innovation through the development of a novel power transformer asset management model meticulously comprising two integral modules: the fault diagnostic module and the life management module. The fault diagnostic module represents a significant advancement, leveraging five gas measurements, H_2 , CH_4 , C_2H_4 , C_2H_6 , C_2H_2 to precisely determine fault conditions and assess their severity levels. Simultaneously, the life management module harnesses the potential of two gas measurements, CO , CO_2 to derive the DP value. The DP value is then utilized to calculate the transformer's remaining life in percentage and degree of deterioration. One

advantage lies in the availability of these gas measurements for numerous critical transformers already equipped with online DGA units. The development of these modules was anchored in the utilization of CNN, a form of deep machine learning. The profound advantage of employing deep machine learning, over conventional methods is its inherent feature selection capability. This enables the direct utilization of raw gas measurements as inputs, streamlining the training process by employing only a single model for each module. The adoption of this approach significantly simplifies training process and substantially reduces training time while maintaining a high degree of accuracy. Notably, the achieved accuracy for both the fault diagnostic and life management modules stands commendably at approximately 86%, affirming the efficacy and reliability of the developed asset management model in advancing the realm of oil-immersed power transformer maintenance and management.

In conclusion, this study has presented a comprehensive framework for transformer health management integrating the fault diagnostics and the life management modules. Through the development of and implementation of these modules, significant advancements in predictive maintenance strategies for power transformers have been achieved.

Appendix A contains the Python script for training this fault diagnostic module, where Appendix B includes the Python script for training the life management module. Both training processes enable users to adapt and enhance the diagnostic capabilities based on specific requirements by adjusting the training data. Appendix C contains the Python script for the asset management module, including an intuitive interface for data entry and visualization (see Figure 5.1).

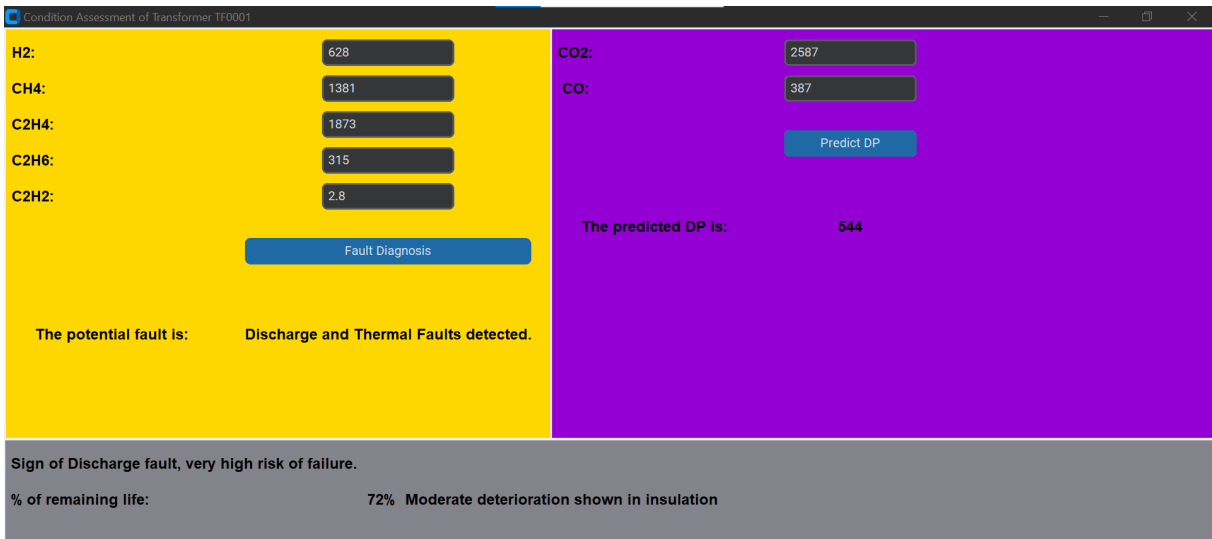


Figure 5.1 Asset Management Module Interface.

When executing the Python script outlined in Appendix C, users will be presented with an interface window featuring two distinct data entry sections. The upper left section is dedicated to the fault diagnostic module, allowing users to input 5-gas measurements for analysis. Upon clicking the “Fault Diagnosis” button, the potential fault will be displayed in this window, along with the corresponding likelihood of failure shown in the lower section. On the upper right, users can input 2-gas measurements within the life management module section. Subsequently, the predicted DP value will be presented in

the window. Additionally, the remaining life expectancy and level of insulation deterioration will be displayed in the lower window, corresponding to the entered data.

5.2. Future Work

Currently, clients can utilize the interface to manually input gas measurements and obtain results promptly. However, a significant advancement lies in transitions towards an online DGA diagnostic system. This system would automate the collection of and processing of data, streamlining the entire diagnostic process.

In this envisioned system, data collected by online DGA units would be wirelessly transmitted back to a central computer or server. These data could be stored in formats such as Excel or a database, ready for analysis. Upon receiving new data, the system would automatically trigger the diagnostic model to process the information without requiring manual intervention.

This transition to an online DGA diagnostic system offers several advantages. Firstly, it significantly reduces the time and effort required for data entry, as measurements are collected and processed in real-time. Secondly, it enhances the efficiency of the diagnostic framework, allowing for continuous monitoring and analysis of transformer health status.

In considering future avenues for research and enhancement, the importance of robust data collection emerges as a cornerstone for refining data-driven machine learning algorithms, pivotal to our developed model. While our model exhibits commendable accuracy, its potential can be further amplified by sourcing datasets derived from real fault conditions observed during transformer open inspections. Augmenting our dataset with this authentic information holds the promise of significantly improving the precision and reliability of our model's predictions.

Expanding our model's diagnostic capabilities to include the identification of additional fault types such as T1, T2, and T3 thermal faults, along with D1 and D2 energy discharge faults, holds substantial promise. By incorporating data on these six primary fault conditions into our training dataset, the model can offer more detailed fault type classification to clients. This enhancement not only enriches the diagnostic capabilities of our model but also provides actionable insights for preventive maintenance strategies, enabling asset managers to proactively address a broader spectrum of transformer issues before they escalate into critical failures.

Moreover, an area ripe for future improvement lies in the amalgamation of the DGA method with other condition monitoring techniques, specifically operational thermal measurements. Previous studies have unveiled the intricate relationship between temperature variations and the generation rates of key DGA gases. Notably, even minor temperature fluctuations can impact these gas generation rates, especially in aged oil samples, rendering them more sensitive to load ramping compared to new oil samples. To mitigate the risk of erroneous online DGA diagnoses, it becomes imperative to record and assess load variations during oil sample collection. This data integration will be pivotal in the development of a new model that comprehensively considers and accounts for these multifaceted factors, thereby

enhancing the accuracy and reliability of our asset management model for oil-immersed power transformers.

References

- [1] M. Dong *et al.*, "A Novel Maintenance Decision Making Model of Power Transformers Based on Reliability and Economy Assessment," *IEEE Access*, vol. 7, pp. 28778-28790, 2019, doi: 10.1109/ACCESS.2019.2897606.
- [2] H. Ma, T. K. Saha, C. Ekanayake, and D. Martin, "Smart Transformer for Smart Grid—Intelligent Framework and Techniques for Power Transformer Asset Management," *IEEE Transactions on Smart Grid*, vol. 6, no. 2, pp. 1026-1034, 2015, doi: 10.1109/TSG.2014.2384501.
- [3] S. Koziel, P. Hilber, P. Westerlund, and E. Shayesteh, "Investments in data quality: Evaluating impacts of faulty data on asset management in power systems," *Applied Energy*, vol. 281, p. 116057, 2021, doi: <https://doi.org/10.1016/j.apenergy.2020.116057>.
- [4] A. Jahromi, R. Piercy, S. Cress, J. Service, and W. Fan, "An approach to power transformer asset management using health index," *IEEE Electrical Insulation Magazine*, vol. 25, no. 2, pp. 20-34, 2009, doi: 10.1109/MEI.2009.4802595.
- [5] L. Jin, D. Kim, A. Abu-Siada, and S. Kumar, "Oil-Immersed Power Transformer Condition Monitoring Methodologies: A Review," *Energies (Basel)*, vol. 15, no. 9, p. 3379, 2022, doi: 10.3390/en15093379.
- [6] G. Odongo, R. Musabe, and D. Hanyurwimfura, "A Multinomial DGA Classifier for Incipient Fault Detection in Oil-Impregnated Power Transformers," *Algorithms*, vol. 14, no. 4, doi: 10.3390/a14040128.
- [7] "IEEE Guide for the Interpretation of Gases Generated in Mineral Oil-Immersed Transformers," *IEEE Std C57.104-2019 (Revision of IEEE Std C57.104-2008)*, pp. 1-98, 2019, doi: 10.1109/IEEESTD.2019.8890040.
- [8] M. Duval and A. dePabla, "Interpretation of gas-in-oil analysis using new IEC publication 60599 and IEC TC 10 databases," *IEEE Electrical Insulation Magazine*, vol. 17, no. 2, pp. 31-41, 2001, doi: 10.1109/57.917529.
- [9] L. Jin, D. Kim, and A. Abu-Siada, "State-of-the-art review on asset management methodologies for oil-immersed power transformers," *Electric Power Systems Research*, vol. 218, p. 109194, 2023/05/01/ 2023, doi: <https://doi.org/10.1016/j.epsr.2023.109194>.
- [10] M. M. Islam, G. Lee, and S. N. Hettiwatte, "A review of condition monitoring techniques and diagnostic tests for lifetime estimation of power transformers," *Electrical engineering*, vol. 100, no. 2, pp. 581-605, 2017, doi: 10.1007/s00202-017-0532-4.
- [11] O. Aljohani and A. Abu-Siada, "Application of DIP to Detect Power Transformers Axial Displacement and Disk Space Variation Using FRA Polar Plot Signature," *IEEE Transactions on Industrial Informatics*, vol. 13, no. 4, pp. 1794-1805, 2017, doi: 10.1109/TII.2016.2626779.
- [12] D. Martin, J. Marks, and T. Saha, "Survey of Australian power transformer failures and retirements," *IEEE electrical insulation magazine*, vol. 33, no. 5, pp. 16-22, 2017, doi: 10.1109/MEI.2017.8014387.
- [13] M. Hamed Samimi and H. Dadashi Ilkhechi, "Survey of different sensors employed for the power transformer monitoring," *IET science, measurement & technology*, vol. 14, no. 1, pp. 1-8, 2020, doi: 10.1049/iet-smt.2019.0103.
- [14] A.-S. Ahmed, *Power Transformer Condition Monitoring and Diagnosis*. Stevenage: Stevenage: The Institution of Engineering and Technology, 2018.
- [15] R. Soni and B. Mehta, "Review on asset management of power transformer by diagnosing incipient faults and faults identification using various testing methodologies," *Engineering failure analysis*, vol. 128, p. 105634, 2021, doi: 10.1016/j.engfailanal.2021.105634.
- [16] T. K. Saha, "Review of modern diagnostic techniques for assessing insulation condition in aged transformers," *IEEE Transactions on Dielectrics and Electrical Insulation*, vol. 10, no. 5, pp. 903-917, 2003, doi: 10.1109/TDEI.2003.1237337.
- [17] S. Li, Z. Ge, A. Abu-Siada, L. Yang, S. Li, and K. Wakimoto, "A New Technique to Estimate the Degree of Polymerization of Insulation Paper Using Multiple Aging Parameters of Transformer Oil," *IEEE Access*, vol. 7, pp. 157471-157479, 2019, doi: 10.1109/ACCESS.2019.2949580.
- [18] "IEEE Guide for Loading Mineral-Oil-Immersed Transformers and Step-Voltage Regulators," *IEEE Std C57.91-2011 (Revision of IEEE Std C57.91-1995)*, pp. 1-123, 2012, doi: 10.1109/IEEESTD.2012.6166928.
- [19] L. Cheim, D. Platts, T. Prevost, and S. Xu, "Furan analysis for liquid power transformers," *IEEE Electrical Insulation Magazine*, vol. 28, no. 2, pp. 8-21, 2012, doi: 10.1109/MEI.2012.6159177.
- [20] A. Abu-Siada, "Correlation of furan concentration and spectral response of transformer oil-using expert systems," *IET science, measurement & technology*, vol. 5, no. 5, pp. 183-188, 2011, doi: 10.1049/iet-smt.2011.0017.
- [21] N. Das, A. Abu-Siada, and S. Islam, "New approach to estimate furan contents in transformer oil using spectroscopic analysis," in *2012 22nd Australasian Universities Power Engineering Conference (AUPEC)*, 26-29 Sept. 2012 2012, pp. 1-4.

- [22] D. Feng, Z. Wang, and P. Jarman, "Transmission power transformer assessment using furan measurement with the aid of thermal model," in *2012 IEEE International Conference on Condition Monitoring and Diagnosis*, 23-27 Sept. 2012 2012, pp. 521-524, doi: 10.1109/CMD.2012.6416194.
- [23] A. Abu-Siada, S. P. Lai, and S. M. Islam, "A Novel Fuzzy-Logic Approach for Furan Estimation in Transformer Oil," *IEEE Transactions on Power Delivery*, vol. 27, no. 2, pp. 469-474, 2012, doi: 10.1109/TPWRD.2012.2186986.
- [24] R. Karthik, T. S. R. Raja, and S. S. Shunmugam, "Performance evaluation of transformer oil using uv-visible spectrophotometer," *Acta Scientiarum. Technology*, vol. 36, no. 2, pp. 245-250, 2014.
- [25] R. Polanský, P. Hahn, P. Kadlec, D. Moravcová, and P. Prosr, "Quantifying the Effect of Catalysts on the Lifetime of Transformer Oil," *Applied Sciences*, vol. 10, no. 4, 2020, doi: 10.3390/app10041309.
- [26] N. A. Bakar and A. Abu-Siada, "A novel method of measuring transformer oil interfacial tension using UV-Vis spectroscopy," *IEEE Electrical Insulation Magazine*, vol. 32, no. 1, pp. 7-13, 2016, doi: 10.1109/MEI.2016.7361098.
- [27] N. A. Baka, A. Abu-Siada, S. Islam, and M. F. El-Naggar, "A new technique to measure interfacial tension of transformer oil using UV-Vis spectroscopy," *IEEE Transactions on Dielectrics and Electrical Insulation*, vol. 22, no. 2, pp. 1275-1282, 2015, doi: 10.1109/TDEI.2015.7076831.
- [28] H. Cui *et al.*, "Effect of Temperature and Pre-stressed Voltage on Breakdown of Oil-Impregnated Paper," in *2018 Condition Monitoring and Diagnosis (CMD)*, 23-26 Sept. 2018 2018, pp. 1-5, doi: 10.1109/CMD.2018.8535932.
- [29] A. A. Suleiman, N. A. Muhamad, N. Bashir, N. S. Murad, Y. Z. Arief, and B. T. Phung, "Effect of moisture on breakdown voltage and structure of palm based insulation oils," *IEEE Transactions on Dielectrics and Electrical Insulation*, vol. 21, no. 5, pp. 2119-2126, 2014, doi: 10.1109/TDEI.2014.004431.
- [30] "IEEE Guide for Acceptance and Maintenance of Insulating Mineral Oil in Electrical Equipment," *IEEE Std C57.106-2015 (Revision of IEEE Std C57.106-2006)*, pp. 1-38, 2016, doi: 10.1109/IEEESTD.2016.7442048.
- [31] S. Li *et al.*, "Effect of AC-voltage harmonics on oil impregnated paper in transformer bushings," *IEEE Transactions on Dielectrics and Electrical Insulation*, vol. 27, no. 1, pp. 26-32, 2020, doi: 10.1109/TDEI.2019.008247.
- [32] J. S. Juris, I. C. Duran, and A. R. Marulanda, "Correlation between Insulation Resistance and Dissolved Gas Analysis Tests in Power Transformers," in *2020 IEEE PES Transmission & Distribution Conference and Exhibition - Latin America (T&D LA)*, 28 Sept.-2 Oct. 2020 2020, pp. 1-6, doi: 10.1109/TDLA47668.2020.9326248.
- [33] H. Torkaman and F. Karimi, "Measurement variations of insulation resistance/polarization index during utilizing time in HV electrical machines – A survey," *Measurement*, vol. 59, pp. 21-29, 2015/01/01/ 2015, doi: <https://doi.org/10.1016/j.measurement.2014.09.034>.
- [34] "IEEE Recommended Practice for Testing Insulation Resistance of Electric Machinery," *IEEE Std 43-2013 (Revision of IEEE Std 43-2000)*, pp. 1-37, 2014, doi: 10.1109/IEEESTD.2014.6754111.
- [35] A. P. Marques *et al.*, "Insulation resistance of power transformers — method for optimized analysis," in *2017 IEEE 19th International Conference on Dielectric Liquids (ICDL)*, 25-29 June 2017 2017, pp. 1-4, doi: 10.1109/ICDL.2017.8124629.
- [36] B. D. Malpure and K. Baburao, "Failure Analysis & Diagnostics of Power Transformer Using Dielectric dissipation factor," in *2008 International Conference on Condition Monitoring and Diagnosis*, 21-24 April 2008 2008, pp. 497-501, doi: 10.1109/CMD.2008.4580334.
- [37] A. Setayeshmehr, A. Akbari, H. Borsi, and E. Gockenbach, "On-line monitoring and diagnoses of power transformer bushings," *IEEE Transactions on Dielectrics and Electrical Insulation*, vol. 13, no. 3, pp. 608-615, 2006, doi: 10.1109/TDEI.2006.1657975.
- [38] G. Faria, M. Pereira, G. Lopes, J. Villibor, P. Tavares, and I. Faria, "Evaluation of Capacitance and Dielectric Dissipation Factor of Distribution Transformers - Experimental Results," in *2018 IEEE Electrical Insulation Conference (EIC)*, 17-20 June 2018 2018, pp. 336-339, doi: 10.1109/EIC.2018.8481052.
- [39] "IEEE Guide for Diagnostic Field Testing of Fluid-Filled Power Transformers, Regulators, and Reactors," *IEEE Std C57.152-2013*, pp. 1-121, 2013, doi: 10.1109/IEEESTD.2013.6544533.
- [40] A. Abu-Siada and S. Islam, "A new approach to identify power transformer criticality and asset management decision based on dissolved gas-in-oil analysis," *IEEE Transactions on Dielectrics and Electrical Insulation*, vol. 19, no. 3, pp. 1007-1012, 2012, doi: 10.1109/TDEI.2012.6215106.
- [41] D. Wang *et al.*, "A New Testing Method for the Dielectric Response of Oil-Immersed Transformer," *IEEE Transactions on Industrial Electronics*, vol. 67, no. 12, pp. 10833-10843, 2020, doi: 10.1109/TIE.2019.2959500.
- [42] C. T. F. 15.01.09, "Dielectric response methods for diagnostics of power transformers," *IEEE Electrical Insulation Magazine*, vol. 19, no. 3, pp. 12-18, 2003, doi: 10.1109/MEI.2003.1203017.
- [43] T. Zhang, X. Tan, B. Zhang, and X. Xu, "Study on Moisture and Aging of Oil-Paper Insulation Using Relative Initial Slope of Recovery Voltage," *IEEE Transactions on Applied Superconductivity*, vol. 26, no. 7, pp. 1-4, 2016, doi: 10.1109/TASC.2016.2600299.

- [44] T. K. Saha and Y. Zheng Tong, "Experience with return voltage measurements for assessing insulation conditions in service-aged transformers," *IEEE Transactions on Power Delivery*, vol. 18, no. 1, pp. 128-135, 2003, doi: 10.1109/TPWRD.2002.803722.
- [45] I. Fofana, A. Bouaicha, and M. Farzaneh, "Aging Characterization of Transformer Oil-Pressboard Insulation using Modern Diagnostic Techniques," *European Transactions on Electrical Power*, vol. 11, pp. 1110–1127, 01/01 2011, doi: 10.1002/etep.499.
- [46] M. A. Talib *et al.*, "Diagnosis of transformer insulation condition using recovery voltage measurements," in *Proceedings. National Power Engineering Conference, 2003. PCon 2003.*, 15-16 Dec. 2003 2003, pp. 329-332, doi: 10.1109/PECON.2003.1437467.
- [47] D. Linhjell, L. Lundgaard, and U. Gafvert, "Dielectric response of mineral oil impregnated cellulose and the impact of aging," *IEEE Transactions on Dielectrics and Electrical Insulation*, vol. 14, no. 1, pp. 156-169, 2007, doi: 10.1109/TDEI.2007.302884.
- [48] T. K. Saha, M. Darveniza, D. J. T. Hill, and T. T. Le, "Electrical and chemical diagnostics of transformers insulation. A. Aged transformer samples," *IEEE Transactions on Power Delivery*, vol. 12, no. 4, pp. 1547-1554, 1997, doi: 10.1109/61.634174.
- [49] T. K. Saha and P. Purkait, "Investigation of polarization and depolarization current measurements for the assessment of oil-paper insulation of aged transformers," *IEEE Transactions on Dielectrics and Electrical Insulation*, vol. 11, no. 1, pp. 144-154, 2004, doi: 10.1109/TDEI.2004.1266329.
- [50] J. Liu, D. Zhang, X. Wei, and H. R. Karimi, "Transformation Algorithm of Dielectric Response in Time-Frequency Domain," *Mathematical problems in engineering*, vol. 2014, pp. 1-7, 2014, doi: 10.1155/2014/547105.
- [51] T. Zhang, X. Li, H. Lv, and X. Tan, "Parameter Identification and Calculation of Return Voltage Curve Based on FDS Data," *IEEE Transactions on Applied Superconductivity*, vol. 24, no. 5, pp. 1-5, 2014, doi: 10.1109/TASC.2014.2344763.
- [52] S. M. Kumara, S.; Bandara, K.; Wickramasuriya, P.; Yousuf, F.; Ekanayake, C.; Fernando, M.; Wang, Z.; Gubanski, S.M. (2021) Frequency Domain Measurements for Diagnosis of Power Transformers: Experiences from Australia, Malaysia, Sri Lanka and UK. *CIGRE Science and Engineering (CSE)*. 82-107.
- [53] A. Abu-Siada and O. Aljohani, "Detecting incipient radial deformations of power transformer windings using polar plot and digital image processing," *IET Science, Measurement & Technology*, vol. 12, no. 4, pp. 492-499, 2018, doi: <https://doi.org/10.1049/iet-smt.2017.0412>.
- [54] M. Bigdeli and A. Abu-Siada, "Clustering of transformer condition using frequency response analysis based on k-means and GOA," *Electric Power Systems Research*, vol. 202, p. 107619, 2022/01/01/ 2022, doi: <https://doi.org/10.1016/j.epsr.2021.107619>.
- [55] S. M. A. N. Al-Ameri *et al.*, "Understanding the Influence of Power Transformer Faults on the Frequency Response Signature Using Simulation Analysis and Statistical Indicators," *IEEE Access*, vol. 9, pp. 70935-70947, 2021, doi: 10.1109/ACCESS.2021.3076984.
- [56] A. Abu-Siada, M. I. Mosaad, D. Kim, and M. F. El-Naggar, "Estimating Power Transformer High Frequency Model Parameters Using Frequency Response Analysis," *IEEE Transactions on Power Delivery*, vol. 35, no. 3, pp. 1267-1277, 2020, doi: 10.1109/TPWRD.2019.2938020.
- [57] O. Aljohani and A. Abu-Siada, "Application of digital image processing to detect transformer bushing faults and oil degradation using FRA polar plot signature," *IEEE Transactions on Dielectrics and Electrical Insulation*, vol. 24, no. 1, pp. 428-436, 2017, doi: 10.1109/TDEI.2016.006088.
- [58] X. Zhao, C. Yao, Z. Zhao, and A. Abu-Siada, "Performance evaluation of online transformer internal fault detection based on transient overvoltage signals," *IEEE Transactions on Dielectrics and Electrical Insulation*, vol. 24, no. 6, pp. 3906-3915, 2017, doi: 10.1109/TDEI.2017.006772.
- [59] V. Behjat, A. Vahedi, A. Setayeshmehr, H. Borsi, and E. Gockenbach, "Diagnosing Shorted Turns on the Windings of Power Transformers Based Upon Online FRA Using Capacitive and Inductive Couplings," *IEEE Transactions on Power Delivery*, vol. 26, no. 4, pp. 2123-2133, 2011, doi: 10.1109/TPWRD.2011.2151285.
- [60] X. Zhao *et al.*, "Experimental Evaluation of Transformer Internal Fault Detection Based on V-I Characteristics," *IEEE Transactions on Industrial Electronics*, vol. 67, no. 5, pp. 4108-4119, 2020, doi: 10.1109/TIE.2019.2917368.
- [61] O. W. Iwanusiw and P. Eng, "The Art and Science of Transformer Ratio Measurement," in *2018 IEEE Electrical Insulation Conference (EIC)*, 17-20 June 2018 2018, pp. 390-394, doi: 10.1109/EIC.2018.8481036.
- [62] A. S. A. Razzaq, M. F. M. Yousof, S. M. Al-Ameri, M. A. Talib, and A. J. Mshkil, "Interpretation of Inter-Turn Fault in Transformer Winding Using Turns Ratio Test and Frequency Response Analysis," 2021.
- [63] E. Osmanbasic, "Importance of using high test voltage for transformer turns ratio test," *Transformers Magazine*, vol. 8, no. 3, pp. 98-105, 2021.

- [64] A. Abu-Siada, M. Arshad, and S. Islam, "Fuzzy logic approach to identify transformer criticality using dissolved gas analysis," in *IEEE PES General Meeting*, 25-29 July 2010 2010, pp. 1-5, doi: 10.1109/PES.2010.5589789.
- [65] A. B. Norazhar, A. Abu-Siada, and S. Islam, "A review on chemical diagnosis techniques for transformer paper insulation degradation," in *2013 Australasian Universities Power Engineering Conference (AUPEC)*, 29 Sept.-3 Oct. 2013 2013, pp. 1-6, doi: 10.1109/AUPEC.2013.6725476.
- [66] A. Abu-Siada, "Improved Consistent Interpretation Approach of Fault Type within Power Transformers Using Dissolved Gas Analysis and Gene Expression Programming," *Energies*, vol. 12, no. 4, p. 730, 2019. [Online]. Available: <https://www.mdpi.com/1996-1073/12/4/730>.
- [67] N. A. Bakar, A. Abu-Siada, and S. Islam, "A review of dissolved gas analysis measurement and interpretation techniques," *IEEE electrical insulation magazine*, vol. 30, no. 3, pp. 39-49, 2014, doi: 10.1109/MEI.2014.6804740.
- [68] J. Chow, R. Lee, E. Wong, K. Leung, and G. Lai, "Novel engineering techniques to overcoming traditional challenges in online condition monitoring systems for power transformer," *Transactions (Hong Kong Institution of Engineers)*, vol. 25, no. 4, pp. 248-254, 2018, doi: 10.1080/1023697X.2018.1539348.
- [69] L.-C. Ma, C. Chen, and J. Y. S. Lin, "Teflon AF2400 Hollow Fiber Membrane Contactor for Dissolved Gas-in-Oil Extraction: Mass Transfer Characteristics," *Ind. Eng. Chem. Res.*, vol. 59, no. 38, pp. 16795-16804, 2020, doi: 10.1021/acs.iecr.0c03178.
- [70] L.-C. Ma, C. Chen, C.-H. Chen, K.-L. Tung, and J. Y. S. Lin, "Gas Transport Properties of Teflon AF2400/Ceramic Composite Hollow Fiber Membranes in Dissolved-Gas-in-Oil Extraction," *Ind. Eng. Chem. Res.*, vol. 59, no. 12, pp. 5392-5401, 2020, doi: 10.1021/acs.iecr.9b06026.
- [71] J. Fan, F. Wang, Q. Sun, F. Bin, J. Ding, and H. Ye, "SOFC detector for portable gas chromatography: High-sensitivity detection of dissolved gases in transformer oil," *IEEE transactions on dielectrics and electrical insulation*, vol. 24, no. 5, pp. 2854-2863, 2017, doi: 10.1109/TDEI.2017.006438.
- [72] J. Fan, F. Wang, Q. Sun, H. Ye, and Q. Jiang, "Application of Polycrystalline SnO₂ Sensor Chromatographic System to Detect Dissolved Gases in Transformer Oil," *Sensors and Actuators B: Chemical*, vol. 267, pp. 636-646, 2018/08/15/2018, doi: <https://doi.org/10.1016/j.snb.2018.04.014>.
- [73] Z. Mao and J. Wen, "Detection of dissolved gas in oil-insulated electrical apparatus by photoacoustic spectroscopy," *IEEE electrical insulation magazine*, vol. 31, no. 4, pp. 7-14, 2015, doi: 10.1109/MEI.2015.7126069.
- [74] H. Cui, L. Yang, Y. Zhu, S. Li, A. Abu-Siada, and S. Islam, "Dissolved Gas Analysis for Power Transformers within Distributed Renewable Generation-Based Systems," *IEEE Transactions on Dielectrics and Electrical Insulation*, vol. 28, no. 4, pp. 1349-1356, 2021, doi: 10.1109/TDEI.2021.009490.
- [75] S. Palzer, "Photoacoustic-based gas sensing: A review," *Sensors (Basel)*, vol. 20, no. 9, p. 2745, 2020, doi: 10.3390/s20092745.
- [76] Y. Yun, W. Chen, Y. Wang, and C. Pan, "Photoacoustic detection of dissolved gases in transformer oil," *Euro. Trans. Electr. Power*, vol. 18, no. 6, pp. 562-576, 2008, doi: 10.1002/etep.191.
- [77] N. Abu Bakar and A. Abu-Siada, "A new method to detect dissolved gases in transformer oil using NIR-IR spectroscopy," *IEEE transactions on dielectrics and electrical insulation*, vol. 24, no. 1, pp. 409-419, 2017, doi: 10.1109/TDEI.2016.006025.
- [78] T. Yang and W. Chen, "Detection of Dissolved Gas in Transformer Oil Based on All-Optical Photoacoustic Spectroscopy," in *2020 IEEE International Conference on High Voltage Engineering and Application (ICHVE)*, 6-10 Sept. 2020 2020, pp. 1-4, doi: 10.1109/ICHVE49031.2020.9279929.
- [79] A. Abu-Siada, S. Hmood, and S. Islam, "A new fuzzy logic approach for consistent interpretation of dissolved gas-in-oil analysis," *IEEE Transactions on Dielectrics and Electrical Insulation*, vol. 20, no. 6, pp. 2343-2349, 2013, doi: 10.1109/TDEI.2013.6678888.
- [80] V. V. Kondalkar, J. Park, and K. Lee, "MEMS hydrogen gas sensor for in-situ monitoring of hydrogen gas in transformer oil," *Sensors and actuators. B, Chemical*, vol. 326, p. 128989, 2021, doi: 10.1016/j.snb.2020.128989.
- [81] F. A. Lewis, "The palladium/hydrogen system," *Berichte der Bunsengesellschaft für physikalische Chemie*, vol. 71, no. 9-10, pp. 1160-1161, 1967.
- [82] C. Christofides and A. Mandelis, "Solid-state sensors for trace hydrogen gas detection," *Journal of applied physics*, vol. 68, no. 6, pp. R1-R30, 1990, doi: 10.1063/1.346398.
- [83] A. Kumar, "Palladium-based trench gate MOSFET for highly sensitive hydrogen gas sensor," *Materials science in semiconductor processing*, vol. 120, p. 105274, 2020, doi: 10.1016/j.mssp.2020.105274.
- [84] L. Zhang, H. Zhao, Y. Li, Y. Han, S. Wang, and Y. Shang, "Study on Multi-parameter On-line Monitoring System for Transformer Bushing," in *2020 Asia Energy and Electrical Engineering Symposium (AEEES)*, 29-31 May 2020 2020, pp. 54-58, doi: 10.1109/AEEES48850.2020.9121465.

- [85] E. Lee, J. M. Lee, J. H. Koo, W. Lee, and T. Lee, "Hysteresis behavior of electrical resistance in Pd thin films during the process of absorption and desorption of hydrogen gas," *International Journal of Hydrogen Energy*, vol. 35, no. 13, pp. 6984-6991, 2010/07/01/ 2010, doi: <https://doi.org/10.1016/j.ijhydene.2010.04.051>.
- [86] "IEEE Guide for Interpretation of Gases Generated in Natural Ester and Synthetic Ester-Immersed Transformers," *IEEE Std C57.155-2014*, pp. 1-52, 2014, doi: 10.1109/IEEESTD.2014.6966710.
- [87] J. Faiz and M. Soleimani, "Dissolved gas analysis evaluation in electric power transformers using conventional methods a review," *IEEE Transactions on Dielectrics and Electrical Insulation*, vol. 24, no. 2, pp. 1239-1248, 2017, doi: 10.1109/TDEI.2017.005959.
- [88] H. Cui *et al.*, "Impact of Load Ramping on Power Transformer Dissolved Gas Analysis," *IEEE Access*, vol. 7, pp. 170343-170351, 2019, doi: 10.1109/ACCESS.2019.2926435.
- [89] E. Wannapring, C. Suwanasri, and T. Suwanasri, "Dissolved Gas Analysis methods for distribution transformers," in *2016 13th International Conference on Electrical Engineering/Electronics, Computer, Telecommunications and Information Technology (ECTI-CON)*, 28 June-1 July 2016 2016, pp. 1-6, doi: 10.1109/ECTICon.2016.7561320.
- [90] B. Sarkar, C. Koley, N. K. Roy, and P. Kumbhakar, "Condition monitoring of high voltage transformers using Fiber Bragg Grating Sensor," *Measurement : journal of the International Measurement Confederation*, vol. 74, pp. 255-267, 2015, doi: 10.1016/j.measurement.2015.07.014.
- [91] G. M. Jun Jiang, "Partial Discharge Detection with Optical Methods," in *Optical sensing in power transformers*. London, England: Wiley, 2021, ch. 5, pp. 137-188.
- [92] D. Kim and A. Abu-Siada, "Partial Discharge Analysis on-site in Various High Voltage Apparatus," in *2018 Condition Monitoring and Diagnosis (CMD)*, 23-26 Sept. 2018 2018, pp. 1-6, doi: 10.1109/CMD.2018.8535987.
- [93] "IEEE Guide for the Detection, Location and Interpretation of Sources of Acoustic Emissions from Electrical Discharges in Power Transformers and Power Reactors," *IEEE Std C57.127-2018 (Revision of IEEE Std C57.127-2007)*, pp. 1-72, 2019, doi: 10.1109/IEEESTD.2019.8664690.
- [94] S. M. B. Neuhold, T.; Braunlich, R.; Behrmann, G.; Schlemper, H.D.; Riechert, U.; Muller, P.; Lehner M.; Schneiter, E.; Sigrist, P., "Return of experience: The CIGRE UHF PD sensitivity verification and on-site detection of critical defects," pp. 1-13, 2018. CIGRE.
- [95] N. D. Roslizan *et al.*, "A Review: Partial Discharge Detection using UHF sensor on High Voltage Equipment," *J. Phys.: Conf. Ser.*, vol. 1432, no. 1, p. 12003, 2020, doi: 10.1088/1742-6596/1432/1/012003.
- [96] H. Chai, B. T. Phung, and S. Mitchell, "Application of UHF Sensors in Power System Equipment for Partial Discharge Detection: A Review," *Sensors (Basel)*, vol. 19, no. 5, p. 1029, 2019, doi: 10.3390/s19051029.
- [97] H. H. Sinaga, B. T. Phung, and T. R. Blackburn, "Partial discharge localization in transformers using UHF detection method," *IEEE Transactions on Dielectrics and Electrical Insulation*, vol. 19, no. 6, pp. 1891-1900, 2012, doi: 10.1109/TDEI.2012.6396945.
- [98] M. K. Chakravarthi, A. V. Giridhar, and D. V. S. S. S. Sarma, "Localization of Incipient Discharge in Power Transformer Using UHF Sensor," in *2019 International Conference on High Voltage Engineering and Technology (ICHVET)*, 7-8 Feb. 2019 2019, pp. 1-3, doi: 10.1109/ICHVET.2019.8724280.
- [99] W. Yuan, G. Chuangli, W. Zhipeng, and D. Pengcheng, "UHF PD Online Monitoring of Huge-Size Transformers and Data Analysis," in *2011 International Conference on Computer Distributed Control and Intelligent Environmental Monitoring*, 19-20 Feb. 2011 2011, pp. 2375-2378, doi: 10.1109/CDCIEM.2011.338.
- [100] S. M. Hoek, M. Krüger, S. Körber, and A. Kraetge, "Application of the UHF technology to detect and locate partial discharges in liquid immersed transformer," *Elektrotechnik und Informationstechnik*, vol. 131, no. 8, pp. 386-392, 2014, doi: 10.1007/s00502-014-0236-7.
- [101] H. Chai, B. T. Phung, and D. Zhang, "Development of UHF Sensors for Partial Discharge Detection in Power Transformer," in *2018 Condition Monitoring and Diagnosis (CMD)*, 23-26 Sept. 2018 2018, pp. 1-5, doi: 10.1109/CMD.2018.8535779.
- [102] H. Y. Zhou, G. M. Ma, M. Zhang, H. C. Zhang, and C. R. Li, "A High Sensitivity Optical Fiber Interferometer Sensor for Acoustic Emission Detection of Partial Discharge in Power Transformer," *IEEE Sensors Journal*, vol. 21, no. 1, pp. 24-32, 2021, doi: 10.1109/JSEN.2019.2951613.
- [103] C. Gao, L. Yu, Y. Xu, W. Wang, S. Wang, and P. Wang, "Partial Discharge Localization Inside Transformer Windings via Fiber-Optic Acoustic Sensor Array," *IEEE Transactions on Power Delivery*, vol. 34, no. 4, pp. 1251-1260, 2019, doi: 10.1109/TPWRD.2018.2880230.
- [104] M. M. Yaacob, M. A. Alsaedi, J. R. Rashed, A. M. Dakhil, and S. F. Atyah, "Review on partial discharge detection techniques related to high voltage power equipment using different sensors," *Photonic Sensors*, vol. 4, no. 4, pp. 325-337, 2014/12/01 2014, doi: 10.1007/s13320-014-0146-7.

- [105] C. Gao, W. Wang, S. Song, S. Wang, L. Yu, and Y. Wang, "Localization of partial discharge in transformer oil using Fabry-Pérot optical fiber sensor array," *IEEE Transactions on Dielectrics and Electrical Insulation*, vol. 25, no. 6, pp. 2279-2286, 2018, doi: 10.1109/TDEI.2018.007065.
- [106] S. Qian, H. Chen, Y. Xu, and L. Su, "High sensitivity detection of partial discharge acoustic emission within power transformer by sagnac fiber optic sensor," *IEEE Transactions on Dielectrics and Electrical Insulation*, vol. 25, no. 6, pp. 2313-2320, 2018, doi: 10.1109/TDEI.2018.007131.
- [107] C. Zachariades, R. Shuttleworth, R. Giussani, and R. MacKinlay, "Optimization of a High-Frequency Current Transformer Sensor for Partial Discharge Detection Using Finite-Element Analysis," *IEEE sensors journal*, vol. 16, no. 20, pp. 7526-7533, 2016, doi: 10.1109/JSEN.2016.2600272.
- [108] G. M. Ma *et al.*, "Distributed Partial Discharge Detection in a Power Transformer Based on Phase-Shifted FBG," *IEEE Sensors Journal*, vol. 18, no. 7, pp. 2788-2795, 2018, doi: 10.1109/JSEN.2018.2803056.
- [109] I. Búa-Núñez, J. E. Posada-Román, J. Rubio-Serrano, and J. A. Garcia-Souto, "Instrumentation System for Location of Partial Discharges Using Acoustic Detection With Piezoelectric Transducers and Optical Fiber Sensors," *IEEE Transactions on Instrumentation and Measurement*, vol. 63, no. 5, pp. 1002-1013, 2014, doi: 10.1109/TIM.2013.2286891.
- [110] I. Búa-Núñez, J. E. Posada-Román, and J. A. García-Souto, "Multichannel detection of acoustic emissions and localization of the source with external and internal sensors for partial discharge monitoring of power transformers," *Energies (Basel)*, vol. 14, no. 23, p. 7873, 2021, doi: 10.3390/en14237873.
- [111] H. Yoshizumi *et al.*, "Consideration of Generation Mechanism of Low Frequency Component of Partial Discharge Signal Detected by Transient Earth Voltage," in *2018 Condition Monitoring and Diagnosis (CMD)*, 23-26 Sept. 2018 2018, pp. 1-4, doi: 10.1109/CMD.2018.8535989.
- [112] A. J. Reid, M. D. Judd, and G. Duncan, "Simultaneous measurement of partial discharge using TEV, IEC60270 and UHF techniques," in *2012 IEEE International Symposium on Electrical Insulation*, 10-13 June 2012 2012, pp. 439-442, doi: 10.1109/ELINSL.2012.6251506.
- [113] W. Liuho *et al.*, "Experimental investigation of transient earth voltage and acoustic emission measurements of partial discharge signals in medium-voltage switchgears," in *2013 2nd International Conference on Electric Power Equipment - Switching Technology (ICEPE-ST)*, 20-23 Oct. 2013 2013, pp. 1-4, doi: 10.1109/ICEPE-ST.2013.6804296.
- [114] A. Itose, M. Kozako, and M. Hikita, "Partial discharge detection and induced surface current analysis using transient earth voltage method for high voltage equipment," in *2016 International Conference on Condition Monitoring and Diagnosis (CMD)*, 25-28 Sept. 2016 2016, pp. 456-460, doi: 10.1109/CMD.2016.7757859.
- [115] J. Seo, H. Ma, and T. Saha, "A novel signal extraction technique for online partial discharge (PD) measurement of transformers," *International Transactions on Electrical Energy Systems*, vol. 26, no. 5, pp. 1032-1048, 2016.
- [116] X. Hu, W. H. Siew, M. D. Judd, and X. Peng, "Transfer function characterization for HFCTs used in partial discharge detection," *IEEE Transactions on Dielectrics and Electrical Insulation*, vol. 24, no. 2, pp. 1088-1096, 2017, doi: 10.1109/TDEI.2017.006115.
- [117] M. Aslam *et al.*, "Dynamic Thermal Model for Power Transformers," *IEEE access*, vol. 9, pp. 71461-71469, 2021, doi: 10.1109/ACCESS.2021.3078759.
- [118] M. Wang, A. J. Vandermaar, and K. D. Srivastava, "Review of condition assessment of power transformers in service," *IEEE Electrical Insulation Magazine*, vol. 18, no. 6, pp. 12-25, 2002, doi: 10.1109/MEI.2002.1161455.
- [119] M. Mikhak-Beyranvand, J. Faiz, and B. Rezaeealam, "Thermal Analysis of Power Transformer Using an Improved Dynamic Thermal Equivalent Circuit Model," *Electric Power Components and Systems*, vol. 47, no. 18, pp. 1598-1609, 2019/11/08 2019, doi: 10.1080/15325008.2019.1689452.
- [120] M. Kunicki, S. Borucki, A. Cichoń, and J. Frymus, "Modeling of the Winding Hot-Spot Temperature in Power Transformers: Case Study of the Low-Loaded Fleet," *Energies*, vol. 12, no. 18, 2019, doi: 10.3390/en12183561.
- [121] T. Mariprasath and V. Kirubakaran, "A real time study on condition monitoring of distribution transformer using thermal imager," *Infrared Physics & Technology*, vol. 90, pp. 78-86, 2018/05/01/ 2018, doi: <https://doi.org/10.1016/j.infrared.2018.02.009>.
- [122] Y. Hu, J. Zheng, and H. Huang, "Experimental Research on Power Transformer Vibration Distribution under Different Winding Defect Conditions," *Electronics*, vol. 8, no. 8, p. 842, 2019. [Online]. Available: <https://www.mdpi.com/2079-9292/8/8/842>.
- [123] A. Secic, M. Krpan, and I. Kuzle, "Vibro-Acoustic Methods in the Condition Assessment of Power Transformers: A Survey," *IEEE Access*, vol. 7, pp. 83915-83931, 2019, doi: 10.1109/ACCESS.2019.2923809.
- [124] S. Ji, P. Shan, Y. Li, D. Xu, and J. Cao, "The vibration measuring system for monitoring core and winding condition of power transformer," in *Proceedings of 2001 International Symposium on Electrical Insulating Materials (ISEIM 2001)*.

- 2001 Asian Conference on Electrical Insulating Diagnosis (ACEID 2001). 33rd Symposium on Electrical and Ele, 22-22 Nov. 2001 2001, pp. 849-852, doi: 10.1109/ISEIM.2001.973811.
- [125] B. Garcia, J. C. Burgos, and A. M. Alonso, "Transformer tank vibration modeling as a method of detecting winding deformations-part II: experimental verification," *IEEE Transactions on Power Delivery*, vol. 21, no. 1, pp. 164-169, 2006, doi: 10.1109/TPWRD.2005.852275.
- [126] A. Abu-Siada and S. Islam, "A Novel Online Technique to Detect Power Transformer Winding Faults," *IEEE Transactions on Power Delivery*, vol. 27, no. 2, pp. 849-857, 2012, doi: 10.1109/TPWRD.2011.2180932.
- [127] O. Aljohani and A. Abu-Siada, "Application of Digital Image Processing to Detect Short-Circuit Turns in Power Transformers Using Frequency Response Analysis," *IEEE Transactions on Industrial Informatics*, vol. 12, no. 6, pp. 2062-2073, 2016, doi: 10.1109/TII.2016.2594773.
- [128] A. Abu-Siada, I. Radwan, and A. F. Abdou, "3D approach for fault identification within power transformers using frequency response analysis," *IET science, measurement & technology*, vol. 13, no. 6, pp. 903-911, 2019, doi: 10.1049/iet-smt.2018.5573.
- [129] M. I. Mossad, M. Azab, and A. Abu-Siada, "Transformer Parameters Estimation From Nameplate Data Using Evolutionary Programming Techniques," *IEEE Transactions on Power Delivery*, vol. 29, no. 5, pp. 2118-2123, 2014, doi: 10.1109/TPWRD.2014.2311153.
- [130] A. Abu-Siada and S. Hmood, "Fuzzy logic approach for power transformer asset management based on dissolved gas-in-oil analysis," *Chemical engineering transactions*, vol. 33, pp. 997-1002, 2013, doi: 10.3303/CET1333167.
- [131] H. Cui, L. Yang, Y. Zhu, S. Li, A. Abu-Siada, and S. Islam, "A comprehensive analyses of aging characteristics of oil-paper insulation system in HVDC converter transformers," *IEEE Transactions on Dielectrics and Electrical Insulation*, vol. 27, no. 5, pp. 1707-1714, 2020, doi: 10.1109/TDEI.2020.008788.
- [132] A. Abu-Siada, J. Budiri, and A. F. Abdou, "Solid State Transformers Topologies, Controllers, and Applications: State-of-the-Art Literature Review," *Electronics*, vol. 7, no. 11, p. 298, 2018. [Online]. Available: <https://www.mdpi.com/2079-9292/7/11/298>.
- [133] M. M. Hasan, A. Abu-Siada, S. M. Islam, and M. S. A. Dahidah, "A New Cascaded Multilevel Inverter Topology with Galvanic Isolation," *IEEE Transactions on Industry Applications*, vol. 54, no. 4, pp. 3463-3472, 2018, doi: 10.1109/TIA.2018.2818061.
- [134] "Condition assessment of power transformers " *Power transformers and reactors, CIGRE Technical Brochure*, vol. A2-761, 2019.
- [135] "Asset health indices for equipment in existing substations," *Substations and electrical installations, CIGRE Technical Brochure*, vol. B3-858, 2021.
- [136] R. Murugan and R. Ramasamy, "Understanding the power transformer component failures for health index-based maintenance planning in electric utilities," *Engineering Failure Analysis*, vol. 96, pp. 274-288, 2019/02/01/ 2019, doi: <https://doi.org/10.1016/j.engfailanal.2018.10.011>.
- [137] G. Odongo, R. Musabe, and D. Hanyurwimfura, "A multinomial dga classifier for incipient fault detection in oil-impregnated power transformers," *Algorithms*, vol. 14, no. 4, p. 128, 2021, doi: 10.3390/a14040128.
- [138] M. Duval and J. Buchacz, "Gas Formation from Arcing Faults in Transformers—Part II," *IEEE electrical insulation magazine*, vol. 38, no. 6, pp. 12-15, 2022, doi: 10.1109/MEI.2022.9916225.
- [139] L. Cheim, M. Duval, and S. Haider, "Combined Duval Pentagons: A Simplified Approach," *Energies (Basel)*, vol. 13, no. 11, p. 2859, 2020, doi: 10.3390/en13112859.
- [140] K. R. M. Nair, *Power and Distribution Transformers: Practical Design Guide*. Milton: Milton: Taylor & Francis Group, 2021.
- [141] T.-D. Do, V.-N. Tuyet-Doan, Y.-S. Cho, J.-H. Sun, and Y.-H. Kim, "Convolutional-Neural-Network-Based Partial Discharge Diagnosis for Power Transformer Using UHF Sensor," *IEEE access*, vol. 8, pp. 207377-207388, 2020, doi: 10.1109/ACCESS.2020.3038386.
- [142] Y. Shi, S. Ji, F. Zhang, Y. Dang, and L. Zhu, "Application of Operating Deflection Shapes to the Vibration-Based Mechanical Condition Monitoring of Power Transformer Windings," *IEEE Transactions on Power Delivery*, vol. 36, no. 4, pp. 2164-2173, 2021, doi: 10.1109/TPWRD.2020.3021909.
- [143] J. Seo, H. Ma, and T. K. Saha, "A Joint Vibration and Arcing Measurement System for Online Condition Monitoring of Onload Tap Changer of the Power Transformer," *IEEE Transactions on Power Delivery*, vol. 32, no. 2, pp. 1031-1038, 2017, doi: 10.1109/TPWRD.2016.2531186.
- [144] X. Zhang and E. Gockenbach, "Asset-Management of Transformers Based on Condition Monitoring and Standard Diagnosis [Feature Article]," *IEEE Electrical Insulation Magazine*, vol. 24, no. 4, pp. 26-40, 2008, doi: 10.1109/MEI.2008.4581371.

- [145] S. Degeratu *et al.*, "Condition monitoring of transformer oil using thermal analysis and other techniques," *Journal of Thermal Analysis and Calorimetry*, vol. 119, no. 3, pp. 1679-1692, 2015/03/01 2015, doi: 10.1007/s10973-014-4276-3.
- [146] J. Lukic *et al.*, "Changes of new unused insulating kraft paper properties during drying—Impact on degree of polymerization," *Cigrè Sci. Enginnering*, vol. 20, pp. 161-170, 2021.
- [147] R. D. Medina, A. A. Romero, E. E. Mombello, and G. Rattá, "Assessing degradation of power transformer solid insulation considering thermal stress and moisture variation," *Electric power systems research*, vol. 151, pp. 1-11, 2017, doi: 10.1016/j.epsr.2017.04.006.
- [148] *IEEE Guide for Loading Mineral-Oil-Immersed Transformers and Step-Voltage Regulators*, 0-7381-7195-6, 2012.
- [149] S. S. M. Ghoneim, "The Degree of Polymerization in a Prediction Model of Insulating Paper and the Remaining Life of Power Transformers," *Energies*, vol. 14, no. 3, p. 670, 2021. [Online]. Available: <https://www.mdpi.com/1996-1073/14/3/670>.
- [150] S. Forouhari and A. Abu-Siada, "Application of adaptive neuro fuzzy inference system to support power transformer life estimation and asset management decision," *IEEE Transactions on Dielectrics and Electrical Insulation*, vol. 25, no. 3, pp. 845-852, 2018, doi: 10.1109/TDEI.2018.006392.
- [151] J. Foros and M. Istad, "Health Index, Risk and Remaining Lifetime Estimation of Power Transformers," *IEEE Transactions on Power Delivery*, vol. 35, no. 6, pp. 2612-2620, 2020, doi: 10.1109/TPWRD.2020.2972976.
- [152] *Mineral Insulating Oils - Methods for the Determination of 2-Furfural and Related Compounds*, 1993.
- [153] "Ageing of liquid impregnated cellulose for power transformers," *CIGRE Technical Brochure*, vol. 738, D1 Materials and emerging test techniques, 2018.
- [154] T. V. Oommen and T. A. Prevost, "Cellulose insulation in oil-filled power transformers: part II maintaining insulation integrity and life," *IEEE Electrical Insulation Magazine*, vol. 22, no. 2, pp. 5-14, 2006, doi: 10.1109/MEI.2006.1618996.
- [155] M. Wu, H. Cao, J. Cao, H. L. Nguyen, J. B. Gomes, and S. P. Krishnaswamy, "An overview of state-of-the-art partial discharge analysis techniques for condition monitoring," *IEEE Electrical Insulation Magazine*, vol. 31, no. 6, pp. 22-35, 2015, doi: 10.1109/MEI.2015.7303259.
- [156] J. Ni, Z. Zhao, S. Tan, Y. Chen, C. Yao, and C. Tang, "The actual measurement and analysis of transformer winding deformation fault degrees by FRA using mathematical indicators," *Electric Power Systems Research*, vol. 184, p. 106324, 2020/07/01/ 2020, doi: <https://doi.org/10.1016/j.epsr.2020.106324>.
- [157] X. Liu, Y. He, and L. Wang, "Adaptive transfer learning based on a two-stream densely connected residual shrinkage network for transformer fault diagnosis over vibration signals," *Electronics (Basel)*, vol. 10, no. 17, p. 2130, 2021, doi: 10.3390/electronics10172130.
- [158] M. Žarković and Z. Stojković, "Analysis of artificial intelligence expert systems for power transformer condition monitoring and diagnostics," *Electric Power Systems Research*, vol. 149, pp. 125-136, 2017/08/01/ 2017, doi: <https://doi.org/10.1016/j.epsr.2017.04.025>.
- [159] S. Gubanski *et al.*, "Dielectric response methods for diagnostics of power transformers," *Electra*, vol. 202, pp. 23-34, 2002.
- [160] C. Lefeng and Y. Tao, "Dissolved Gas Analysis Principle-Based Intelligent Approaches to Fault Diagnosis and Decision Making for Large Oil-Immersed Power Transformers: A Survey," *Energies (Basel)*, vol. 11, no. 4, p. 913, 2018.
- [161] J. I. Aizpurua, S. D. J. McArthur, B. G. Stewart, B. Lambert, J. G. Cross, and V. M. Catterson, "Adaptive Power Transformer Lifetime Predictions Through Machine Learning and Uncertainty Modeling in Nuclear Power Plants," *IEEE Transactions on Industrial Electronics*, vol. 66, no. 6, pp. 4726-4737, 2019, doi: 10.1109/TIE.2018.2860532.
- [162] N. Lelekakis, D. Martin, and J. Wijaya, "Ageing Rate of Paper Insulation used in Power Transformers Part 1: Oil/paper System with Low Oxygen Concentration," *Dielectrics and Electrical Insulation, IEEE Transactions on*, vol. 19, pp. 1999-2008, 12/01 2012, doi: 10.1109/TDEI.2012.6396958.
- [163] D. Bormann and P. Picher, *Mechanical condition assessment of transformer windings using frequency response analysis (FRA)*. 2008.
- [164] A. S. A. Razzaq, M. F. M. Yousof, S. M. Al-Ameri, M. A. Talib, and A. J. Mshkil, "Interpretation of Inter-Turn Fault in Transformer Winding Using Turns Ratio Test and Frequency Response Analysis," vol. 11, pp. 218-225, 2022, doi: 10.18178/ijeetc.11.3.218-225.
- [165] K. H. Ibrahim, N. R. Korany, and S. M. Saleh, "Effects of power transformer high-frequency equivalent circuit parameters non-uniformity on fault diagnosis using SFRA test," *Ain Shams Engineering Journal*, vol. 13, no. 4, p. 101674, 2022/06/01/ 2022, doi: <https://doi.org/10.1016/j.asej.2021.101674>.
- [166] M. A. Tsili, E. I. Amoiralis, A. G. Kladas, and A. T. Souflaris, "Power transformer thermal analysis by using an advanced coupled 3D heat transfer and fluid flow FEM model," *International Journal of Thermal Sciences*, vol. 53, pp. 188-201, 2012/03/01/ 2012, doi: <https://doi.org/10.1016/j.iijthermalsci.2011.10.010>.

- [167] H. Hongsheng, Q. Suxiang, and C. Jian, "Monitoring and fault diagnosing system design for power transformer based on temperature field model and DGA feature extraction," in *2008 7th World Congress on Intelligent Control and Automation*, 25-27 June 2008 2008, pp. 1800-1805, doi: 10.1109/WCICA.2008.4593195.
- [168] P. Lu *et al.*, "Real-Time Monitoring of Temperature Rises of Energized Transformer Cores With Distributed Optical Fiber Sensors," *IEEE Transactions on Power Delivery*, vol. 34, no. 4, pp. 1588-1598, 2019, doi: 10.1109/TPWRD.2019.2912866.
- [169] Y. Cui, H. Ma, T. Saha, C. Ekanayake, and D. Martin, "Moisture-Dependent Thermal Modelling of Power Transformer," *IEEE Transactions on Power Delivery*, vol. 31, no. 5, pp. 2140-2150, 2016, doi: 10.1109/TPWRD.2016.2569123.
- [170] A. Santisteban, F. Delgado, A. Ortiz, I. Fernández, C. J. Renedo, and F. Ortiz, "Numerical analysis of the hot-spot temperature of a power transformer with alternative dielectric liquids," *IEEE Transactions on Dielectrics and Electrical Insulation*, vol. 24, no. 5, pp. 3226-3235, 2017, doi: 10.1109/TDEI.2017.006228.
- [171] L. Li, S. Niu, S. L. Ho, W. N. Fu, and Y. Li, "A Novel Approach to Investigate the Hot-Spot Temperature Rise in Power Transformers," *IEEE Transactions on Magnetics*, vol. 51, no. 3, pp. 1-4, 2015, doi: 10.1109/TMAG.2014.2359956.
- [172] W. H. Tang and Q. H. Wu, *Condition Monitoring and Assessment of Power Transformers Using Computational Intelligence*. London: London: Springer London, 2011.
- [173] H. Wu, X. Wang, and J. Zhang, "Online monitoring and diagnosis method of transformer winding deformation," *IEEE transactions on electrical and electronic engineering*, vol. 14, no. 12, pp. 1747-1753, 2019, doi: 10.1002/tee.23000.
- [174] A. S. Masoum, N. Hashemnia, A. Abu-Siada, M. A. S. Masoum, and S. M. Islam, "Online Transformer Internal Fault Detection Based on Instantaneous Voltage and Current Measurements Considering Impact of Harmonics," *IEEE Transactions on Power Delivery*, vol. 32, no. 2, pp. 587-598, 2017, doi: 10.1109/TPWRD.2014.2358072.
- [175] A. G. C. Menezes, M. M. Araujo, O. M. Almeida, F. R. Barbosa, and A. P. S. Braga, "Induction of Decision Trees to Diagnose Incipient Faults in Power Transformers," *IEEE Transactions on Dielectrics and Electrical Insulation*, vol. 29, no. 1, pp. 279-286, 2022, doi: 10.1109/TDEI.2022.3148453.
- [176] N. Haque, A. Jamshed, K. Chatterjee, and S. Chatterjee, "Accurate Sensing of Power Transformer Faults From Dissolved Gas Data Using Random Forest Classifier Aided by Data Clustering Method," *IEEE Sensors Journal*, vol. 22, no. 6, pp. 5902-5910, 2022, doi: 10.1109/JSEN.2022.3149409.
- [177] Y. Kim, T. Park, S. Kim, N. Kwak, and D. Kweon, "Artificial Intelligent Fault Diagnostic Method for Power Transformers using a New Classification System of Faults," *Journal of electrical engineering & technology*, vol. 14, no. 2, pp. 825-831, 2019, doi: 10.1007/s42835-019-00105-0.
- [178] O. Kherif, Y. Benmahamed, M. Tegar, A. Boubakeur, and S. S. M. Ghoneim, "Accuracy Improvement of Power Transformer Faults Diagnostic Using KNN Classifier With Decision Tree Principle," *IEEE Access*, vol. 9, pp. 81693-81701, 2021, doi: 10.1109/ACCESS.2021.3086135.
- [179] Y. D. Almoallem, I. B. M. Taha, M. I. Mosaad, L. Nahma, and A. Abu-Siada, "Application of logistic regression algorithm in the interpretation of dissolved gas analysis for power transformers," *Electronics (Basel)*, vol. 10, no. 10, p. 1206, 2021, doi: 10.3390/electronics10101206.
- [180] M. Božić, M. Stojanović, Z. Stajić, and Đ. Vukić, "Power transformer fault diagnosis based on dissolved gas analysis with logistic regression," *Przegląd Elektrotechniczny*, vol. 6, pp. 83-87, 2013.
- [181] H. A. Illias and W. Z. Liang, "Identification of transformer fault based on dissolved gas analysis using hybrid support vector machine-modified evolutionary particle swarm optimisation," *PLoS One*, vol. 13, no. 1, pp. e0191366-e0191366, 2018, doi: 10.1371/journal.pone.0191366.
- [182] K. Bacha, S. Souahlia, and M. Gossa, "Power transformer fault diagnosis based on dissolved gas analysis by support vector machine," *Electric power systems research*, vol. 83, no. 1, pp. 73-79, 2012, doi: 10.1016/j.epsr.2011.09.012.
- [183] J. I. Aizpurua *et al.*, "Power transformer dissolved gas analysis through Bayesian networks and hypothesis testing," *IEEE Transactions on Dielectrics and Electrical Insulation*, vol. 25, no. 2, pp. 494-506, 2018, doi: 10.1109/TDEI.2018.006766.
- [184] R. A. Hooshmand, M. Parastegari, and Z. Forghani, "Adaptive neuro-fuzzy inference system approach for simultaneous diagnosis of the type and location of faults in power transformers," *IEEE Electrical Insulation Magazine*, vol. 28, no. 5, pp. 32-42, 2012, doi: 10.1109/MEI.2012.6268440.
- [185] J. Faiz and M. Soleimani, "Assessment of computational intelligence and conventional dissolved gas analysis methods for transformer fault diagnosis," *IEEE Transactions on Dielectrics and Electrical Insulation*, vol. 25, no. 5, pp. 1798-1806, 2018, doi: 10.1109/TDEI.2018.007191.
- [186] H. A. Illias, X. R. Chai, and A. H. Abu Bakar, "Hybrid modified evolutionary particle swarm optimisation-time varying acceleration coefficient-artificial neural network for power transformer fault diagnosis," *Measurement*, vol. 90, pp. 94-102, 2016/08/01/ 2016, doi: <https://doi.org/10.1016/j.measurement.2016.04.052>.

- [187] T. Kari *et al.*, "An integrated method of ANFIS and Dempster-Shafer theory for fault diagnosis of power transformer," *IEEE Transactions on Dielectrics and Electrical Insulation*, vol. 25, no. 1, pp. 360-371, 2018, doi: 10.1109/TDEI.2018.006746.
- [188] T. K. Abdel-Gail, R. M. Sharkawy, M. M. A. Salama, and R. Bartnikas, "Partial discharge pattern classification using the fuzzy decision tree approach," *IEEE Transactions on Instrumentation and Measurement*, vol. 54, no. 6, pp. 2258-2263, 2005, doi: 10.1109/TIM.2005.858143.
- [189] Y. Sun *et al.*, "Partial Discharge Pattern Recognition of Transformers Based on MobileNets Convolutional Neural Network," *Applied sciences*, vol. 11, no. 15, p. 6984, 2021, doi: 10.3390/app11156984.
- [190] X. Zhou *et al.*, "Research on transformer partial discharge uhf pattern recognition based on cnn-lstm," *Energies (Basel)*, vol. 13, no. 1, p. 61, 2019, doi: 10.3390/en13010061.
- [191] Y. Xi, L. Yu, B. Chen, G. Chen, and Y. Chen, "Research on Pattern Recognition Method of Transformer Partial Discharge Based on Artificial Neural Network," *Security and communication networks*, vol. 2022, 2022, doi: 10.1155/2022/5154649.
- [192] J. Wang *et al.*, "Evaluation on Partial Discharge Intensity of Electrical Equipment Based on Improved ANFIS and Ultraviolet Pulse Detection Technology," *IEEE Access*, vol. 7, pp. 126561-126570, 2019, doi: 10.1109/ACCESS.2019.2938784.
- [193] J. R. Secue and E. Mombello, "Sweep frequency response analysis (SFRA) for the assessment of winding displacements and deformation in power transformers," *Electric Power Systems Research*, vol. 78, no. 6, pp. 1119-1128, 2008/06/01/2008, doi: <https://doi.org/10.1016/j.epsr.2007.08.005>.
- [194] Z. Zhao, C. Tang, Q. Zhou, L. Xu, Y. Gui, and C. Yao, "Identification of Power Transformer Winding Mechanical Fault Types Based on Online IFRA by Support Vector Machine," *Energies (Basel)*, vol. 10, no. 12, p. 2022, 2017, doi: 10.3390/en10122022.
- [195] G. Bucci, F. Ciancetta, E. Fiorucci, S. Mari, and A. Fioravanti, "Deep Learning Applied to SFRA Results: A Preliminary Study," presented at the 2021 7th International Conference on Computing and Artificial Intelligence, Tianjin, China, 2021. [Online]. Available: <https://doi.org/10.1145/3467707.3467753>.
- [196] A. Tavakoli, L. D. Maria, B. Valecillos, D. Bartalesi, S. Garatti, and S. Bittanti, "A Machine Learning approach to fault detection in transformers by using vibration data," *IFAC PapersOnLine*, vol. 53, no. 2, pp. 13656-13661, 2020, doi: 10.1016/j.ifacol.2020.12.866.
- [197] Z. Wang and A. Sharma, "Research on transformer vibration monitoring and diagnosis based on Internet of things," *Journal of intelligent systems*, vol. 30, no. 1, pp. 677-688, 2021, doi: 10.1515/jisys-2020-0111.
- [198] K. Hong, M. Jin, and H. Huang, "Transformer Winding Fault Diagnosis Using Vibration Image and Deep Learning," *IEEE transactions on power delivery*, vol. 36, no. 2, pp. 676-685, 2021, doi: 10.1109/TPWRD.2020.2988820.
- [199] A. Doolgindachbaporn, G. Callender, P. Lewin, E. A. Simonson, and G. Wilson, "Data Driven Transformer Thermal Model for Condition Monitoring," *IEEE transactions on power delivery*, pp. 1-1, 2021, doi: 10.1109/TPWRD.2021.3123957.
- [200] G. M. dos Santos, R. R. B. de Aquino, and M. M. S. Lira, "Thermography and artificial intelligence in transformer fault detection," *Electrical engineering*, vol. 100, no. 3, pp. 1317-1325, 2017, doi: 10.1007/s00202-017-0595-2.
- [201] M. Hui, T. K. Saha, and C. Ekanayake, "Machine learning techniques for power transformer insulation diagnosis," 2011: IEEE, pp. 1-6.
- [202] M. Hui, T. K. Saha, and C. Ekanayake, "Statistical learning techniques and their applications for condition assessment of power transformer," *IEEE transactions on dielectrics and electrical insulation*, vol. 19, no. 2, pp. 481-489, 2012, doi: 10.1109/TDEI.2012.6180241.
- [203] S. Amidedin Mousavi, A. Hekmati, M. Sedighizadeh, M. Bigdeli, and A. Bazargan, "ANN based temperature compensation for variations in polarization and depolarization current measurements in transformer," *Thermal Science and Engineering Progress*, vol. 20, p. 100671, 2020/12/01/2020, doi: <https://doi.org/10.1016/j.tsep.2020.100671>.
- [204] Y. Zhang, S. Li, X. Fan, J. Liu, and J. Li, "Prediction of Moisture and Aging Conditions of Oil-Immersed Cellulose Insulation Based on Fingerprints Database of Dielectric Modulus," (in English), *Polymers*, vol. 12, no. 8, p. 1722, 2020-08-05 2020, doi: <http://dx.doi.org/10.3390/polym12081722>.
- [205] J. Liu *et al.*, "A BPNN Model Based AdaBoost Algorithm for Estimating Inside Moisture of Oil-Paper Insulation of Power Transformer," *IEEE transactions on dielectrics and electrical insulation*, vol. 29, no. 2, pp. 1-1, 2022, doi: 10.1109/TDEI.2022.3157909.
- [206] B. A. Thango and P. N. Bokoro, "Prediction of the Degree of Polymerization in Transformer Cellulose Insulation Using the Feedforward Backpropagation Artificial Neural Network," *Energies*, vol. 15, no. 12, p. 4209, 2022. [Online]. Available: <https://www.mdpi.com/1996-1073/15/12/4209>.

- [207] M. Nezami, M. Equbal, S. A. Khan, and S. Sohail, "An ANFIS based comprehensive correlation between diagnostic and destructive parameters of transformer's paper insulation," *Arabian Journal for Science and Engineering*, vol. 46, no. 2, pp. 1541-1547, 2021.
- [208] R. A. Prasojo, K. Diwyacitta, S. Suwarno, and H. Gumilang, "Transformer paper expected life estimation using ANFIS based on oil characteristics and dissolved gases (Case study: Indonesian transformers)," *Energies (Basel)*, vol. 10, no. 8, p. 1135, 2017, doi: 10.3390/en10081135.
- [209] P. K. Pandey, Z. Husain, and R. K. Jarial, "ANFIS Based Approach to Estimate Remnant Life of Power Transformer by Predicting Furan Contents," *International journal of electrical and computer engineering (Malacca, Malacca)*, vol. 4, no. 4, p. 463, 2014, doi: 10.11591/ijece.v4i4.5567.
- [210] L. Ruijin, Z. Hanbo, S. Grzybowski, Y. Lijun, Z. Yiyi, and L. Yuxiang, "An Integrated Decision-Making Model for Condition Assessment of Power Transformers Using Fuzzy Approach and Evidential Reasoning," *IEEE transactions on power delivery*, vol. 26, no. 2, pp. 1111-1118, 2011, doi: 10.1109/TPWRD.2010.2096482.
- [211] M. Arshad, S. M. Islam, and A. Khaliq, "Fuzzy logic approach in power transformers management and decision making," *IEEE Transactions on Dielectrics and Electrical Insulation*, vol. 21, no. 5, pp. 2343-2354, 2014, doi: 10.1109/TDEI.2014.003859.
- [212] R. M. Arias Velásquez, "Support vector machine and tree models for oil and Kraft degradation in power transformers," *Engineering failure analysis*, vol. 127, p. 105488, 2021, doi: 10.1016/j.engfailanal.2021.105488.
- [213] "Machine Learning Tools in Support of Transformer Diagnostics," *CIGRE Technical Brochure*, vol. A2-206, 2018.
- [214] S. obulareddy and S. K. Munagala, "Application of Machine learning algorithms for Power transformer Internal faults identification," 2021, vol. 1: IEEE, pp. 331-335, doi: 10.1109/ICACCS51430.2021.9441719.
- [215] Z. Zhao, J. Xu, Y. Zang, and R. Hu, "Adaptive Abnormal Oil Temperature Diagnosis Method of Transformer Based on Concept Drift," *Applied sciences*, vol. 11, no. 14, p. 6322, 2021, doi: 10.3390/app11146322.
- [216] M. E. A. Senoussaoui, M. Brahami, and I. Fofana, "Transformer oil quality assessment using random forest with feature engineering," *Energies (Basel)*, vol. 14, no. 7, p. 1809, 2021, doi: 10.3390/en14071809.
- [217] A. Alqudsi and A. El-Hag, "Application of machine learning in transformer health index prediction," *Energies (Basel)*, vol. 12, no. 14, p. 2694, 2019, doi: 10.3390/en12142694.
- [218] S. S. M. Ghoneim and I. B. M. Taha, "Comparative Study of Full and Reduced Feature Scenarios for Health Index Computation of Power Transformers," *IEEE Access*, vol. 8, pp. 181326-181339, 2020, doi: 10.1109/ACCESS.2020.3028689.
- [219] S.-W. Fei and Y. Sun, "Forecasting dissolved gases content in power transformer oil based on support vector machine with genetic algorithm," *Electric power systems research*, vol. 78, no. 3, pp. 507-514, 2008, doi: 10.1016/j.epsr.2007.04.006.
- [220] C. H. Wei, W. H. Tang, and Q. H. Wu, "A Hybrid Least-square Support Vector Machine Approach to Incipient Fault Detection for Oil-immersed Power Transformer," *Electric power components and systems*, vol. 42, no. 5, pp. 453-463, 2014, doi: 10.1080/15325008.2013.857180.
- [221] S. A. Wani, A. S. Rana, S. Sohail, O. Rahman, S. Parveen, and S. A. Khan, "Advances in DGA based condition monitoring of transformers: A review," *Renewable & sustainable energy reviews*, vol. 149, p. 111347, 2021, doi: 10.1016/j.rser.2021.111347.
- [222] T. Kari, W. Gao, A. Tuluhong, Y. Yaermaimaiti, and Z. Zhang, "Mixed kernel function support vector regression with genetic algorithm for forecasting dissolved gas content in power transformers," *Energies (Basel)*, vol. 11, no. 9, p. 2437, 2018, doi: 10.3390/en11092437.
- [223] Z. Zhe-wen, W. Yong, Y. Ding, T. lei, and Z. Ying-jian, "A Transformer Fault Diagnosis Method Based on Bayesian Network," *J. Phys.: Conf. Ser.*, vol. 1213, no. 5, p. 52002, 2019, doi: 10.1088/1742-6596/1213/5/052002.
- [224] L. Cheim, L. Lin, and A. Dagnino, "Probabilistic transformer fault tree analysis using Bayesian networks," in *2014 IEEE PES T&D Conference and Exposition*, 14-17 April 2014 2014, pp. 1-5, doi: 10.1109/TDC.2014.6863177.
- [225] C. Hu, C. Zhang, Z. Zhang, and S. Xie, "Comparative Study on Defects and Faults Detection of Main Transformer Based on Logistic Regression and Naive Bayes Algorithm," *J. Phys.: Conf. Ser.*, vol. 1732, no. 1, p. 12075, 2021, doi: 10.1088/1742-6596/1732/1/012075.
- [226] A. Li, X. Yang, H. Dong, Z. Xie, and C. Yang, "Machine learning-based sensor data modeling methods for power transformer PHM," *Sensors (Basel)*, vol. 18, no. 12, p. 4430, 2018, doi: 10.3390/s18124430.
- [227] C. Yan, M. Li, and W. Liu, "Transformer Fault Diagnosis Based on BP-Adaboost and PNN Series Connection," *Mathematical problems in engineering*, vol. 2019, pp. 1-10, 2019, doi: 10.1155/2019/1019845.

- [228] S. Chen, H. Ge, H. Li, Y. Sun, and X. Qian, "Hierarchical deep convolution neural networks based on transfer learning for transformer rectifier unit fault diagnosis," *Measurement : journal of the International Measurement Confederation*, vol. 167, p. 108257, 2021, doi: 10.1016/j.measurement.2020.108257.
- [229] J. Lin, J. Ma, and J. Zhu, "Hierarchical Federated Learning for Power Transformer Fault Diagnosis," *IEEE Transactions on Instrumentation and Measurement*, vol. 71, pp. 1-11, 2022, doi: 10.1109/TIM.2022.3196736.
- [230] S. A. Khan, M. D. Equbal, and T. Islam, "ANFIS based identification and location of paper insulation faults of an oil immersed transformer," in *2014 6th IEEE Power India International Conference (PIICON)*, 5-7 Dec. 2014 2014, pp. 1-6, doi: 10.1109/POWERI.2014.7117715.
- [231] F. Cheng, L. Qu, and W. Qiao, "A case-based data-driven prediction framework for machine fault prognostics," in *2015 IEEE Energy Conversion Congress and Exposition (ECCE)*, 20-24 Sept. 2015 2015, pp. 3957-3963, doi: 10.1109/ECCE.2015.7310219.
- [232] H. Metin Ertunc and M. Hosoz, "Comparative analysis of an evaporative condenser using artificial neural network and adaptive neuro-fuzzy inference system," *International Journal of Refrigeration*, vol. 31, no. 8, pp. 1426-1436, 2008/12/01/ 2008, doi: <https://doi.org/10.1016/j.iijrefrig.2008.03.007>.
- [233] S. A. Khan, M. D. Equbal, and T. Islam, "A comprehensive comparative study of DGA based transformer fault diagnosis using fuzzy logic and ANFIS models," *IEEE Transactions on Dielectrics and Electrical Insulation*, vol. 22, no. 1, pp. 590-596, 2015, doi: 10.1109/TDEI.2014.004478.
- [234] M. S. Katooli and A. Koochaki, "Detection and Classification of Incipient Faults in Three-Phase Power Transformer Using DGA Information and Rule-based Machine Learning Method," *Journal of control, automation & electrical systems*, vol. 31, no. 5, pp. 1251-1266, 2020, doi: 10.1007/s40313-020-00625-5.
- [235] T. A. Aman, A. S. Mokhtar, and M. AizamTalib, "Assessment The Overall Health Condition of Transformer Using Health Index and Critical Index Approach: TNB Grid Case Study," in *2020 IEEE International Conference on Power and Energy (PECon)*, 7-8 Dec. 2020 2020, pp. 235-239, doi: 10.1109/PECon48942.2020.9314483.
- [236] M. M. Islam, G. Lee, and S. N. Hettiwatte, "Application of a general regression neural network for health index calculation of power transformers," *International Journal of Electrical Power & Energy Systems*, vol. 93, pp. 308-315, 2017/12/01/ 2017, doi: <https://doi.org/10.1016/j.ijepes.2017.06.008>.
- [237] "Pattern Recognition Techniques for Determining the Health Index of Oil-Paper Insulation of In-service Power Transformers," *CIGRE Technical Brochure*, vol. A2_105_2014, 2014.
- [238] R. A. Prasojo, N. U. Maulidevi, B. A. Soedjarno, and S. Suwarno, "Health Index Analysis of Power Transformer with Incomplete Paper Condition Data," in *2019 IEEE 4th International Conference on Condition Assessment Techniques in Electrical Systems (CATCON)*, 21-23 Nov. 2019 2019, pp. 1-4, doi: 10.1109/CATCON47128.2019.CN0073.
- [239] A. Alqudsi and A. El-Hag, "Assessing the power transformer insulation health condition using a feature-reduced predictor mode," *IEEE Transactions on Dielectrics and Electrical Insulation*, vol. 25, no. 3, pp. 853-862, 2018, doi: 10.1109/TDEI.2018.006630.
- [240] M. Islam, G. Lee, S. N. Hettiwatte, and K. Williams, "Calculating a Health Index for Power Transformers Using a Subsystem-Based GRNN Approach," *IEEE Transactions on Power Delivery*, vol. 33, no. 4, pp. 1903-1912, 2018, doi: 10.1109/TPWRD.2017.2770166.
- [241] D. G. T. Da Silva, H. J. Braga Da Silva, F. P. Marafão, H. K. M. Paredes, and F. A. S. Gonçalves, "Enhanced health index for power transformers diagnosis," *Engineering Failure Analysis*, vol. 126, p. 105427, 2021/08/01/ 2021, doi: <https://doi.org/10.1016/j.engfailanal.2021.105427>.
- [242] D. Rediansyah, R. A. Prasojo, Suwarno, and A. Abu-Siada, "Artificial Intelligence-Based Power Transformer Health Index for Handling Data Uncertainty," *IEEE access*, vol. 9, pp. 150637-150648, 2021, doi: 10.1109/ACCESS.2021.3125379.
- [243] R. M. Arias Velásquez, J. V. Mejía Lara, and A. Melgar, "Converting data into knowledge for preventing failures in power transformers," *Engineering Failure Analysis*, vol. 101, pp. 215-229, 2019/07/01/ 2019, doi: <https://doi.org/10.1016/j.engfailanal.2019.03.027>.
- [244] M. S. Yahaya, N. Azis, M. Z. A. Ab Kadir, J. Jasni, M. H. Hairi, and M. A. Talib, "Estimation of Transformers Health Index Based on the Markov Chain," *Energies*, vol. 10, no. 11, p. 1824, 2017. [Online]. Available: <https://www.mdpi.com/1996-1073/10/11/1824>.
- [245] R. Murugan and R. Raju, "Evaluation of in-service power transformer health condition for Inspection, Repair, and Replacement (IRR) maintenance planning in electric utilities," *International journal of system assurance engineering and management*, vol. 12, no. 2, pp. 318-336, 2021, doi: 10.1007/s13198-021-01083-1.
- [246] P. Bohatyrewicz, J. Płowucha, and J. Subocz, "Condition Assessment of Power Transformers Based on Health Index Value," *Applied sciences*, vol. 9, no. 22, p. 4877, 2019, doi: 10.3390/app9224877.

- [247] M. Pompili and F. Scatiggio, "Classification in iso-attention classes of hv transformer fleets," *IEEE Transactions on Dielectrics and Electrical Insulation*, vol. 22, no. 5, pp. 2676-2683, 2015, doi: 10.1109/TDEI.2015.005252.
- [248] A. M. Selva *et al.*, "Application of statistical distribution models to predict health index for condition-based management of transformers," *Applied sciences*, vol. 11, no. 6, p. 2728, 2021, doi: 10.3390/app11062728.
- [249] J. H. Jürgensen, L. Nordström, and P. Hilber, "Estimation of Individual Failure Rates for Power System Components Based on Risk Functions," *IEEE Transactions on Power Delivery*, vol. 34, no. 4, pp. 1599-1607, 2019, doi: 10.1109/TPWRD.2019.2913777.
- [250] W. Zuo, H. Yuan, Y. Shang, Y. Liu, and T. Chen, "Calculation of a Health Index of Oil-Paper Transformers Insulation with Binary Logistic Regression," *Mathematical Problems in Engineering*, vol. 2016, p. 6069784, 2016/06/15 2016, doi: 10.1155/2016/6069784.
- [251] A. E. B. Abu-Elanien, M. M. A. Salama, and M. Ibrahim, "Calculation of a Health Index for Oil-Immersed Transformers Rated Under 69 kV Using Fuzzy Logic," *IEEE Transactions on Power Delivery*, vol. 27, no. 4, pp. 2029-2036, 2012, doi: 10.1109/TPWRD.2012.2205165.
- [252] R. D. Medina, D. A. Zaldivar, A. A. Romero, J. Zuñiga, and E. E. Mombello, "A fuzzy inference-based approach for estimating power transformers risk index," *Electric Power Systems Research*, vol. 209, p. 108004, 2022/08/01/ 2022, doi: <https://doi.org/10.1016/j.epsr.2022.108004>.
- [253] A. Mohmad, M. Ibrahim Shapiai, M. Solehin Shamsudin, M. A. Abu, and A. A. Hamid, "Investigating performance of transformer health index in machine learning application using dominant features," *J. Phys.: Conf. Ser.*, vol. 2128, no. 1, p. 12025, 2021, doi: 10.1088/1742-6596/2128/1/012025.
- [254] K. Ibrahim, R. M. Sharkawy, H. K. Temraz, and M. M. A. Salama, "Selection criteria for oil transformer measurements to calculate the Health Index," *IEEE Transactions on Dielectrics and Electrical Insulation*, vol. 23, no. 6, pp. 3397-3404, 2016, doi: 10.1109/TDEI.2016.006058.
- [255] A. D. Ashkezari, H. Ma, T. K. Saha, and C. Ekanayake, "Application of fuzzy support vector machine for determining the health index of the insulation system of in-service power transformers," *IEEE Transactions on Dielectrics and Electrical Insulation*, vol. 20, no. 3, pp. 965-973, 2013, doi: 10.1109/TDEI.2013.6518966.
- [256] H. Zeinoddini-Meymand and B. Vahidi, "Health index calculation for power transformers using technical and economical parameters," *IET Science, Measurement & Technology*, vol. 10, no. 7, pp. 823-830, 2016, doi: <https://doi.org/10.1049/iet-smt.2016.0184>.
- [257] S. K. Abeygunawardane, P. Jirutitijaroen, and H. Xu, "Adaptive Maintenance Policies for Aging Devices Using a Markov Decision Process," *IEEE Transactions on Power Systems*, vol. 28, no. 3, pp. 3194-3203, 2013, doi: 10.1109/TPWRS.2012.2237042.
- [258] S. Milosavljevic and A. Janjic, "Integrated Transformer Health Estimation Methodology Based on Markov Chains and Evidential Reasoning," *Mathematical Problems in Engineering*, vol. 2020, p. 7291749, 2020/05/30 2020, doi: 10.1155/2020/7291749.
- [259] P. Sarajcevic, D. Jakus, and M. Nikolic, "Wide & Deep Machine Learning Model for Transformer Health Analysis," in *2019 4th International Conference on Smart and Sustainable Technologies (SpliTech)*, 18-21 June 2019 2019, pp. 1-6, doi: 10.23919/SpliTech.2019.8783122.
- [260] M. M. S. NAKAI; M.YOSHIDA; K.AOKI, "Rationalization and high precision of transformer lifetime evaluation method," *CIGRE Technical Brochure*, vol. A2-315, 2020.
- [261] C. P. Krause, A.d.; Devaux, F.; Ding, H.; Katshuna, V.; Lukic, J.; Melzer, L.; Miyazaki, S.; Munro, M.; Peixoto, A.; Scala, M.; Walker, D., "The Condition of Solid Transformer Insulation at End-of-Life," *CIGRE Reference Paper*, vol. A2-321, 2022.
- [262] R. A. Prasojo and S. Suwarno, "Power transformer paper insulation assessment based on oil measurement data using SVM-classifier," *International Journal on Electrical Engineering and Informatics*, vol. 10, no. 4, pp. 661-673, 2018, doi: 10.15676/ijeei.2018.10.4.4.
- [263] B. Gorgan *et al.*, "Calculation of the remaining lifetime of power transformers paper insulation," in *2012 13th International Conference on Optimization of Electrical and Electronic Equipment (OPTIM)*, 24-26 May 2012 2012, pp. 293-300, doi: 10.1109/OPTIM.2012.6231792.
- [264] L. Kong, W. Mo, X. Ge, T. Liu, F. Zhou, and H. Chen, "Application of Insulation Aging Evaluation Method for Distribution Transformers in Practice," in *2020 IEEE International Conference on High Voltage Engineering and Application (ICHVE)*, 6-10 Sept. 2020 2020, pp. 1-4, doi: 10.1109/ICHVE49031.2020.9279932.
- [265] "Ageing of Cellulose in Mineral-Oil Insulated Transformers," *CIGRE TASK FORCE D1.01.10*, vol. 323, 2007.
- [266] *AS/NZS 60076.7 Power Transformers Part 7: Loading guide for oil-immersed power transformers (IEC 60076-7, Ed. 1.0 (2005) MOD)*, 2013.

- [267] P. K. Sen and P. Sarunpong, "Overloading and loss-of-life assessment guidelines of oil-cooled transformers," in *2001 Rural Electric Power Conference. Papers Presented at the 45th Annual Conference (Cat. No.01CH37214)*, 29 April-1 May 2001 2001, pp. B4/1-B4/8, doi: 10.1109/REPCON.2001.949516.
- [268] H. Gorginpour, H. Ghimatgar, and M. S. Toulabi, "Lifetime Estimation and Optimal Maintenance Scheduling of Urban Oil-Immersed Distribution-Transformers Considering Weather-Dependent Intelligent Load Model and Unbalanced Loading," *IEEE transactions on power delivery*, pp. 1-1, 2022, doi: 10.1109/TPWRD.2022.3146154.
- [269] V. M. Catterson, "Prognostic modeling of transformer aging using Bayesian particle filtering," in *2014 IEEE Conference on Electrical Insulation and Dielectric Phenomena (CEIDP)*, 19-22 Oct. 2014 2014, pp. 413-416, doi: 10.1109/CEIDP.2014.6995874.
- [270] A. Bagheri, M. Allahbakhshi, M. M. Arefi, N. Najafi, and M. S. Javadi, "A new approach for top-oil thermal modelling of power transformers using Unscented Kalman filter considering IEEE C57.91 standard," *IET electric power applications*, vol. 16, no. 5, pp. 536-547, 2022, doi: 10.1049/elp2.12174.
- [271] W. Chen and X. Su, "Application of Kalman filter to hot-spot temperature monitoring in oil-immersed power transformer," *IEEJ Transactions on Electrical and Electronic Engineering*, <https://doi.org/10.1002/tee.21862> vol. 8, no. 4, pp. 322-327, 2013/07/01 2013, doi: <https://doi.org/10.1002/tee.21862>.
- [272] W. Lai, H. Luo, W. Li, Y. Cao, L. Ye, and Y. Wang, "Prediction of top oil temperature for oil-immersed transformer based on Kalman filter algorithm," in *2017 2nd International Conference on Power and Renewable Energy (ICPRE)*, 20-23 Sept. 2017 2017, pp. 132-136, doi: 10.1109/ICPRE.2017.8390514.
- [273] S. Li, H. Ma, T. K. Saha, Y. Yang, and G. Wu, "On Particle Filtering for Power Transformer Remaining Useful Life Estimation," *IEEE Transactions on Power Delivery*, vol. 33, no. 6, pp. 2643-2653, 2018, doi: 10.1109/TPWRD.2018.2807386.
- [274] D. Martin, C. Yi, C. Ekanayake, M. Hui, and T. Saha, "An Updated Model to Determine the Life Remaining of Transformer Insulation," *IEEE transactions on power delivery*, vol. 30, no. 1, pp. 395-402, 2015, doi: 10.1109/TPWRD.2014.2345775.
- [275] E. Zhang *et al.*, "Aging state assessment of transformer cellulosic paper insulation using multivariate chemical indicators," *Cellulose*, vol. 28, no. 4, pp. 2445-2460, 2021.
- [276] V. Vasovic *et al.*, "Aging of transformer insulation — experimental transformers and laboratory models with different moisture contents: Part I — DP and furans aging profiles," *IEEE Transactions on Dielectrics and Electrical Insulation*, vol. 26, no. 6, pp. 1840-1846, 2019, doi: 10.1109/TDEI.2019.008183.
- [277] C. P. Krause, Alfonso de; Devaux, Francois; Ding, Hongzi; Katshuna, Victor; Lukic, Jelena; Melzer, Lena; Miyazaki, Satoru; Munro, Mike; Peixoto, Anabela; Scala, Mario; Walker, David;, "The Condition of Solid Transformer Insulation at End-of-Life," *CIGRE Reference Paper*, vol. Electra 321, 2022.
- [278] A. d. Pablo, "Furfural and ageing: how are they related," in *IEE Colloquium on Insulating Liquids (Ref. No. 1999/119)*, 27-27 May 1999 1999, pp. 5/1-5/4, doi: 10.1049/ic:19990667.
- [279] "Furanic Compounds for Diagnosis," *CIGRE Working Group D1.01(TF13)*, vol. 494, 2012.
- [280] B. A. Thango, A. O. Akumu, L. S. Sikhosana, A. F. Nnachi, and J. A. Jordaan, "Study of the Impact of Degree of Polymerization on the Remnant Life of Transformer Insulation," in *2021 IEEE PES/IAS PowerAfrica*, 23-27 Aug. 2021 2021, pp. 1-5, doi: 10.1109/PowerAfrica52236.2021.9543450.
- [281] P. Sen and S. Pansuwan, "Overloading and loss-of-life assessment guidelines of oil-cooled transformers," in *2001 Rural Electric Power Conference. Papers Presented at the 45th Annual Conference (Cat. No. 01CH37214)*, 2001: IEEE, pp. B4/1-B4/8.
- [282] Z. Tian, "An artificial neural network method for remaining useful life prediction of equipment subject to condition monitoring," *Journal of Intelligent Manufacturing*, vol. 23, no. 2, pp. 227-237, 2012/04/01 2012, doi: 10.1007/s10845-009-0356-9.
- [283] A. R. Abbasi, "Fault detection and diagnosis in power transformers: a comprehensive review and classification of publications and methods," *Electric Power Systems Research*, vol. 209, p. 107990, 2022/08/01/ 2022, doi: <https://doi.org/10.1016/j.epsr.2022.107990>.
- [284] M. Arshad and S. M. Islam, "A Novel Fuzzy Logic Technique for Power Transformer Asset Management," in *Conference Record of the 2006 IEEE Industry Applications Conference Forty-First IAS Annual Meeting*, 8-12 Oct. 2006 2006, vol. 1, pp. 276-286, doi: 10.1109/IAS.2006.256536.
- [285] R. M. Arias Velasquez and J. V. Mejia Lara, "Root cause analysis improved with machine learning for failure analysis in power transformers," *Engineering failure analysis*, vol. 115, p. 104684, 2020, doi: 10.1016/j.engfailanal.2020.104684.
- [286] S. Li, G. Wu, H. Dong, L. Yang, and X. Zhen, "Probabilistic Health Index-Based Apparent Age Estimation for Power Transformers," *IEEE Access*, vol. 8, pp. 9692-9701, 2020, doi: 10.1109/ACCESS.2020.2963963.

- [287] A. Abu-Siada, "Improved consistent interpretation approach of fault type within power transformers using dissolved gas analysis and gene expression programming," *Energies (Basel)*, vol. 12, no. 4, p. 730, 2019, doi: 10.3390/en12040730.
- [288] L. Dias *et al.*, "An unsupervised approach for fault diagnosis of power transformers," *Quality and Reliability Engineering International*, vol. 37, no. 6, pp. 2834-2852, 2021, doi: <https://doi.org/10.1002/qre.2892>.
- [289] J. Wu, K. Li, J. Sun, and L. Xie, "A novel integrated method to diagnose faults in power transformers," *Energies (Basel)*, vol. 11, no. 11, p. 3041, 2018, doi: 10.3390/en11113041.
- [290] Y. Benmahamed, M. Tegar, and A. Boubakeur, "Application of SVM and KNN to Duval Pentagon 1 for transformer oil diagnosis," *IEEE transactions on dielectrics and electrical insulation*, vol. 24, no. 6, pp. 3443-3451, 2017, doi: 10.1109/TDEI.2017.006841.
- [291] J. Fan, F. Wang, Q. Sun, F. Bin, F. Liang, and X. Xiao, "Hybrid RVM-ANFIS algorithm for transformer fault diagnosis," *IET generation, transmission & distribution*, vol. 11, no. 14, pp. 3637-3643, 2017, doi: 10.1049/iet-gtd.2017.0547.
- [292] Y. Wang and L. Zhang, "A Combined Fault Diagnosis Method for Power Transformer in Big Data Environment," *Mathematical Problems in Engineering*, vol. 2017, p. 9670290, 2017/05/18 2017, doi: 10.1155/2017/9670290.
- [293] L. Zhang, G. Sheng, H. Hou, and X. Jiang, "A Fault Diagnosis Method of Power Transformer Based on Cost Sensitive One-Dimensional Convolution Neural Network," in *2020 5th Asia Conference on Power and Electrical Engineering (ACPEE)*, 4-7 June 2020 2020, pp. 1824-1828, doi: 10.1109/ACPEE48638.2020.9136223.
- [294] C. Sun, Y. Chen, and N. Tang, "Fault Diagnosis of Power Transformer Based on DGA and Information Fusion," in *2022 IEEE/IAS Industrial and Commercial Power System Asia (I&CPS Asia)*, 8-11 July 2022 2022, pp. 247-251, doi: 10.1109/ICPSAsia55496.2022.9949927.
- [295] J. Li, C. Hai, Z. Feng, and G. Li, "A Transformer Fault Diagnosis Method Based on Parameters Optimization of Hybrid Kernel Extreme Learning Machine," *IEEE Access*, vol. 9, pp. 126891-126902, 2021, doi: 10.1109/ACCESS.2021.3112478.
- [296] Y. Cui, H. Ma, and T. Saha, "Improvement of power transformer insulation diagnosis using oil characteristics data preprocessed by SMOTEBoost technique," *IEEE Transactions on Dielectrics and Electrical Insulation*, vol. 21, no. 5, pp. 2363-2373, 2014, doi: 10.1109/TDEI.2014.004547.
- [297] S. Kim *et al.*, "A Semi-Supervised Autoencoder With an Auxiliary Task (SAAT) for Power Transformer Fault Diagnosis Using Dissolved Gas Analysis," *IEEE Access*, vol. 8, pp. 178295-178310, 2020, doi: 10.1109/ACCESS.2020.3027830.
- [298] M. Elsis, M. Q. Tran, K. Mahmoud, D.-E. A. Mansour, M. Lehtonen, and M. M. F. Darwish, "Effective IoT-based deep learning platform for online fault diagnosis of power transformers against cyberattacks and data uncertainties," *Measurement : journal of the International Measurement Confederation*, vol. 190, p. 1, 2022, doi: 10.1016/j.measurement.2021.110686.
- [299] I. B. M. Taha, S. S. M. Ghoneim, and H. G. Zaini, "Improvement of Rogers four ratios and IEC Code methods for transformer fault diagnosis based on Dissolved Gas Analysis," in *2015 North American Power Symposium (NAPS)*, 4-6 Oct. 2015 2015, pp. 1-5, doi: 10.1109/NAPS.2015.7335098.
- [300] A. Peimankar, S. J. Weddell, T. Jalal, and A. C. Laphorn, "Evolutionary multi-objective fault diagnosis of power transformers," *Swarm and Evolutionary Computation*, vol. 36, pp. 62-75, 2017/10/01/ 2017, doi: <https://doi.org/10.1016/j.swevo.2017.03.005>.
- [301] A. Kirkbas, A. Demircali, S. Koroglu, and A. Kizilkaya, "Fault diagnosis of oil-immersed power transformers using common vector approach," *Electric Power Systems Research*, vol. 184, p. 106346, 2020/07/01/ 2020, doi: <https://doi.org/10.1016/j.epsr.2020.106346>.
- [302] L. V. Ganyun, C. Haozhong, Z. Haibao, and D. Lixin, "Fault diagnosis of power transformer based on multi-layer SVM classifier," *Electric Power Systems Research*, vol. 74, no. 1, pp. 1-7, 2005/04/01/ 2005, doi: <https://doi.org/10.1016/j.epsr.2004.07.008>.
- [303] W. Mang-Hui, "A novel extension method for transformer fault diagnosis," *IEEE Transactions on Power Delivery*, vol. 18, no. 1, pp. 164-169, 2003, doi: 10.1109/TPWRD.2002.803838.
- [304] M. Badawi *et al.*, "Reliable Estimation for Health Index of Transformer Oil Based on Novel Combined Predictive Maintenance Techniques," *IEEE Access*, vol. 10, pp. 25954-25972, 2022, doi: 10.1109/ACCESS.2022.3156102.
- [305] B. Zeng, J. Guo, W. Zhu, Z. Xiao, F. Yuan, and S. Huang, "A transformer fault diagnosis model based on hybrid grey wolf optimizer and LS-SVM," *Energies (Basel)*, vol. 12, no. 21, p. 4170, 2019, doi: 10.3390/en12214170.
- [306] Y. Zhang, X. Ding, Y. Liu, and P. J. Griffin, "An artificial neural network approach to transformer fault diagnosis," *IEEE Transactions on Power Delivery*, vol. 11, no. 4, pp. 1836-1841, 1996, doi: 10.1109/61.544265.
- [307] X. Hao and S. Cai-xin, "Artificial Immune Network Classification Algorithm for Fault Diagnosis of Power Transformer," *IEEE Transactions on Power Delivery*, vol. 22, no. 2, pp. 930-935, 2007, doi: 10.1109/TPWRD.2007.893182.

- [308] V. Duraisamy, N. Devarajan, D. Somasundareswari, A. A. M. Vasanth, and S. N. Sivanandam, "Neuro fuzzy schemes for fault detection in power transformer," *Applied Soft Computing*, vol. 7, no. 2, pp. 534-539, 2007/03/01/ 2007, doi: <https://doi.org/10.1016/j.asoc.2006.10.001>.
- [309] N. Yadaiah and N. Ravi, "Internal fault detection techniques for power transformers," *Applied Soft Computing*, vol. 11, no. 8, pp. 5259-5269, 2011/12/01/ 2011, doi: <https://doi.org/10.1016/j.asoc.2011.05.034>.
- [310] A. R. G. Castro and V. Miranda, "Knowledge discovery in neural networks with application to transformer failure diagnosis," *IEEE Transactions on Power Systems*, vol. 20, no. 2, pp. 717-724, 2005, doi: 10.1109/TPWRS.2005.846074.
- [311] M. M. Ibrahim, M. M. Sayed, and E. E. A. El-Zahab, "Diagnosis of power transformer incipient faults using Fuzzy Logic-IEC Based Approach," in *2014 IEEE International Energy Conference (ENERGYCON)*, 13-16 May 2014 2014, pp. 242-245, doi: 10.1109/ENERGYCON.2014.6850435.
- [312] H. Malik and S. Mishra, "Selection of Most Relevant Input Parameters Using Principle Component Analysis for Extreme Learning Machine Based Power Transformer Fault Diagnosis Model," *Electric power components and systems*, vol. 45, no. 12, pp. 1339-1352, 2017, doi: 10.1080/15325008.2017.1338794.
- [313] H. He and E. A. Garcia, "Learning from Imbalanced Data," *IEEE Transactions on Knowledge and Data Engineering*, vol. 21, no. 9, pp. 1263-1284, 2009, doi: 10.1109/TKDE.2008.239.
- [314] K. N. V. P. S. Rajesh, U. M. Rao, I. Fofana, P. Rozga, and A. Paramane, "Influence of Data Balancing on Transformer DGA Fault Classification With Machine Learning Algorithms," *IEEE Transactions on Dielectrics and Electrical Insulation*, vol. 30, no. 1, pp. 385-392, 2023, doi: 10.1109/TDEI.2022.3230377.
- [315] M. M. Alam *et al.*, "Assessing Transformer Oil Quality using Deep Convolutional Networks," in *2019 29th Australasian Universities Power Engineering Conference (AUPEC)*, 26-29 Nov. 2019 2019, pp. 1-6, doi: 10.1109/AUPEC48547.2019.211896.
- [316] J. Lin, J. Ma, J. G. Zhu, and Y. Cui, "A Transfer Ensemble Learning Method for Evaluating Power Transformer Health Conditions With Limited Measurement Data," *IEEE Transactions on Instrumentation and Measurement*, vol. 71, pp. 1-10, 2022, doi: 10.1109/TIM.2022.3175268.
- [317] "D1/A2 Technical Brochure - Advances in DGA interpretation," vol. 771, July 2019. CIGRE.
- [318] A. Teymouri and B. Vahidi, "CO₂/CO concentration ratio: A complementary method for determining the degree of polymerization of power transformer paper insulation," *IEEE Electrical Insulation Magazine*, vol. 33, no. 1, pp. 24-30, 2017, doi: 10.1109/MEI.2017.7804313.
- [319] M. Duval, A. D. Pablo, I. Atanasova-Hoehlein, and M. Grisar, "Significance and detection of very low degree of polymerization of paper in transformers," *IEEE Electrical Insulation Magazine*, vol. 33, no. 1, pp. 31-38, 2017, doi: 10.1109/MEI.2017.7804314.
- [320] F. R. Barbosa, O. M. Almeida, A. P. S. Braga, M. A. B. Amora, and S. J. M. Cartaxo, "Application of an artificial neural network in the use of physicochemical properties as a low cost proxy of power transformers DGA data," *IEEE Transactions on Dielectrics and Electrical Insulation*, vol. 19, no. 1, pp. 239-246, 2012, doi: 10.1109/TDEI.2012.6148524.
- [321] S. Kim *et al.*, "A Semi-Supervised Autoencoder With an Auxiliary Task (SAAT) for Power Transformer Fault Diagnosis Using Dissolved Gas Analysis," *IEEE access*, vol. 8, pp. 178295-178310, 2020, doi: 10.1109/ACCESS.2020.3027830.
- [322] M. M. Nezami, S. A. Wani, S. A. Khan, N. Khera, and M. A. Khan, "Fuzzy approach for residual life assessment of paper insulation," in *2017 3rd International Conference on Condition Assessment Techniques in Electrical Systems (CATCON)*, 16-18 Nov. 2017 2017, pp. 26-30, doi: 10.1109/CATCON.2017.8280178.
- [323] D. A. Zaldivar, A. A. Romero, and S. R. Rivera, "Risk assessment algorithm for power transformer fleets based on condition and strategic importance," *Algorithms*, vol. 14, no. 11, p. 319, 2021, doi: 10.3390/a14110319.
- [324] M. M. Nezami, M. D. Equbal, S. A. Khan, S. Sohail, and S. S. M. Ghoneim, "Classification of Cellulosic Insulation State Based on Smart Life Prediction Approach (SLPA)," *Processes*, vol. 9, no. 6, p. 981, 2021. [Online]. Available: <https://www.mdpi.com/2227-9717/9/6/981>.
- [325] L. Tao, X. Yang, Y. Zhou, and L. Yang, "A Novel Transformers Fault Diagnosis Method Based on Probabilistic Neural Network and Bio-Inspired Optimizer," *Sensors*, vol. 21, no. 11, p. 3623, 2021. [Online]. Available: <https://www.mdpi.com/1424-8220/21/11/3623>.
- [326] Y. Zhou, L. Tao, X. Yang, and L. Yang, "Novel Probabilistic Neural Network Models Combined with Dissolved Gas Analysis for Fault Diagnosis of Oil-Immersed Power Transformers," *ACS Omega*, vol. 6, no. 28, pp. 18084-18098, 2021/07/20 2021, doi: 10.1021/acsomega.1c01878.

Appendix A Python Script for Fault Diagnostic Module Training

```
1 import matplotlib.pyplot as plt
2 import numpy as np
3 import pandas as pd
4 from imblearn.over_sampling import SMOTE
5 from sklearn.preprocessing import MultiLabelBinarizer
6 from sklearn.utils import shuffle
7 from keras.models import Sequential
8 from keras.layers import Conv1D, Flatten, Dense, BatchNormalization
9 from sklearn.preprocessing import MinMaxScaler
10 import joblib
11
12 # Load csv file into a Pandas DataFrame
13 data = pd.read_csv('C:/Users/20884857/OneDrive - Curtin University of
14 Technology Australia/'
15 'AM model datasets/Classification/Data sets from
16 references REV11a - labels.csv',
17 usecols=[0, 1, 2, 3, 4, 5],
18 header=0)
19
20 # Exclude the 1st column from normalization
21 numeric_cols = data.select_dtypes(include=['float64', 'int64']).columns
22
23 # Normalize the data using the Min-Max normalization method
24 scaler = MinMaxScaler()
25 data[numeric_cols] = scaler.fit_transform(data[numeric_cols])
26
27 # Save the scaler object for App use
28 joblib.dump(scaler, 'scaler1.joblib')
29
30 # Define fault labels using binary encoding
31 fault_labels = data['Fault'].apply(lambda x: x.split(';'))
32 mlb = MultiLabelBinarizer()
33 fault_labels_encoded = pd.DataFrame(mlb.fit_transform(fault_labels), columns=
34 mlb.classes_)
35
36 # Add the encoded labels to the DataFrame
37 data = pd.concat([data, fault_labels_encoded], axis=1)
38
39 # Drop the original fault column
40 data = data.drop('Fault', axis=1)
41
42 # Shuffle the datasets
43 data = shuffle(data, random_state=42)
44
45 # Split data into training, validation, and testing sets
46 train_data = data[:int(0.65 * len(data))]
47 val_data = data[int(0.65 * len(data)):int(0.8 * len(data))]
48 test_data = data[int(0.8 * len(data)):]
49
50 train_features = train_data.iloc[:, :5].values
51 train_targets = train_data.iloc[:, 5:].values
52 val_features = val_data.iloc[:, :5].values
53 val_targets = val_data.iloc[:, 5:].values
54 test_features = test_data.iloc[:, :5].values
55 test_targets = test_data.iloc[:, 5:].values
56
57 # Calculate the binary representation of each label combination
58 label_combinations = np.arange(2 ** train_targets.shape[1])
59 power_labels = np.array([list(bin(x)[2:].zfill(train_targets.shape[1])) for x
60 in label_combinations], dtype=int)
```

```

57
58 # Calculate the multi-class targets for each instance
59 # and convert train targets to multi-class
60 train_targets_multi_class = []
61 for j in range(train_targets.shape[0]):
62     train_targets_multi_class.append(np.where((power_labels == train_targets
        [j]).all(axis=1))[0][0])
63
64 train_targets_multi_class = np.array(train_targets_multi_class)
65
66 # Add the multi-class targets as a new column to the DataFrames
67 train_data = train_data.assign(multi_class_targets=train_targets_multi_class
    )
68
69 # Generate class labels based on unique values in train_targets_multi_class
70 class_labels = [str(label) for label in np.unique(train_targets_multi_class
    )]
71
72 # Use SMOTE to balance the training data
73 sm = SMOTE(random_state=42, k_neighbors=1)
74 train_features_resampled, train_targets_resampled = sm.fit_resample(
    train_features,
75     train_targets_multi_class.reshape(-1, 1))
76
77 # Convert resampled train targets from multi-class back to binary encoding
78 train_targets_binary = [] # Initialize empty list for binary targets
79 # Loop through each target value in train_targets_resampled
80 for target in train_targets_resampled:
81     index = target # Find the index of the target value in power_labels
82     binary_values = power_labels[index] # Get the corresponding binary
        values from power_labels
83     train_targets_binary.append(binary_values) # Append the binary values
        to train_targets_binary
84 # Convert train_targets_binary to a numpy array
85 train_targets_binary = np.array(train_targets_binary)
86
87 # train_features_resampled array needs to be reshaped to 3D array so that it
        can be used as input of 1DCNN.
88 n_samples = train_features_resampled.shape[0]
89 n_features = train_features_resampled.shape[1]
90 train_features_resampled = np.reshape(train_features_resampled, (n_samples,
    1, n_features))
91
92 # define the input shape
93 input_shape = (1, n_features)
94
95 # Define the model architecture
96 model = Sequential()
97 model.add(Conv1D(64, 3, padding='same', activation='ReLU', input_shape=
    input_shape))
98 model.add(BatchNormalization())
99 model.add(Flatten())
100 model.add(Dense(16, activation='ReLU'))
101 model.add(Dense(fault_labels_encoded.shape[1], activation='sigmoid'))
102 model.summary()
103
104 # Compile the model
105 val_features = np.reshape(val_features, (val_features.shape[0], 1,
    val_features.shape[1]))

```

```
106 test_features = np.reshape(test_features, (test_features.shape[0], 1,
    test_features.shape[1]))
107
108 # opt = AdamW()
109 model.compile(optimizer='Nadam',
110               loss='binary_crossentropy',
111               metrics=['accuracy'])
112
113 history = model.fit(train_features_resampled, train_targets_binary,
114                   validation_data=(val_features, val_targets),
115                   epochs=1000, batch_size=16)
116
117 # Evaluate the model on the test set
118 test_loss, test_acc = model.evaluate(test_features, test_targets)
119 print('Test accuracy:', test_acc)
120
121 # save the model
122 model.save('FDDGACNN1083SC19.h5')
123
124 loss = history.history['loss']
125 val_loss = history.history['val_loss']
126 epochs = range(1, len(loss) + 1)
127 plt.plot(epochs, loss, 'y', label='Training loss')
128 plt.plot(epochs, val_loss, 'r', label='Validation loss')
129 plt.title('Training and validation loss')
130 plt.xlabel('Epochs')
131 plt.ylabel('Loss')
132 plt.legend()
133 plt.show()
134
135 acc = history.history['accuracy']
136 val_acc = history.history['val_accuracy']
137 plt.plot(epochs, acc, 'y', label='Training acc')
138 plt.plot(epochs, val_acc, 'r', label='Validation acc')
139 plt.title('Training and validation accuracy')
140 plt.xlabel('Epochs')
141 plt.ylabel('Accuracy')
142 plt.legend()
143 plt.show()
144
```

Appendix B Python Script for Life Management Module Training

```
1 # This model uses CO and CO2 measurements to predict DP.
2 import matplotlib.pyplot as plt
3 import pandas as pd
4 from keras.layers import Dense, Conv1D, Flatten
5 from keras.models import Sequential
6 from sklearn.model_selection import train_test_split
7 from sklearn.preprocessing import MinMaxScaler
8 import joblib
9
10 # Load data into a pandas DataFrame
11 data = pd.read_csv('C:/Users/20884857/OneDrive - Curtin University of
    Technology Australia/'
12                   'AM model datasets/Regression/RLCOCO2ratioDP.csv',
13                   usecols=[1, 2, 3],
14                   header=0)
15
16 # shuffle data
17 data = data.sample(frac=1)
18
19 # convert DataFrame to numpy arrays
20 X = data.iloc[:, :2].values # use columns 2 and 3 as input features
21 y = data.iloc[:, 2].values
22
23 # apply max-min normalization to X
24 scaler = MinMaxScaler()
25 X = scaler.fit_transform(X)
26
27 # save the scaler object for later use
28 joblib.dump(scaler, 'scalerCOCO2DP2.joblib')
29
30 # reshape X to have a 3D shape (samples, time steps, features)
31 X = X.reshape((X.shape[0], 1, X.shape[1]))
32
33 # split data into training and testing sets
34 X_train, X_test, y_train, y_test = train_test_split(X, y, test_size=0.2,
    random_state=42)
35
36 # create and compile the 1D CNN model
37 model = Sequential()
38 model.add(Conv1D(filters=128, kernel_size=1, activation='relu', input_shape=(
    1, X.shape[2])))
39 model.add(Flatten())
40 model.add(Dense(64, activation='relu'))
41 model.add(Dense(1))
42 model.compile(loss='mse', optimizer='adam')
43 model.summary()
44
45 # train the model
46 history = model.fit(X_train, y_train, epochs=5000,
47                    batch_size=16, verbose=1, validation_data=(X_test, y_test
    ))
48
49 # evaluate the model on the testing set
50 mse = model.evaluate(X_test, y_test, verbose=0)
51 print("Mean squared error on testing set:", mse)
52
53 # save the model
54 model.save('DPCOCO2_3.h5')
55
56 # plot the training and validation loss
```



```
57 plt.plot(history.history['loss'], label='Training loss')
58 plt.plot(history.history['val_loss'], label='Validation loss')
59 plt.title('Training and validation loss')
60 plt.xlabel('Epoch')
61 plt.ylabel('Loss')
62 plt.legend()
63 plt.show()
```

Appendix C Python Script for Asset Management Model

```
1 import math
2 import numpy as np
3 import joblib
4 from keras.models import load_model
5 from tkinter import *
6 import customtkinter as ctk
7 from customtkinter import *
8
9 ctk.set_appearance_mode("dark")
10
11
12 class App(ctk.CTk):
13     def __init__(self):
14         super().__init__()
15
16         self.geometry("1000x600")
17         self.title("Condition Assessment of Transformer TF0001")
18
19         # define Frames
20         self.grid_columnconfigure(0, weight=1)
21         self.grid_rowconfigure(0, weight=1)
22
23         self.frameBody = ctk.CTkFrame(master=self)
24         self.frameBody.grid(row=0, column=0, sticky="nswe")
25
26         # Main pane body
27         self.paneBody = PanedWindow(self.frameBody)
28         self.paneBody.pack(fill="both", expand=TRUE)
29
30         # other panes
31         self.paneLeftBody = PanedWindow(self.paneBody, orient="vertical")
32         self.paneBody.add(self.paneLeftBody)
33
34         self.paneTop = PanedWindow(self.paneLeftBody, height=650)
35         self.paneLeftBody.add(self.paneTop)
36
37         self.paneFD = PanedWindow(self.paneTop, bg="#FFD700", width=750)
38         self.paneTop.add(self.paneFD)
39
40         self.paneRL = PanedWindow(self.paneTop, bg="#9400D3")
41         self.paneTop.add(self.paneRL)
42
43         self.paneBottom = PanedWindow(self.paneLeftBody, bg="#83838B")
44         self.paneLeftBody.add(self.paneBottom)
45
46         self.label_H2 = ctk.CTkLabel(self.paneFD,
47                                     text="H2:",
48                                     text_color="black",
49                                     font=("Helvetica", 16, "bold"))
50         self.label_H2.grid(row=0, column=0, padx=5, pady=(10, 0), sticky="w"
51 )
52
53         self.entry_H2 = ctk.CTkEntry(self.paneFD)
54         self.entry_H2.grid(row=0, column=1, padx=5, pady=(10, 0))
55
56         self.label_CH4 = ctk.CTkLabel(self.paneFD,
57                                     text="CH4:",
58                                     text_color="black",
59                                     font=("Helvetica", 16, "bold"))
60         self.label_CH4.grid(row=1, column=0, padx=5, pady=(10, 0), sticky="w"
```

```

59 ")
60
61     self.entry_CH4 = ctk.CTkEntry(self.paneFD)
62     self.entry_CH4.grid(row=1, column=1, padx=5, pady=(10, 0))
63
64     self.label_C2H4 = ctk.CTkLabel(self.paneFD,
65                                 text="C2H4:",
66                                 text_color="black",
67                                 font=("Helvetica", 16, "bold"))
68     self.label_C2H4.grid(row=2, column=0, padx=5, pady=(10, 0), sticky=
"w")
69
70     self.entry_C2H4 = ctk.CTkEntry(self.paneFD)
71     self.entry_C2H4.grid(row=2, column=1, padx=5, pady=(10, 0))
72
73     self.label_C2H6 = ctk.CTkLabel(self.paneFD,
74                                 text="C2H6:",
75                                 text_color="black",
76                                 font=("Helvetica", 16, "bold"))
77     self.label_C2H6.grid(row=3, column=0, padx=5, pady=(10, 0), sticky=
"w")
78
79     self.entry_C2H6 = ctk.CTkEntry(self.paneFD)
80     self.entry_C2H6.grid(row=3, column=1, padx=5, pady=(10, 0))
81
82     self.label_C2H2 = ctk.CTkLabel(self.paneFD,
83                                 text="C2H2:",
84                                 text_color="black",
85                                 font=("Helvetica", 16, "bold"))
86     self.label_C2H2.grid(row=4, column=0, padx=5, pady=(10, 0), sticky=
"w")
87
88     self.entry_C2H2 = ctk.CTkEntry(self.paneFD)
89     self.entry_C2H2.grid(row=4, column=1, padx=5, pady=(10, 0))
90
91     self.button_FD = CTkButton(self.paneFD, text="Fault Diagnosis",
command=self.predict_fault)
92     self.button_FD.grid(row=5, column=1, padx=30, pady=30, sticky="ew")
93
94     self.label_FD = ctk.CTkLabel(self.paneFD,
95                                 text="The potential fault is:",
96                                 text_color="black",
97                                 font=("Helvetica", 16, "bold"))
98     self.label_FD.grid(row=6, column=0, padx=30, pady=30)
99
100    self.potentialFault = ctk.CTkLabel(self.paneFD, text="")
101    self.potentialFault.grid(row=6, column=1, padx=30, pady=30)
102
103    self.comment_FD = ctk.CTkLabel(self.paneBottom, text="")
104    self.comment_FD.grid(row=1, column=0, padx=5, pady=(10, 0))
105
106    # -----
107    -----
108    self.label_CO2 = ctk.CTkLabel(self.paneRL,
109                                text="CO2:",
110                                text_color="black",
111                                font=("Helvetica", 16, "bold"))
112    self.label_CO2.grid(row=0, column=0, padx=5, pady=(10, 0), sticky="
w")

```

```

112     self.entry_CO2 = ctk.CTkEntry(self.paneRL)
113     self.entry_CO2.grid(row=0, column=1, padx=5, pady=(10, 0))
114
115     self.label_CO = ctk.CTkLabel(self.paneRL,
116                               text="CO:",
117                               text_color="black",
118                               font=("Helvetica", 16, "bold"))
119     self.label_CO.grid(row=1, column=0, padx=10, pady=(10, 0), sticky="
w")
120
121     self.entry_CO = ctk.CTkEntry(self.paneRL)
122     self.entry_CO.grid(row=1, column=1, padx=10, pady=(10, 0))
123
124
125     # -----
126     self.button_DP = CTkButton(self.paneRL, text="Predict DP", command=
self.predict_DPoutput)
127     self.button_DP.grid(row=4, column=1, padx=30, pady=30, sticky="ew")
128
129     self.label_predictDP = ctk.CTkLabel(self.paneRL,
130                                       text="The predicted DP is:",
131                                       text_color="black",
132                                       font=("Helvetica", 16, "bold"))
133     self.label_predictDP.grid(row=5, column=0, padx=30, pady=30)
134     self.predicted_DP = ctk.CTkLabel(self.paneRL, text="")
135     self.predicted_DP.grid(row=5, column=1, padx=30, pady=30)
136
137     self.label_remaining_life = ctk.CTkLabel(self.paneBottom,
138                                             text="% of remaining life:"
,
139                                             text_color="black",
140                                             font=("Helvetica", 16, "
bold"))
141     self.label_remaining_life.grid(row=2, column=0, padx=5, pady=(10, 0
), sticky="w")
142
143     self.remaining_life = ctk.CTkLabel(self.paneBottom, text="")
144     self.remaining_life.grid(row=2, column=1, padx=5, pady=(10, 0))
145
146     self.insulation_status = ctk.CTkLabel(self.paneBottom, text="")
147     self.insulation_status.grid(row=2, column=2, padx=5, pady=(10, 0))
148
149
150     # -----
151     def predict_FD(self, input_measurements, scaler, model):
152         # Apply max-min normalization to the input measurements
153         x = np.array(input_measurements).reshape((1, 5))
154         x = scaler.transform(x)
155         # Reshape the input measurements to have a 3D shape (samples, time
steps, features)
156         x = x.reshape((1, 1, 5))
157         # Make a prediction using the model
158         y_pred = model.predict(x)
159         # convert to binary
160         threshold = 0.5
161         binary_pred = np.where(np.array(y_pred) >= threshold, 1, 0)

```

```

162     # Return the predicted Fault
163     return (binary_pred)
164
165     def get_fault_label(self, condition):
166         if np.array_equal(condition, [[0, 1, 0, 0]]) or np.array_equal(
condition, [[0, 0, 0, 0]]):
167             return "No Fault detected."
168         elif np.array_equal(condition, [[0, 0, 0, 1]]) or np.array_equal(
condition, [[0, 1, 0, 1]]):
169             return "Thermal Fault detected."
170         elif np.array_equal(condition, [[0, 0, 1, 0]]) or np.array_equal(
condition, [[0, 1, 1, 0]]):
171             return "Partial Discharge Fault detected."
172         elif np.array_equal(condition, [[0, 0, 1, 1]]) or np.array_equal(
condition, [[0, 1, 1, 1]]):
173             return "Partial Discharge and Thermal Faults detected."
174         elif np.array_equal(condition, [[1, 0, 0, 0]]) or np.array_equal(
condition, [[1, 1, 0, 0]]):
175             return "Discharge Fault detected."
176         elif np.array_equal(condition, [[1, 0, 0, 1]]) or np.array_equal(
condition, [[1, 1, 0, 1]]):
177             return "Discharge and Thermal Faults detected."
178         elif np.array_equal(condition, [[1, 0, 1, 0]]) or np.array_equal(
condition, [[1, 1, 1, 0]]):
179             return "Discharge and Partial Discharge Faults detected."
180         else:
181             return "Discharge, Partial Discharge and Thermal Faults detected
."
182
183
184     def comment_fault(self, condition):
185         if np.array_equal(condition, [[0, 1, 0, 0]]) or \
np.array_equal(condition, [[0, 0, 0, 0]]):
186             return "No fault detected, very low likelihood of failure."
187         elif np.array_equal(condition, [[0, 0, 1, 0]]) or \
np.array_equal(condition, [[0, 1, 1, 0]]):
188             return "Sign of Partial Discharge fault, low risk of failure."
189         elif np.array_equal(condition, [[0, 0, 0, 1]]) or \
np.array_equal(condition, [[0, 0, 1, 1]]) or \
np.array_equal(condition, [[0, 1, 0, 1]]) or \
np.array_equal(condition, [[0, 1, 1, 1]]):
190             return "Sign of Thermal fault, moderate risk of failure."
191         else:
192             return "Sign of Discharge fault, very high risk of failure."
193
194
195     def predict_fault(self):
196         # Get the input measurements from the line edits
197         H2 = float(self.entry_H2.get())
198         CH4 = float(self.entry_CH4.get())
199         C2H4 = float(self.entry_C2H4.get())
200         C2H6 = float(self.entry_C2H6.get())
201         C2H2 = float(self.entry_C2H2.get())
202
203         # Load the saved model
204         model = load_model('FDDGACNN1083SC19.h5')
205
206         # Load the scaler
207         scaler = joblib.load('scaler1.joblib')
208
209         # Make a prediction using the function

```

```

214     input_measurements = [H2, CH4, C2H4, C2H6, C2H2]
215     condition = self.predict_FD(input_measurements, scaler, model)
216
217     # Get the fault Label
218     label = self.get_fault_label(condition)
219
220     # Display the predicted output in a message box
221     # CtkMessageBox(title="Prediction", message=f"The predicted output
is: {label}\nCondition: {condition}")
222     self.potentialFault.configure(text=f"{label}", text_color="black",
font=("Helvetica", 16, "bold"))
223
224     # Comment on the fault condition
225     comment = self.comment_fault(condition)
226     self.comment_FD.configure(text=f"{comment}", text_color="black",
font=("Helvetica", 16, "bold"))
227
228     # -----
-----
229
230     def predict_DP(self, input_COCO2, scaler3, model3):
231         # Apply max-min normalization to the input measurements
232         x = np.array(input_COCO2).reshape((1, 2))
233         x = scaler3.transform(x)
234         # Reshape the input measurements to have a 3D shape (samples, time
steps, features)
235         x = x.reshape((1, 1, 2))
236         # Make a prediction using the model
237         DP_pred = model3.predict(x)[0][0]
238         # Return the predicted 2FAL value
239         return DP_pred
240
241     def predict_DPoutput(self):
242         # Get the input measurements from the line edits
243         CO2 = float(self.entry_CO2.get())
244         CO = float(self.entry_CO.get())
245
246         # Load the saved model
247         model3 = load_model('DPCOCO2_3.h5')
248
249         # Load the scaler
250         scaler3 = joblib.load('scalerCOCO2DP.joblib')
251
252         # Make a prediction using the function
253         input_COCO2 = [CO2, CO]
254         dp = self.predict_DP(input_COCO2, scaler3, model3)
255
256         # Display the predicted output in a message box
257         self.predicted_DP.configure(text=f"{int(dp)}",
text_color="black",
258                                     font=("Helvetica", 16, "bold"))
259
260
261         r1 = 166.1 * math.log10(dp) - 382.2
262
263         self.remaining_life.configure(text=f"{int(r1)}" + "%",
text_color="black",
264                                     font=("Helvetica", 16, "bold"))
265
266
267         if dp > 700:

```

```
268     status = "Health insulation"
269     elif 450 < dp <= 700:
270         status = "Moderate deterioration shown in insulation"
271     elif 250 < dp <= 450:
272         status = "Extensive deterioration shown in insulation"
273     else:
274         status = "End of insulation life"
275
276     self.insulation_status.configure(text=status,
277                                     text_color="black",
278                                     font=("Helvetica", 16, "bold"))
279
280
281 if __name__ == "__main__":
282     app = App()
283     app.mainloop()
284
```